# Respiration monitoring based on information fusion from Impedance pneumography and Electrocardiography

Feng Ma

# RESPIRATION MONITORING BASED ON INFORMATION FUSION FROM IMPEDANCE PNEUMOGRAPHY AND ELECTROCARDIOGRAPHY

by

**Feng Ma**

in partial fulfillment of the requirements for the degree of

**Master of Science**

in Electrical Engineering

at the Delft University of Technology,

| | | |
|---|---|---|
| Student number: | 4616170 | |
| Project duration: | November 1, 2017 – August 1, 2018 | |
| Supervisor: | Dr. Richard C. Hendriks | |
| Thesis committee: | Prof. Dr. ir. Alle-Jan van der Veen, | TU Delft |
| | Dr. ir. Richard C. Hendriks, | TU Delft |
| | Dr. Faruk Uysal, | TU Delft |
| | Dr. ir. Willemijn Groenendaal, | imec |
| | Ir. Patrick van der Heijden | imec |

TU Delft Delft University of Technology

# ABSTRACT

In the hospital environment, the variations in respiratory information (RI) are typically used for indicating the health condition of the patients. With RI known, corresponding parameters in both time domain (respiratory rate) and frequency domain (respiratory power) can be extracted to indicate the health condition. However, the monitoring technologies available in the clinical environment commonly work obtrusively, which can result in discomfort for patients during a long-term monitoring. Meanwhile, these technologies also possess high false alarm rates, especially during movement of the subjects. Thus, designing an unobtrusive equipment suitable for moving patients that could collect as well as the algorithm to analyze such signals to provide an accurate and robust estimate of respiratory information obviously becomes very interesting.

The base signals of interest for estimating respiratory information are two commonly used bio-medical signals, Impedance pneumography (IP) and electrocardiography (ECG). Impedance pneumography is a commonly used method for respiratory rate monitoring. Electrocardiography is a measurement of the electrical activity of heart and respiration modulates the ECG in both time domain and frequency domain so that it is feasible to estimate the RI also from ECG. These two signals can be utilized with the same measurement electrodes attached to the surface of the body from the same device which provides a potential wearable method for real-time RI monitoring.

This thesis investigates the feasibility of using these two unobtrusive bio-medical signals, IP and ECG, to monitor respiratory rate (RR) in home environments especially during various movements. Algorithm development focused on creating accurate and robust respiratory rate estimates both from impedance pneumography and ECG-derived methods based on the modulation of respiration. Furthermore, the RI estimate from individual signals will be further fused by the way of information fusion and investigate the feasibility of giving more accurate respiratory information than that obtained using one signal alone. Finally, we also investigate the feasibility of using acceleration recordings (Acc) to attenuate the motion artefact distorting the underlying signals.

Signal quality indicators (SQI) and respiration quality indicators (RQI) together play a key role in providing a more accurate RR estimate. Performance of all methods is evaluated against spirometer recordings, as a golden reference, based on a set of typical statistical metrics.

The main results are that IP signal can provide a more accurate RR estimate compared with the ECG signal. Furthermore, the derived signal quality indicators, SQI and RQI, could distinguish data of good quality from bad quality and the RR smoothing process could improve the result both of IP and ECG-derived methods with the help of signal quality indicator. Another main finding is that the correlation between the motion artefacts and Acc recordings is not high enough, resulting in that Acc is not a proper reference signal for motion artefacts attenuation. Finally, it's also found that information fusion methods could improve the overall estimate from multiple signal sources.

For the future work, a better reference signal for motion artefacts attenuation should be explored. Furthermore, since only the respiratory rate estimation is investigated in this thesis, more respiratory information, like tidal volume, should also be explored.

*Feng Ma*
*Eindhoven, August 2018*

# ACKNOWLEDGEMENT

This thesis, Respiration Monitoring Based on Information Fusion From Impedance pneumography and Electrocardiography, has been carried by the cooperation between the imec, the Netherlands and the Delft University of Technology, The Netherlands. I feel this is the best time to express my gratitude to all the people from imec and TU Delft who gave me a lot of help during this thesis project.

Firstly, I would like to thank imec the Netherlands and Senior researcher Willemijn Groenendaal for providing the great thesis opportunity. I've been working in the group Connected Health Solution and all the People in this group are very friendly and always willing to help each other. Specifically, I would like to thank my supervisors Willemijn Groenendaal and Patrick van der Heijden for the great enthusiasm and for all the valuable weekly meetings on the track of the project and the impressive suggestions on the algorithm development. Big thanks also to my colleague Jorge Herranz Olazabal for his valuable and impressive expertise and the help for my project.

I also would like to express my gratitude to Dr. Richard Hendriks, my daily supervisor at TU Delft, for his continuous enthusiasm for support and help. Richard gives me ideas for the direction of the research and new thoughts on my projects as well as helps me with the graduation issues.

*Feng Ma*
*Eindhoven, August 2018*

# NOMENCLATURE

| | |
|---|---|
| $ANS$ | Autonomic nervous system |
| $AR$ | Auto-regressive |
| $Bioz$ | bioimpedance, same as impedance pneumography |
| $Bpm$ | Beat per minute |
| $cICA$ | Constrained independent component analysis |
| $DWT$ | Discrete wavelet transform |
| $ECG$ | Electrocardiography |
| $EDR$ | ECG-derived respiration |
| $FFT$ | Fast Fourier transform |
| $GALL$ | Gradient adaptive Laguerre Lattice |
| $HRV$ | Heart rate variability |
| $IP$ | impedance pneumography |
| $LDA$ | Linear discriminant analysis |
| $MA$ | Motion artifact |
| $MPA$ | Maximum peak area |
| $OSQI$ | Overall signal quality |
| $PPG$ | Photoplethysmogram |
| $QDA$ | Quadratic discriminant analysis |
| $RQI$ | Respiration quality indicator |
| $RR$ | Respiration rate |
| $RSA$ | Respiratory Sinus Arrhythmia |
| $SNR$ | Signal to noise ratio |
| $SQI$ | Signal quality indicator |
| $TI$ | Transthoracic inductance |
| $TRA$ | Total respiratory area |

# CONTENTS

# LIST OF FIGURES

# LIST OF TABLES

# 1

# INTRODUCTION

In hospital environments, the patients are under careful monitoring and a set of vital signs are monitored to indicate the health condition [12]. One essential vital sign is the respiratory rate (RR) and it's also found to be an importantly informative indicator for conditions of the patients in physiology, especially for clinical deterioration[13]. Early recognition of the changes in the vital signs, like RR, can be of great help to prevent severe and even life-threatening situations [14]. Thus continuous monitoring of RR can provide valuable information indicating patient health status in the hospital as well as in home environments.
The RR estimation can be achieved by a great number of methods from different physiological signals and can be mainly divided into direct and indirect methods [12]. Normally in practice, only those direct methods that measure the amount of air which can be inhaled and exhaled in breath cycles can provide a robust and satisfactory recording of respiratory information for every breath cycle, thus we can derive an accurate estimate of the RR. However, such methods often work in an obtrusive way and somehow result in discomfort if the patients wear it for a long time.
For the indirect methods, due to the modulations of respiration on certain bio-medical signals, a small number of sensors could be attached on the human body and able to record the respiratory rate in real-time and they don't work really well especially when there are too many artefacts resulted from the movement [15]. Two commonly used sensors are impedance plethysmography and inductance plethysmography sensors and more details of these two will be introduced in Chapter 2. However, whether the direct or indirect methods we have introduced so far are not suitable for long-term RR monitoring. As a consequence, there is a constant demand for a non-invasive and unobtrusive wearable method for RR estimation of which the performance can reach certain clinical standards accuracy.
In this thesis, two physiological signals of interest are utilized for estimating RR and these are **Impedance pneumography (IP)** and **electrocardiography(ECG)**. Physiological mechanisms can result in modulations by respiration on both signals.
Impedance pneumography, also known as bio-impedance (Bioz), is a commonly-used technique to monitor the respiration information of the patients by measuring the variations of the electrical impedance of the thorax during the breath cycle in an unobtrusive way [16]. For the ECG signals, various types of modulation can be observed thus the respiratory signals could be derived from ECG [3]. As a consequence, these two signals can be used to estimate the respiratory rate without extra sensors.
This thesis concentrates on investigating the feasibility of using IP and ECG to achieve robust and accurate RR estimation. In particular, the target is to improve accuracy especially during movement in the typical home environment, where few studies have been found. A set of methods of complete signal processing pipelines are introduced. Further, to judge the reliability of RR estimate from the individual signals, we have two indi-

cators, signal quality indicator (SQI) and respiratory quality indicator (RQI) to indicate the signal quality from the aspect of morphology for ECG and also the presence of respiratory component respectively and both of them are evaluated based on an available dataset from imec. In order to make full use of these two signals, a set of fusion methods are also introduced and they fuse respiratory rate estimates from these two base signals. The main target is to clarify if it's possible to provide more accurate and robust RR estimates in the way of information fusion than only from a single signal. Finally, spirometer recording, a technology to measure the breathing volume directly, is used to provide a golden standard of the RR for the algorithm development.

## 1.1. PROJECT TARGET

The overall target of this thesis is to investigate the feasibility of performing reliable respiratory monitoring from a set of unobtrusive sensors under different motions. The signals of interest utilized in this thesis are:

- Impedance plethysmography signal (IP)
- Electrocardiography (ECG)
- Accelerometer recordings (Acc)

These three signals are chosen for investigation because they can all be obtained in a non-invasive way from a wearable imec data collection device and the first two signals are known to be influenced by respiration and both are currently measured in clinical environments. The Acc recordings could be a potential reference signal to improve the signal quality of the first two, especially when the signals are distorted by motion artefacts. Hence a successful solution based on these signals would not require additional hardware or monitoring devices. In addition, spirometer recording is also obtained as a reference signal which measures the breath volume directly.

## 1.2. OBJECTIVES

The objective of this thesis is to develop methods to provide an accurate and robust RR estimate from IP and ECG these two physiological signals base on certain signal processing methods. The main objectives of the work are now summarized.
The first objective of this thesis is to:

- Develop a complete framework for respiration estimation based on IP and ECG signals.

Methods developed in this work for obtaining respiration are tested and compared with methods from imec. Since both the base signals, IP and ECG, are sensitive to motion and normally they have an overlapping frequency band with the artefact [17]. Therefore, a logical question to ask is whether certain reference signals can be utilized to attenuate the motion artefact. Therefore, the second objective is to:

- Investigate if the acceleration recordings (Acc) are a valid reference signal for motion artefact reduction by evaluating the correlation between the Acc and the motion artefact.

The performance of the developed framework is also needed to be evaluated, tuhs the third objective is to:

- Evaluate the proposed framework for RR estimation and search for reproducible evaluation procedure based on possible statistical metrics in a quantified way.

## 1.3. OVERVIEW OF THE THESIS

This thesis consists of the following parts.
Chapter 2 gives a more detailed introduction to the two utilized bio-medical signals namely ECG and IP. Furthermore, the modulation of respiration on the on these signals is also described. Finally, the databases used in this thesis are also introduced.
Chapter 3 gives an overview of the typical signal processing techniques used in this thesis. Techniques both in the time domain and frequency domain are introduced. An overview of data fusion is also given, which is an essential part of this thesis.
Chapter 4 introduces the development framework used in this thesis. The selected signal processing techniques are described in more details together with the implementation. An overview of the evaluation methods is also given.
In Chapter 5, evaluation results and further discussions are given. Various statistical metrics introduced in Chapter 4 are applied to the results of RR estimate obtained from different methods and a comparison on the performance of different methods is given. We also gain an understanding of what intensity of movement can this framework handle by applying this framework to the data collected from different intensity of movement.
Chapter 6 summarizes the thesis and concludes the thesis. Possible further work are also discussed.

# 2

# THE PRIMARY SIGNALS FOR RR ESTIMATION

## 2.1. INTRODUCTION

The target of this thesis is to develop a framework which is suitable for long-term RR monitoring. The primary signals of interest utilized in this thesis are the electrocardiography (ECG) and impedance pneumography (IP) signal, also called Bioz signal. The reason for the selection of these two signals is explained in more details in section 2.2.
The thesis work is carried out on three databases, both of the first two are from imec, which have ECG, IP, Acc recording and spirometer recordings. The last database is an online public database, namely PhysioNet [18], which has clean long enough ECG recording from subjects in the hospital as well as the realistic noise recordings.
This chapter gives an overview of the physiological origin of the signals, how they are collected and how they affect the respiration. Finally, an introduction is given to the databases on which the work is carried on.

## 2.2. MONITORING METHODS AND SIGNAL SELECTION

In this section, the typical methods used for respiration monitoring, the direct way and indirect way, are introduced in more details. Furthermore, we make a comparison of these two methods and explain why we choose the indirect method and the certain signals: IP and ECG.
As for the direct methods, they record the respiration information directly from the movement of the flowing air, for example, spirometer can measure the amount of air breathed in and breathed out of the lung during the breath cycles [19].
As for indirect methods, respiration information can also be recorded indirectly from certain physiological signals which reflect the volume change of human chest and examples of such techniques are transthoracic inductance (TI) and impedance pneumography [13]. For the former one, a band containing sinusoidal wire coils along will placed around the chest or belly of the patients. The area of the coils will change due to the change of the volume of the chest and belly, resulting in the variation of the inductance, which can be used to generate the respiratory signal [20]. As for the latter one, impedance pneumography is a measurement of the variations in electrical impedance across the chest and abdomen during the breath-breath cycle to reflect the respiration information.

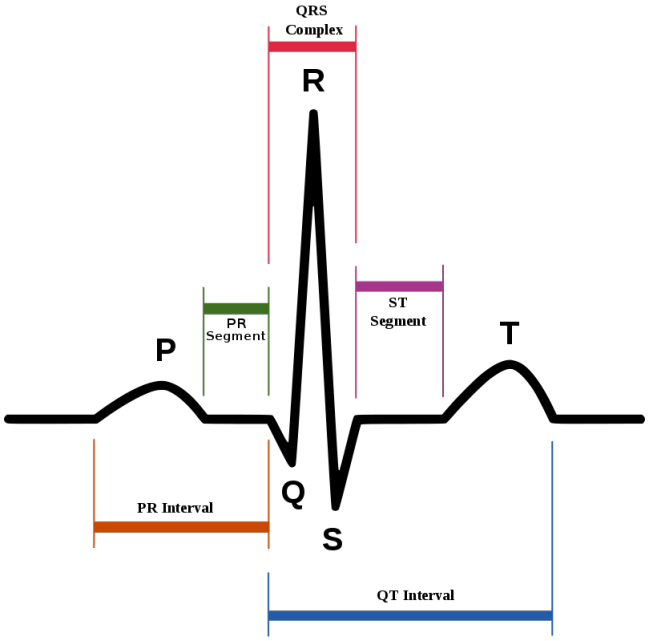


Figure 2.1: A schematic view of one normal ECG including the complete QRS complex waveform and P, T wave. The individual time intervals are also present. Image adapted from [1]

One more method can also be categorized into the in-direct methods: ECG. ECG is the measurement reflecting the electric activity of the heart and visible respiratory information is buried into the ECG in multiple ways due to the modulations of respiration on ECG [12]. Consequently, we can extract the ECG-derived respiratory (EDR) signals from the ECG, from which we can estimate the respiratory rate based on certain methods.
Each method has advantages and disadvantages. Direct measurements are more accurate, however, they can interfere with normal respiration since they normally work in an obtrusive way. Meanwhile, it's normally not possible to be embedded into a wearable device. Thus, the direct methods are not suitable for unobtrusive and long-term respiration monitoring. Thus, the indirect methods are selected since both IP and ECG can be measured with the same electrodes attached on the human body in an unobtrusive and non-invasive way from the wearable data collection device and can achieve long-term monitoring without resulting any discomfort to the subjects. However, these two signals also have shortcomings. The IP can be highly accurate and does not interfere with respiration but it requires data acquisition from still patient without any movements, otherwise the signal can be distorted by motion artefact and result in a poor RR estimate due to the poor signal quality. As for the ECG signal, the overall modulations of the respiratory ECG are relatively small compared with IP signal meaning that typical algorithms designed to extract the respiratory signals from ECG cannot tell whether these modulations are actually present in the signal or not [12].

## 2.3. THE ELECTROCARDIOGRAPHY(ECG)

The ECG is a measurement of the electrical activities of the heartbeat. During one heartbeat, the related heart muscles will pump the blood from the atria to the ventricles and finally to the body's blood circulatory system [21]. Typically, a number of electrodes are attached on certain positions of the body and during the heartbeats, the ionic current generated by the repetitive muscle activity will be converted into electric current which results in a small but still measurable voltage drop throughout the whole human body [22].
A typical ECG waveform which could be found in any healthy people is present in Figure 2.1 adapted from [1] and it contains a $P$ wave, a $QRS$ complex and a $T$ wave. This cycle is repeated in every heartbeat.
The morphology of the ECG waveform depend on the position of the electrodes attached on the body. A typical ECG configuration normally has four electrodes and can give three independent measurements reflecting the heart's electrical activity denoted as lead [23]. There are also many signal leads which have two

electrodes. One electrode is normally used as a body bias to attenuate the interference. A lead provides a vector of the heart's electrical activity within a certain direction related to the position of the electrodes. Most ECG configurations include the three limb leads: lead I, lead II and lead III. The electrodes forming these leads are located on the limb. One on each arm and one on the left leg. These leads form the basics of what is known as Einthoven's lead system [24].

- **Lead I** is the voltage difference between the left arm and right arm.
- **Lead II** is the voltage difference between the left leg and right arm.
- **Lead III** is the voltage difference between the left leg and left arm.

A 12-lead ECG is usually used in clinical environments and can provide the information of the heart's functionality in various angles [2]. Figure 2.2 shows a 12-lead ECG system and all the angles it can cover. In this work, information from a single lead ECG is used, Lead II.

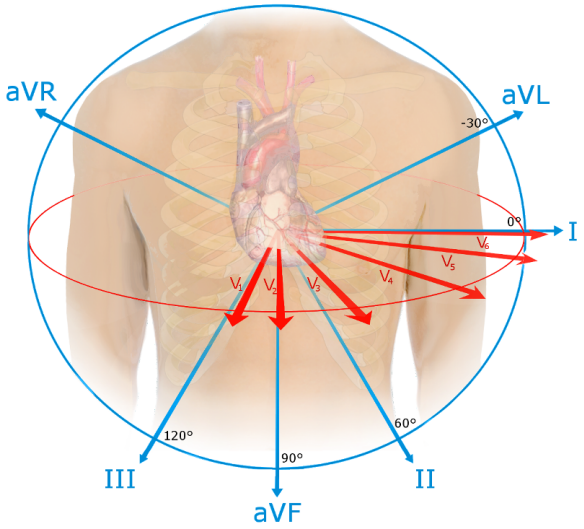


Figure 2.2: An representation of 12-lead ECG . Each lead can provide information of the electrical activity of the heart from a particular angle indicated in the figure. These contain limb leads (I, II and III) and augmented leads (aVR, aVF, aVL) and precordial leads (V1, V2, V3, V4, V5, V6) at the transverse plane. Image from [2]

### 2.3.1. THE ECG AND RESPIRATION

In this section, modulations of the respiration on the ECG signals are introduced and this is the base how we extract the respiration information from the ECG signal.
Breath-related modulations have been found and analyzed already in 1913 by Einthoven et al[24]. Nowadays they are commonly called ECG-derived respiration (EDR) signals. The commonly visible EDR signals are demonstrated in Figure 2.3. This figure shows the illustration of respiratory signals extraction based on three types of the modulation respiration has on ECG: baseline wander (BW), amplitude modulation (AM), and frequency modulation (FM) [3]. The dominant effects in more details of respiration on the ECG are listed below:

1. **Cardiac movement within the thoracic cavity** On the one hand, it has been shown experimentally, the change of the thoracic impedance distribution results from the volume change of the lung during the

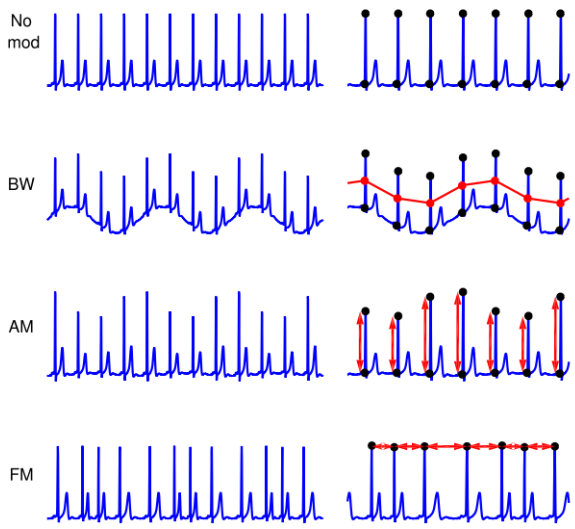


Figure 2.3: modulations of respiration on ECG signal. On the left section, the ECG with no modulation, baseline wander (BW), amplitude modulation (AM), and frequency modulation (FM) are shown from the top. In the right section, the QRS detection are shown in black dots and also the resulting EDR signals are present in red. Adapted from [3]

breath cycles. When the lung is full of air, it becomes a poor conductor and results in the increase in the electrical impedance during inspiration, thus the ECG amplitude will decrease [25]. Similarly, expiration would increase ECG amplitude. On the other hand, the heart will move during the respiration in the chest, furthermore, the relative positions of the electrodes to the heart will also change, which could result in a change on the morphology of ECG.
Two typical measures of the amplitude modulation are the voltage difference between the R peak and S peak and the amplitude of R peak against the baseline of ECG, respectively. In literature, these two are typically referred to as "amplitude modulation" methods [10].

2. **Respiratory Sinus Arrhythmia(RSA)** RSA refers to change of cardiac rhythm associated to respiration and it is the record of the variations between the consecutive heartbeat intervals. The heart rate increases during the inhalation and decreases during the exhalation, which makes it possible to derive the respiratory signal from the variation [12]. However, RSA really has its shortcomings as follows.
   - RSA effect could be weakened for elder people and it is found that smoking and certain diseases could also weaken the RSA variation [26].
   - The variation of RSA is depending on respiratory rate and according to one study in [12], from the experiment, the RSA is shown to decrease for lower respiratory rate, which means it requires a higher breathing rate to extract the EDR signal of good quality based on RSA from ECG.
3. **ECG baseline wandering** Low frequency wander of the ECG signal can be caused by respiration [3]. The baseline wander in the ECG is mainly caused by the change of the position of electrodes relative to the heart during the respiration, usually only seen in deep breathing [12]. Normally, in the preprocessing of ECG, this baseline wandering is often is removed by a high-pass filtering method for further processing. Thus the baseline wandering could only be visible from the raw ECG data.

## 2.4. IMPEDANCE PNEUMOGRAPHY(IP)

The IP signal is a commonly used bio-medical measurement to reflect respiratory information the clinical environment. It has already been a cost-effective method suitable for long-term respiration monitoring and even can be embedded into wearable devices, which makes it possible for monitoring during movement [27]. However, due to the fact that IP is really sensitive to movement, the most robust solutions are still under in-

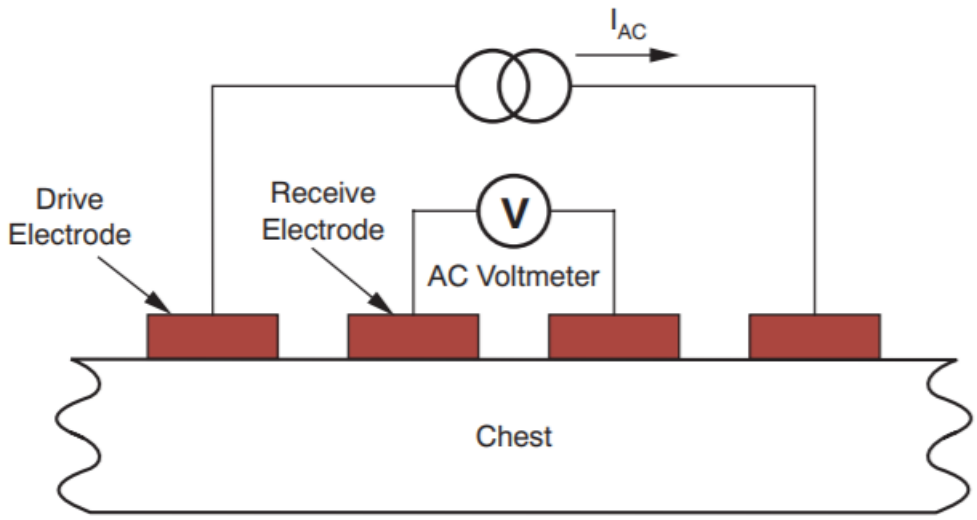


Figure 2.4: A Four-Terminal Measurement with two current injecting and two receiver electrodes.Adapted from [4]

vestigation and it's still troublesome to get the IP signal of good quality from people during speech or physical activity [28].

As shown in Figure 2.4, the configuration of IP typically has four electrodes and the principle of IP is that two electrodes of these four are injecting current with high enough frequency and a relatively low amplitude. Then the voltage difference is measured along the current path between another two electrodes, called receive electrodes [28]. The amplitude of the injecting current is commonly less than 100 $\mu A$ and normally the corresponding frequency for respiration monitoring is between 20–100 $kHz$ and this range can also be a bit larger [29].

The way IP measures the respiratory information is kind of straightforward and the respiratory information is reflected by the change of the impedance during the breath cycles. During the breath cycle, when people are breathing in and breathing out, the volume of the lung will change and this can result in a change of the path between the two receive electrodes and furthermore the variation of the electrical impedance [12]. Meanwhile, during the heartbeat, the change of the volume of blood could also result in the variation of the impedance which has a similar frequency as the heartbeat [30]. As a consequence, the two main components of the impedance change are caused by the respiratory activity and also cardiac activity. Usually, the amplitude of the change caused by cardiac activity in impedance is weaker than that resulted from the respiration which makes it possible to split these two components for most cases. However, as for the really fast and shallow respiration, the amplitudes of these two components from respiration and cardiac activity are of the same order and they may also have an overlapping frequency band so that the commonly used monitor may take the cardiac component as the respiratory information, resulting in a wrong RR estimate [5].

As for the placement of the electrodes for IP signal, it's concluded from on study that the most suitable configuration for long-term monitoring which could provide a signal of good quality is that the four electrodes are placed on intersections of right and left auxiliary mid-line at the fifth and seventh ribs, respectively [31].

It is also of great interest to measure more respiratory information like tidal volume from the IP signal. In some studies, it is found that the relationship between the IP and tidal volume is approximately linear [32], however, most of the studies are carried out when there are no motions of the subject, which means further validation is needed under more movements [33].

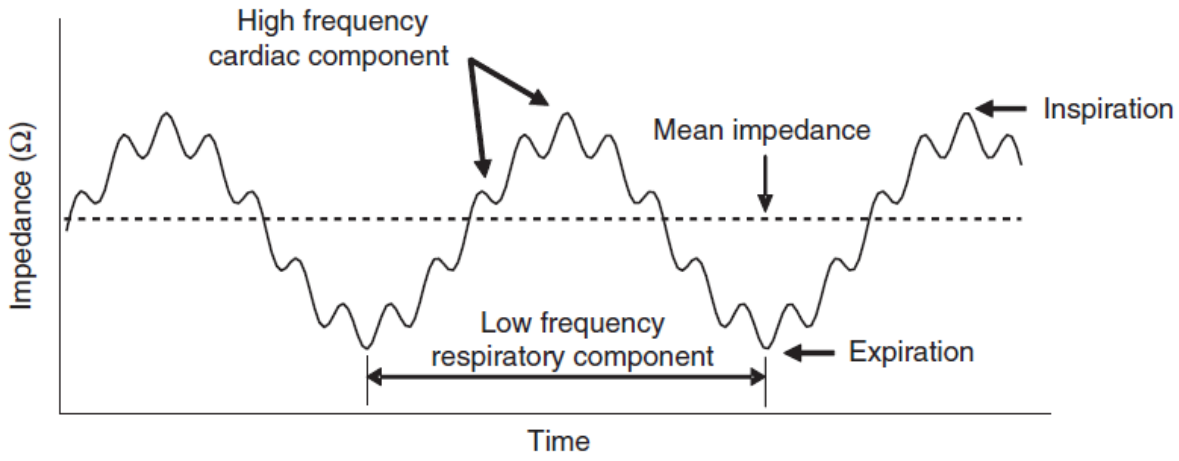


Figure 2.5: Simulated impedance waveform which is composed of two frequency component: the cardiac component with higher frequency and the respiratory component with lower frequency. The dotted line is the calculated mean impedance. Adapted from [5]

Figure 2.5 adapted from [5] shows the two main components of a different frequency band in the IP signal, where the cardiac component with a higher frequency is visible on the top of the respiratory component with lower frequency. Furthermore, from the frequency domain, the cardiac component normally has a frequency band of 0.8-3.0 $Hz$ while for the respiratory component is 0.1-0.7$Hz$ [34]. This frequency difference is the base for the extraction of each signal by filtering techniques. From this figure, we can also see the starts of the expiration and inspiration, which are the corresponding valley and peak points, respectively.

## 2.5. MATERIALS

In this section, we give a brief introduction to the databases on which this work is carried. The first two are the existing database from online public resource and imec. The last one is newly designed and the basic information of the protocol design is given. Finally, the information of all the volunteers are summarized.

### 2.5.1. DATABASES

The following databases are used for this thesis project:

- **Database 1**: This is an existing database from imec and this is used for evaluating the performance of the proposed respiratory signal quality (RQI) in section 4.2.2. The following signals are recorded: reference signal as a gold standard signal collected by the spirometer, ECG, IP and three-axis accelerometer recordings. In this database, the volunteers are required to lie on the bed to breathe following certain respiration patterns, e.g. breathing at different rates and also holding the breath for some time to simulate a period of apnoea.
- **Database 2**: This is an existing database from an online public resource, namely Physionet [18]. The clean ECG as well as three realistic noises, including muscle noise, motion noise and baseline wandering, are recording from 20 subjects in a clinical environment. This database is used for evaluating the performance of the proposed signal quality indicator for ECG signal in section 4.2.2.
- **Database 3**: This is a newly designed database for this thesis project and it is used to evaluate the performance of the proposed framework on respiratory rate monitoring. The following signals are recorded: one reference signal as a gold standard signal collected by the spirometer, three more desired signals,

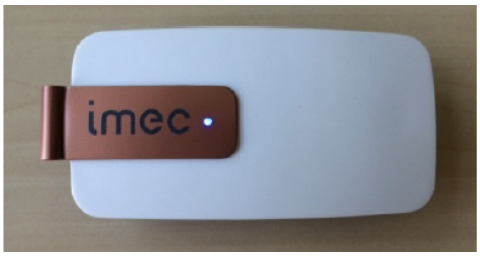


(a) Robin platform


(b) sprirometer from Biopac company

Figure 2.6: The data collection devices

the first two, ECG and IP for respiration monitoring and the last one as a reference signal, three-axis accelerometer recordings, for the investigation of motion artefacts attenuation.

### 2.5.2. MEASUREMENT EQUIPMENT AND SIGNALS OF DATABASE 3

in this database, four different signals were acquired in measurements: ECG, IP, acceleration recordings (ACC) and breath volume recording from the spirometer. The first three are measured using a wearable platform from imec named Robin device, which has a connector measuring the ECG and IP simultaneously as well as ACC recording in three axis collected by the accelerometer embedded inside the device. The breath volume is measured by the spirometer from Biopac, which is composed of a data acquisition model together with a transducer. The corresponding devices are shown in Figure 2.6.
In more detail, the collected signals and sampling frequencies used during data acquisition were:

- **ECG**: This is sampled at **512 Hz**, which utilizes three electrodes in single lead placed on the upper left, lower right of the body and right above the belly button. The position of the electrodes is slightly different among the volunteers due to many electrodes attached to the body.
- **IP**: This is collected by the Robin device using the same electrodes as ECG with a sampling rate of **1024 Hz**.
- **acceleration(Acc) recordings**: This is collected by the accelerometer embedded in the Robin device in three axes at a sampling rate of **32 Hz**.
- **spirometer recordings**: This is the measurement of the volume of the breath cycle, which can be taken as a reference signals for extracting the true RR from comparison purpose. It is sampled at **100 Hz**.

As for the lead of the ECG used in this database, it is selected as lead II since from the literature this could provide the most visible $QRS$ complex. For the IP signal, one lead is also learned from literature introduced above which gives the most waveform of good quality, where the electrodes are placed on the high midaxillary line and close to the nipples. The data acquisition device is also attached in the middle of the chest to record the accelerations in three axes with a rate of $32 Hz$. The electrodes positions are shown in Figure 2.7.

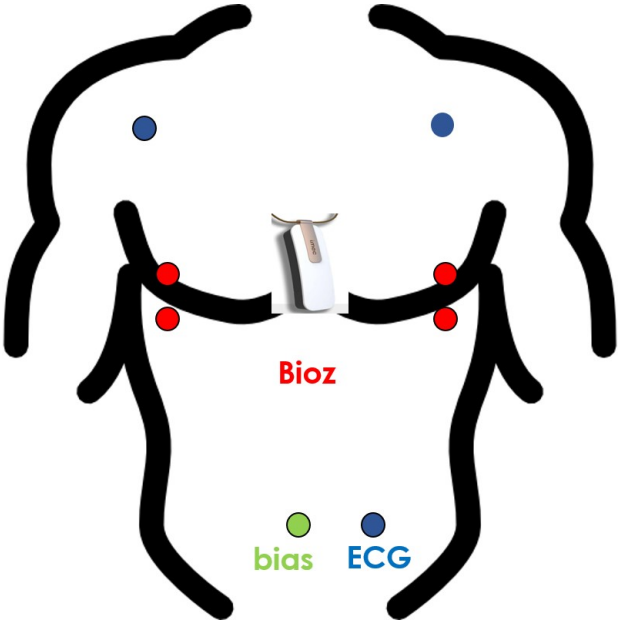


Figure 2.7: The positions of the electrodes of the corresponding signals are presented: IP(red), ECG(blue) and the Robin device.

### 2.5.3. PROTOCOL DESIGN

This measurement protocol is created to present the typical daily activities in the general home environment. The protocol includes five sections, lying on the bed, sitting on the chair, standing, running and free breath. For each section, there are varying amounts of stages of the periodical or random movement. The combined length of all the section is approximately 45 minutes. Between each section and the stage, there will be a period long enough (e.g. 1 min) for leading the volunteer to the next one. In the beginning of each section of this protocol, a deep breathing in followed by a breath hold for 7 seconds is set to synchronize different recorded signals.
Full protocol details for the measurements can be found in Appendix A.1. Each section in the protocol was categorized into one of the five activity categories. For the running section, this is carried out on the treadmill at different speed. In each section, these categories and their total target duration in the protocol are:

- **Lying** (5 min) lying on the with both periodical and random movement.
- **Sitting** (4 min) sitting on the chair with typical daily movement.
- **Standing** (4 min) standing with random movement.
- **Running** (10 min) On the treadmill, subjects are required to start walking jogging to running at different speed.
- **Free breath** (5 min) On the chair the subjects are required to breathe freely and this data is used as a learning period for optimizing the parameters for algorithms.

### 2.5.4. VOLUNTEER DEMOGRAPHICS

Totally 12 volunteers are involved in the data acquisition. We give a brief introduction to all the volunteers in the following table.

| items / value | Age(year) | Weight(Kg) | Height(cm) |
|---|---|---|---|
| **Range** | 24 - 28 | 55 - 87 | 172 - 188 |
| **Average** | 25.4 | 69 | 177.8 |

Table 2.1: The information of the volunteers involved in data collection for **database 3**

# 3

# LITERATURE OVERVIEW OF SIGNAL PROCESSING METHODS FOR RESPIRATORY SIGNALS

This section gives an overall introduction to signal processing techniques used in various studies as a literature overview. The base signals of interest are mainly ECG and IP since these two signals are the ones used in the framework chapter 4 of this thesis.
In most cases, the respiratory components are visible from the ECG and IP signals, however, the raw signals of both two are not of good enough signal quality to achieve an automatic estimation for respiratory rate due to noise components like motion artefact and system noise [23]. Before estimating the respiratory information, preprocessing for both IP and ECG signals are needed and the raw signals must be filtered or processed by certain techniques to make sure that the signal is good enough to extract accurate respiratory rate. Briefly, signal processing framework for estimating the respiratory rate is composed of four stages [12]:

- **Respiratory signal extraction** Extract the respiratory signals from the base signals based on the modulations of respiration on the underlying signals.
- **Noise reduction on the signals** Attenuate the noises buried in the signals based on basic filtering or more advanced methods, for example, adaptive filtering with the help of the reference signal correlated to the true signal or the noise.
- **RR estimation** Estimate the RR from the processed signals either based on **time-domain** techniques, normally detecting the peaks and valleys or **frequency-domain** techniques.
- **Information fusion** Fuse the RR estimate from different signals based on certain methods.

In this thesis, the respiratory signals are extracted from the IP and ECG signals. The noise reduction part is optional and an overview of all these four stages in the framework is given in the following sections.

## 3.1. RESPIRATORY SIGNAL EXTRACTION

### 3.1.1. ECG-DERIVED RESPIRATORY SIGNAL

As is described in chapter 2, it is known that the modulations of respiration on ECG can be divided into three categories: Amplitude modulation (AM), Frequency modulation (FM) and Baseline wandering (BM) and corresponding techniques for extracting each modulation may also be different.
Generally, the techniques for extracting the EDR signals can be divided into two categories: **feature-based** and **filter-based based** techniques [10]. Working in a more direct way, filter-based techniques are implemented to eliminate the frequency content outside of the range of normal respiratory frequencies by band-pass filtering. In most studies, simple band-pass filtering is utilized to get the EDR signals[35]. However, the filter-based techniques have more limitations due to the sensitivity to noise compared with feature-based technique [35]. In this thesis, more efforts are put into the feature-based techniques.

#### FEATURE-BASED TECHNIQUES

Feature-based techniques work in a way of extracting the features of beat-by-beat related to respiratory activity and typically work in the time domain [10]. A set of filtering methods are used to eliminate both low and high-frequency noise and also the main interference frequency component from the device at 50 $Hz$. Furthermore, QRS detector methods are used to detect the QRS waveform of the ECG. More details of QRS detection methods can be found in [36]. Normally, $R$ peaks in the QRS waveform are detected by the detectors and the corresponding $Q$ and $S$ valleys detected as the minimas with a certain window of length 0.2s centred at the R peaks[37]. Furthermore, after detecting all the QRS complex waveform, the EDR signals can be extracted with the help of all the QRS points and the discrete series of the EDR signals are further resampled at a constant frequency based on linear cubic interpolation since subsequent processing required to obtain an evenly sampled EDR. Finally, the resampled EDR signals will also be passing through a band-pass filter to remove the frequency components outside of the range of normal respiratory frequencies.
For **FM-based** techniques, EDR signal based on $RSA$ is the most commonly used method since many studies about $HRV$ have been published and documented [12]. As a consequence, the way to extract the $EDR_{RSA}$ is based on QRS detection and after we get the R-R intervals, a cubic spline interpolation at a constant sampling frequency is further used to generate a continuous respiratory signal. In a relevant study, the $EDR_{RSA}$ signal is filtered with fourth-order Butterworth band-pass filter with a passband of 0.1–0.6 Hz (6–36 bpm) frequency band. This frequency band is only related to normal respiratory rates and ensured that cardiac frequency components are removed from the respiratory signals [38].
As for **AM-based** techniques, this is based on the amplitude modulation on the $QRS$ complex of respiration on the ECG. The first study about this is described in[13]. In this study, two calculated $QRS$ area changes from two orthogonal leads are used to follow the change of the heart electrical axis angle. This angle is calculated at every $QRS$ complex and all the discrete values of this angle are further interpolated by cubic splines and an evenly sampled respiratory signal is generated, denoted as $EDR_{area}$. In some studies, the $QRS$ area calculated from single-lead ECG is utilized to obtain the respiratory signal for simplicity and the area is taken from some part of the ECG signal within a fixed window with a length of 100 ms, of which the center is at R peak of the QRS complex [9]. A high correlation between the estimate from the $EDR_{area}$ and from the reference signal is also found in this study.
A simpler way to derive the respiratory signal compared with the area-based method can be based on the amplitude of the QRS complex[39], denoted as $EDR_{amp}$. After detecting all the R peaks in the ECG signal, the $EDR_{amp}$ respiratory series is taken as the amplitude of successive $R$ peaks with respect to the baseline level of ECG. Two median filters, 200$ms$ and 600$ms$, are used to remove $QRS$ complexes, $P$ waves and $T$ wave from the ECG signal, respectively. The output of these tow median filters is the baseline. Meanwhile, the $EDR_{amp}$ can be extracted by taking the amplitude difference between $R$ peak and $S$ trough in the ECG and the $S$ trough is the minima found within 0.1 seconds after $R$ peak, for each QRS complex[39].
There are also some other novel ways to derive the EDR signals from literature. One study a new method is presented and it is measuring the changes of $QRS$ slopes and R-wave angle during the breath cycles [6] to generate the EDR series. An example of QRS angle is shown in Figure 3.1. There are two steps to derive the QRS angle. Firstly, for each QRS complex, line fitting methods are used to measure both upward and downward slope of the $R$ wave. After that, the smallest angle generated by these two lines are obtained, which is

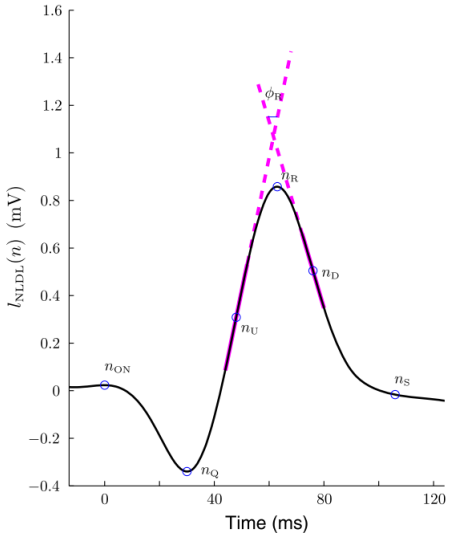


Figure 3.1: An example of The QRS slope and R-wave angle. The two thick magenta lines are the best fitting curve of the the QRS slopes in a sense of least square and the QRS angle can be derived from them. Adapted from [6]

taken as the R wave slope respiratory signal.
All the mentioned methods to extract the EDR signals are summarized in the following table 3.1 adapted and then modified from [3] and the general block diagram is also shown in Figure 3.2.

| Methods | Technique |
|---|---|
| | Featured-based |
| $EDR_{RSA}$ | **FM:** R-R peak intervals from the ECG QRS complex waveform [40] |
| $EDR_{Ramp}, EDR_{Rsamp}$ | **AM:** Amplitude of the R peaks respect to the baseline; Amplitude difference between the R peak ans S valley [39] |
| $EDR_{bw}$ | mean signal values between consecutive troughs.[3] |
| $ESR_{area}$ | The area of the QRS complex after removing the baseline wandering by the subtraction of interpolation between Q and S valleys. [9] |
| | Novel methods |
| $EDR_{PCA}$ | Pricinple component analysis on QRS complex and the eigenvecotr corresponding to the first PC is taken as EDR signal.[41] |
| $EDR_{slope}$ | The variation of the R angle in the ECG QRS complex waveform [6] |

Table 3.1: Techniques for extracting EDR signals. Adapted and modified from [9]

### 3.1.2. IMPEDANCE PNEUMOGRAPHY

As for the IP signals, the processing methods are more straightforward as the IP signal itself already represents the pattern of respiration. In some studies, It has been shown that the main component of the impedance signal is highly correlated to respiration [42].
Normally, the steps for reprocessing the IP signal include a high-pass and low-pass filtering to remove the frequency band which is not representing the respiratory activities [12]. The low-pass filtering is used to

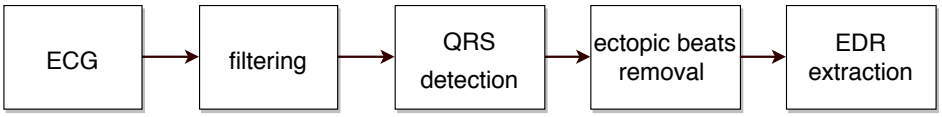


Figure 3.2: The general block diagram for EDR extraction in literature

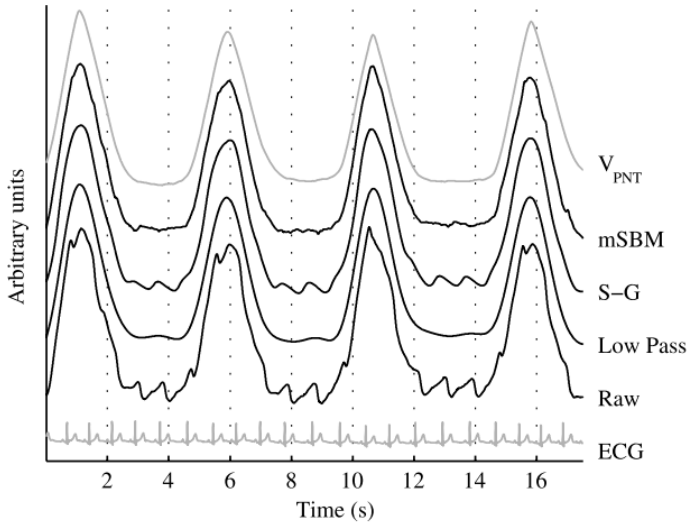


Figure 3.3: Example of all different filtering methods on the IP signal to remove the cardiac artefact. $V_{PNT}$ is the lung volume signal as a golden reference. The raw IP signal has cardiac component right following all the R peaks of the corresponding ECG. $S-G$ and $mSBM$ are the output from the Savitzky– Golay smoothing method and modified Schuessler–Bates methods, respectively. Adapted from [7]

remove the cardiac oscillations as well as with the instrumentation noise (like quantization noise) higher than true respiratory rate, e.g., with a 1.5 Hz (90 bpm) cut-off frequency. As there is also commonly baseline wandering in the IP signal, the high-pass filtering is used to eliminate this kind of low-frequency noise to make IP signal of good enough quality for further processing.
Some studies investigate the methods for suppressing cardiogenic oscillations in impedance pneumography and as shown in Figure 3.3, the cardiac oscillations can also be present in the IP signal if we look at the raw IP signal together with the ECG signal.
Normally, the cardiac oscillation can be filtered out using a low-pass filtering set at a proper cut-off frequency. More advanced technologies are investigated in some studies. One technique described in [7] is using the R peaks in ECG to obtain the cardiac oscillations from the IP signal. More details can be found in [7]. The methods show great attenuation on the cardiac artefact in the IP signal with little distortion to it. However, from their study, the low-pass filtering method has almost the same performance in removing the cardiac artefact as the more advanced one since they also preserve the peaks of the respiratory signals at almost the same timing. A set of example signals flitted by various the techniques in this study is shown in Figure 3.3. As a consequence, simple low-pass filtering is enough to get the respiratory signal from IP of good quality.

## 3.2. MOTION ARTEFACT, NOISE REDUCTION AND SIGNAL QUALITY

In this section, we describe the nature of the motion artefact and introduce typical techniques for attenuating the noise.
Motion artefacts are considered as the most troublesome limitation to respiration monitoring methods [15]. A data example is shown in Figure 3.4, from stage d in section one from the **database 3** in Chapter 2, where

the volunteers are required to move randomly on the bed. Within the red square, the signal is distorted by the artefacts which make it difficult to derive correct respiratory information from it. The Acc recordings on the right side show that the subject was moving randomly.
From many studies, motion artefact reduction is related to the design of the electrodes and it has been proven that the motion artefact could be attenuated in a certain extent by increasing the contact area between the electrodes and human skin[43]. Furthermore, signal processing methods could also be used to eliminate the artefact present in the signal during the post-processing[44]. However, due to the fact that the MA and true bio-medical signals could have an overlapping frequency band, which makes it impossible to split them by simple filterings, like band-pass filtering [15]. Thus, many studies investigate the feasibility of removing MA from the underlying signals to provide a more robust and accurate respiration monitoring.
One typical technique suitable for noise reduction is adaptive filtering [45]. The principle of this technique

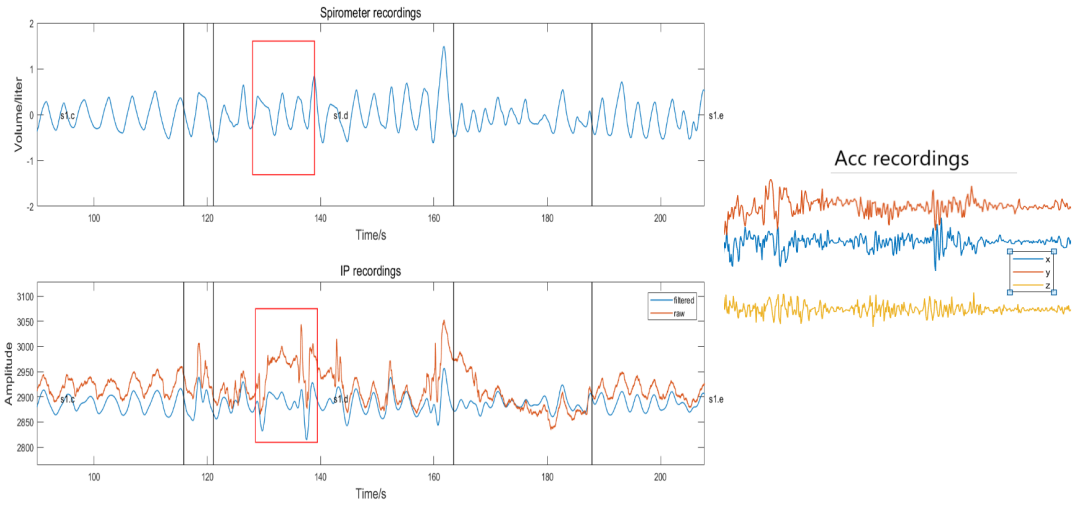


Figure 3.4: Example of IP signal distorted by motion artifacts and the corresponding spirometer recordings and Acc recordings

is shown in 3.5. The observation signal $X(n)$ is consisted of both the true signal $S(n)$ and the noise $N_0(n)$. under the condition that the reference signal $N_1(n)$ correlates well with the noise or the true signal in the observation signal $X(n)$, the adaptive filters is capable to tracking the change of the noise or true signal and finally generate an optimal estimate of the noise $N_0(n)$ as $\hat{N}_0(n)$, in statistical sense. As a consequence, the true signal can be further obtained and of good enough quality for further processing [46].
One performance study of various adaptive filter algorithm for noise reduction in respiratory signals was

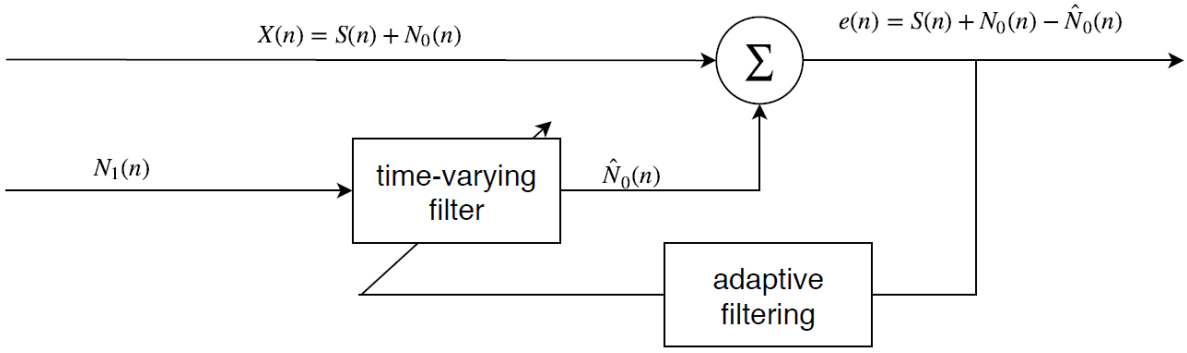


Figure 3.5: Adaptive filtering

carried out in [47]. In this study, the true respiratory signal has been corrupted by synthetic noises and six different adaptive filtering methods are used to remove the noises. It is concluded with the help of a proper reference signal, all the adaptive filtering have good performance on attenuating the noise in the signals and

there will be always a trade-off between step sizes and the convergence rate.
In practice, one typical problem for adaptive filtering techniques is how to find a proper reference signal. It has been found in a lot of studies, the triaxial accelerometer recordings are commonly used as a reference signal indicating the motion artefact and it is fed into the adaptive filter to generate an estimate of the motion artefact. In [48], three axial outputs of the Acc are used as the input reference signal to estimate the motion artefact in the ECG and IP signals with the help of gradient adaptive Laguerre lattice (GALL) filter, then all the three outputs are further fused by a Kalman filter to generate the final motion estimate. It has been concluded that the MA in the ECG signal could not be attenuated greatly by this proposed method while for the respiratory signals, it has a good performance on attenuating the noise. One possible reason stated in [48] for this from this study is that MA on ECG waveform is that the artefacts in the ECG signal are mostly the variations of potential between the electrodes by the relative sliding between the electrodes and the skin, while the measured Acc signals are actually capturing the absolute physical movement. Thus, Acc signal and motion artefact is actually two different signals generated from two different mechanisms. For the transthoracic inductance (TI) signal, it is found that Acc signals are correlated well with the motion artefact in TI signal since MA in the TI signal is generated by the mechanical movement which can be captured by Acc signal. From this studies, it can be concluded for adaptive filtering technique, a proper reference signal correlated well to the noise is essential for the noise attenuation.
Since noise attenuation is difficult and still underway, some studies recommended that signal quality indicator should be assigned to the underlying signals to indicate the reliability of the respiratory information estimated from them. A few relevant papers have described their own signal quality indices. For example in [49], a signal quality indicator(SQI) is created which measures the regularity of the peaks, which is believed to be capable to indicate the true respiratory activities. This SQI value is then scaled to be between 0–1 in a nonlinearly way. It is concluded that this SQI value could help to fuse RR from two EDR signals to achieve a lower error compared with the RR from only one EDR. compared with the SQI proposed for ECG mentioned above, which is relatively straight-forward, one study proposes respiratory quality indices (RQIs) that indicates the quality of the respiratory signals extracted from ECG and PPG signals in [50]. Specifically, RQI is used to detect the presence of the respiratory modulations on the underlying bio-medical signals. Four different RQIs measuring different features of the respiratory signals are derived. It is concluded that the proposed RQI-based method in this study could provide a more robust and accurate RR estimate.

## 3.3. RESPIRATORY RATE ESTIMATE

Although the IP and EDR signals seem to be sinusoidal waveforms in some cases, it is still difficult to estimate the RR automatically from the raw signals [23].
In some early studies[3], the researchers try to get the RR from the respiratory signals through visual inspection by identifying the peaks and troughs which truly reflect the respiratory activities. However, the results of this human annotation are not reproducible. Furthermore, some studies investigate the feasibility of estimating the respiratory activities automatically based on some algorithms, which can be mainly divided into frequency-based methods and time-domain methods [10] .
Generally, the time-domain methods could provide more robust and accurate RR estimate compared with frequency-domain methods because time-domain techniques are based on the peak detection which does not require that the underlying respiratory signal needs to be quasi-stationary, which is required for frequency-domain techniques[10]. Therefore, more focus remains on time-domain methods. Results from different methods are also briefly presented. However, due to the reason that the various data acquisition and evaluation metrics from different studies, for example, some studies have the protocols which collect data from less intensive movement if compared with other studies, it's extremely difficult to compare the results from different studies.

### 3.3.1. TIME DOMAIN TECHNIQUE

Typically, for a respiratory signal of ideal quality, it will be very similar to a pure sine wave such that the simplest way for breath detection in time-domain is to detect the peaks and valleys and take them as the beginning and end of the breath cycle. However, the signals are often distorted by motion artefact and noise which makes the simple detection method not work well [12]. Normally, motion artefact and noise could result in random fluctuations on the top of the clean signal, which make it possible to remove those ripples by setting a proper threshold to the detected peaks and valleys [8]. However, it is hard to determine a constant distinct value as the threshold for all the situations. Many studies are trying to determine the threshold in an adaptive way.
An adaptive threshold algorithm is investigated in [8] and a threshold is determined as 0.2 times the $75-th$ percentile of all the detected peaks and any peaks of which the corresponding amplitude is below this threshold will be not taken as real respiratory activities and then removed. One additional criterion is also given: for every breath, there must be exactly one minimum below zero. After removing the wrongly detected peaks and valleys, the RR estimate can be calculated by the following equation:

$$RR_{inst} = \frac{60}{\Delta t} \tag{3.1}$$

Where $\Delta t$ is the time interval (in seconds) between consecutive peaks that satisfy the requirements. The resulting RR is in a unit of breath per minute (bpm). This method was first described in [51], denoted as "$Count-orig$" ((refer to "$Count-orig$" method in Figure 3.6). In this study, it had provided better results than spectral calculation based methods since either the RR estimated from the Fast Fourier Transform (FFT)-based method or autoregressive modelling-based method provides a low correlation below 0.2 with the reference RR and the new algorithm has a much higher correlation value as 0.87.
A modified version of the "$Count-orig$" is raised in [8], denoted as "$Count-adv$" ((refer to "Count-adv" method in Figure 3.6). The threshold is determined with the help of a third quartile of the amplitude differences between consecutive extrema pairs (peaks and valleys) instead of maxima. If the amplitude difference of the corresponding pair of extrema is below this threshold, they are considered as the random fluctuations due to the artefact which is not representing the true respiratory activities. After removing the random fluctuations, the RR is calculated by equation 3.1.

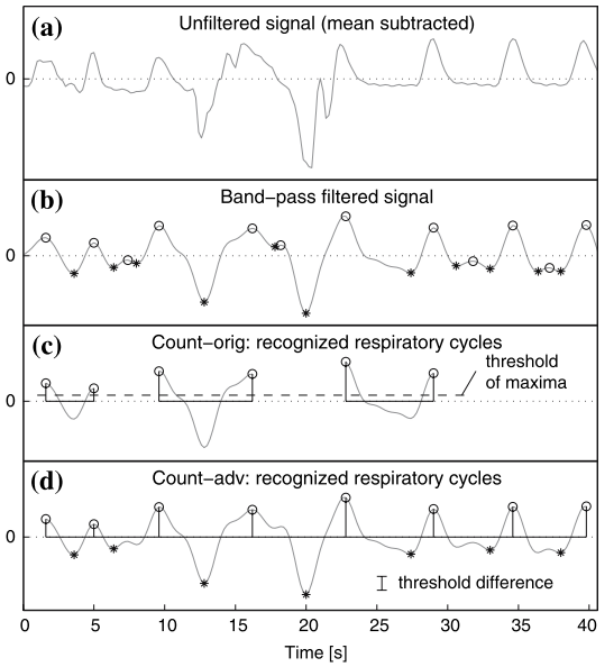


Figure 3.6: Illustration of the two time-domain RR estimation methods, c) and d). Steps a) and b) are preprocessing steps. Adapted from [8].

### 3.3.2. FREQUENCY DOMAIN TECHNIQUE

Frequency analysis of the respiratory signal is much simpler compared with time-domain methods. The normal way to estimate the RR is to transform the respiratory signal into the frequency domain and then look for the dominant component representing the respiratory activities [10]. In many studies, two commonly used spectrum estimation methods are Fast Fourier Transform (FFT) and Auto-regressive (AR) modelling.
In [52], the FFT is applied to three EDR signals from the ECG signal using a 30-second sliding window with an overlapping of 6 seconds. It is found that correlation coefficients are approximately 0.90 between the developed methods and reference respiratory signals. The data are collected from 24 subjects who were under a full standard sleep test.
Auto-regressive (AR) modelling is a linear predictive modelling technique which is capable to predict the output variable (RR) with the help of a certain amount of the past signal and this method could improve the frequency resolution compared with the FFT method [12]. A key factor for the AR model is the selection of the order and it determines how many previous samples we use to predict the current value. For EDR methods, model orders between 5 and 7 were found to be best in [12]. In some other studies, in order to solve the problem of finding the optimal order for the AR model, the median spectrum for model orders 2–20 is calculated and the pole in the respiratory range with the highest magnitude pole is selected and the corresponding frequency is taken as the respiratory rate [53]. It is reported that the median spectrum method can provide a more accurate RR estimate compared with the method based only on one spectrum with a certain order.
All the methods in time-domain and frequency-domain are summarized in table 3.2 which are adapted and then modified from [10].

## 3.4. INFORMATION FUSION FOR RESPIRATORY SIGNALS

Information fusion is a more advanced way to fuse the information from a set of signals and provide a more correct output of the real-world phenomena. It has been reported from many studies that certain fusion methods could gain great improvement on some applications which could be found in [36].
Data fusion is the term used to describe the integration and combination of information. In RR sense, data fusion can be used to fusion RR estimate from a set of biomedical signals (e.g. ECG and IP), or from the same source signal but based on different methods (e.g. various EDRs from the same ECG ). The stages where data fusion is taking place in the signal processing path can be categorized into three processing levels [12]:

- **Data level**: The lowest level of data fusion. Raw signals from different sources are fused to obtain a better signal.
- **Feature level** In this level, features extracted from different sensor data are combined to make a fused feature. In this thesis, RR is considered as a feature of the respiratory signals.
- **Decision level** The highest level of data fusion. It can mainly be divided into two categories: the hard decision or soft decisions.

For the respiratory application, data level fusion is a troublesome task. It's not possible to fuse the data from different bio-medical signals. The reason for this is that the respiratory signals from different source signals may have different latency due the different response time of the underlying signal to represent the respiratory signals, which makes it difficult to fusion the data in the lowest level. Thus, this thesis will focus on feature level fusion. The following subsections will give an overview of different fusion methods used in various respiratory rate estimation studies. As a summary, most studies conclude that the fusion methods could provide a better result but often the improvements are kind of minor for certain situations.

#### SMART FUSION

In [36], a smart fusion is for RR estimation proposed. The idea is that RR estimates from BW, AM and FM-based EDR respiratory signals will be further corrected by the quality assessment. If the standard deviation

| Methods | Description |
|---|---|
| | Time-domain methods |
| $T_1$ | detect the breath cycle with the help of the detected peaks and valleys [54] |
| $T_2$ | Detect the breath cycle by combining peak and trough detection with thresholds both in time and amplitude [55]: remove all the peaks less than the mean as well as the valleys greater than the mean; remove all the peaks or valleys within a window of 0.5s centred at the previous peaks or valleys |
| $T_3$ | Detect the breath cycles using 'Count-orig' method. [8]. |
| $T_4$ | Detect the breath cycles using $Count-adv$ [8]. |
| | Frequency-domian methods |
| $F_1$ | Spectral analysis of the respiratory signal by Fast Fourier transform [36]. |
| $F_2$ | Spectral analysis of the respiratory signal by Welch periodogram [36] |
| $F_3$ | Spectral analysis of the respiratory signal by the Auto-regressive method with a model order of 8 [53]. |
| $F_4$ | The Auto-regressive all-pole modelling method is used for the spectral analysis of the respiratory signal with the model order of 8 and the pole with the highest amplitude is selected which indicates the true respiratory activity [56]. |

Table 3.2: Methods for respiratory rate estimation. Adapted and then modified from [10]

of the RR estimates from all the EDR signal is less than 4 bpm and the mean of the individual RR estimates is calculated and further taken as the final RR estimate, otherwise, the RRs from all EDR signals are not reliable and no RR is output. It is concluded the Smart Fusion can remove the wrongly detected RR estimate and thus produce a better result.

### FREQUENCY DOMAIN FUSION

In [57], the data fusion is based on the RR estimated by frequency-domain methods. The frequency spectrum of BW, AM and FM respiratory signals are calculated based on the Welch periodogram and then a mean spectrum is obtained. One additional criterion for the spectrum is that the underlying signal must have a certain power of the frequency component in the predefined respiratory range, otherwise, it's removed from the fusion step to get the mean spectrum. Finally, the RR estimate for the corresponding signal frame is taken as the frequency component which has the maximum power in the estimated mean spectrum. under the best combination of the underlying signals for data fusion, this method was reported to obtain an error of $-2.16 \pm 12.69$ mHz, equivalent to $-0.13 \pm 0.77$ bpm, on respiratory rate.

### KALMAN FILTER

After obtaining the noisy RR estimates by the breath detection methods from the underlying respiratory signals, more advanced techniques can be used to estimate the true state of this dynamic system. A typical technique for solving this problem is Kalman filter (KF) [58].
The Kalman filter is the optimal estimator in the statistical sense since it can minimize the mean square error of a state when there is uncertainty present in the state in the form of Gaussian noise [12].
The state and the observation at a discrete time can be formed in the following equations:

$$x_{k+1} = A_k x_k + w_k \tag{3.2}$$
$$z_k = H_k x_k + v_k \tag{3.3}$$

where $x$ is the state and $y$ is the observation. $w_k$ and $v_k$ are state and measurement noises respectively and these two noises are assumed to be independent and obey normally probability $w_k \sim N(0, Q_k)$ and $v_k \sim N(0, R_k)$, where $Q_k$ is noise covariance of the state while $R_k$ is the covariance of the measurement. $A_k$ is physical model matrix for the state and $H_k$ is the measurement matrix for the observation.
The pricinple of Kalman filter is that it gives an optimal estimate of the current state based on the help of prior knowledge of physical model as well as the information of the current observation. Normally, KF has two distinct steps: **"Predict"** and **"Update"** [12].

- **Predict** In this step, the KF provide a state estimate for the current time index based on the estimate from previous time frame.(for a more detailed derivation of these equations, refer to [12]).

  $$\hat{x}_{K|k-1} = A_{k-1} x_{k-1} \tag{3.4}$$
  $$\hat{P}_{k|k-1} = A_{k-1} P_{k-1|k-1} A_{k-1}^T + Q_{k-1} \tag{3.5}$$

  where the $\hat{x}_{K|k-1}$ is the state estimate for current time $k$ based on the state from time $k-1$ as well as the prior physical model. $P_k$ is the error covariance matrix at time k.

- **Update** In this step, with the obtained new observation for the current time index, a posteriori estimate is derived based on the following equations:

  $$r_k = y_k - H_k \hat{x}_{k|k-1} \tag{3.6}$$
  $$S_k = H_k \hat{P}_{k|k-1} H_k^T + R_k \tag{3.7}$$
  $$K_k = \hat{P}_{k|k-1} H_k^T S_k^{-1} \tag{3.8}$$
  $$\hat{x}_{k|k} = \hat{x}_{k|k-1} + K_k r_k \tag{3.9}$$
  $$P_{k|k} = \hat{P}_{k|k-1} - K_k S_k K_k^T \tag{3.10}$$

where the $r_k$ is the residual innovation, the difference between the state prediction and the observation. The innovation is often the only measure available in the Kalman filter to indicate the performance of the estimator [12]. $S_k$ is the innovation covariance and $K_k$ is the kalman gain. The recursions of the Kalman fitler need to be initialized with a predefined estimates of $\hat{x}_{(0|0)}$ and $P_{0|0}$.
for the application of respiratory rate estimation, the KF was first taken in [12]. The Kalman filter is used to track the true RR estimated from a set of respiratory signals. Based on the assumption that the respiratory rate is approximately constant only with minor changes between two measurements and the predicted state is set as the same value previous one ( $A_k$ is set to 1), thus the corresponding equations are simplified and the state transition equation in 3.4 is switched into scalar. The researchers used KF to smooth the RR estimates from $IP$, $EDR_{RSA}$ and $EDRR_{Ramp}$. The process noise $w$ is set based on the variation on the true RR. As a consequence, the dynamic model is set as follows:

$$x_{k+1} = x_k + w_k \tag{3.11}$$

Meanwhile, $H_k$ is set to one since the measurement is directly set from the state. The measurement model is then formed as follows togehter with the observation noise $v_k$:

$$y_k = x_k + v_k \tag{3.12}$$

Normally, the covariances $Q_k$ and $R_k$ for the noise term $w_k$ and $v_k$ are rather difficult to estimate. In this study [12], the $Q_k$ is set to 2 as a reasonable value for a good track of the RR variability for the consecutive breath cycles. As a consequence, the measurement noise $R_k$ is even more difficult to estimate since it the measurement noise varies from the configurations of the different source signals from which the respiratory signals are derived. To simplify this, scalar values $R_k$ are set differently for each individual measurement method ( ECG and IP), ranging between 18–38 (standard deviation 4-6 bpm). Process covariance $P_k$ was set ten times $Q_k$ and the state $x_{0|0}$ is initialized by taking the average RR from all the underlying respiratory signals. The KF works as a smoothing filter to smooth the RR estimate from the individual signal and it's reported that the Kalman filter could give more correct RR estimates which has a higher correlation value with the reference signal compared with the instinct RR estimate without filtering.
In the same study [12], an alternative method for fusing the RR estimate is also proposed. the KF innovation residual $r_k$ from Equation 3.6 works as an indicator for the reliability of the RR estimate. In KF filtering the difference between the value of the true state and the value of the prediction should be zero-mean and white, thus the variance of the state can be taken as the square of the residual.

$$\sigma_k^2 = r_k^2 \tag{3.13}$$

The fusion idea is that if based on the variance$\sigma_{k,s}^2$ for each respiratory signal $s$ at time $k$, working as the confidence of the RR estimate $RR_{inst}$, a fusion method can be combining RR estimates from each signal using the inverse proportion of each signal's variance since this linear combination minimizes the mean square error [12]. The fusion formula is as following:

$$\hat{z}_0 = \sum_{n=1}^{n} \alpha_p \hat{z}_p \tag{3.14}$$

where a weighting parameter $\alpha_p$ is defined as:

$$\alpha_p = \frac{1}{\sigma_p^2 \sum_{i=1}^{n} \frac{1}{\sigma_i^2}} \tag{3.15}$$

For simplicity, the way to fuse RR from two measurements is as follows:

$$RR_k = \frac{\sigma_{k,2}^2}{\sigma_{k,2}^2 + \sigma_{k,1}^2} RR_{k,1}^{inst} + \frac{\sigma_{k,1}^2}{\sigma_{k,2}^2 + \sigma_{k,1}^2} RR_{k,2}^{inst} \tag{3.16}$$

The ideas behind this equation is that: if one measurement is under artefact, resulting in a larger error on the corresponding RR estimate, then the residual will be lager than the others, a smaller weight will be assigned to the corresponding RR estimate compared with others, which means the output from the fusion step will focus more on the RR estimate from signal of good quality. It is reported that that this innovation fusion methods could provide a more accurate RR estimate and a higher correlation value with the reference RR as

0.74. However, there are also some limitations of this method and this method does not give accurate results when all source measurements are noisy. The setting of this KF methods is summarized in the table 1.

**Algorithm 2** Summary of the KF algorithm in [12]

**procedure** KF FUSION — The procedure of KF in [12]

**Initialization** $b$ — Initialize the parameters

$$Q_k = 2 \quad R_k = [4,6]$$

$$P_k = 20 \quad x_{0|0} = \sum_{i=1}^{N} RR_{EDR_i} / N$$

**while** $i < N$ **do** — stop the loop when reach the last segment

Apply KF to $N$ respiratory signals and get $RR_{EDR_i}$ $i = 1,2...N$

Get the corresponding residual $\sigma_i^2$ of each $EDR_i$

Do information fusion based on equation 3.15 and get $RR_{fusion_i}$.

**end while**

**return** series $RR_{fusion_i}$ — The final series of RR estimates

**end procedure**

# 4

# DEVELOPMENT FRAMEWORK FOR RESPIRATORY RATE ESTIMATE

This chapter describes the framework that is developed in RR algorithm development. The final target is to create a respiratory rate estimate as accurate as possible in a way of information fusion based on IP and ECG signals. Respiratory rates estimated from spirometer are considered as the gold reference for the comparison against RR estimates from this framework. Furthermore, a set of evaluation coefficients from the related literature are also introduced to create reproducible procedures evaluating the performance of the proposed methods in a quantified way.

## 4.1. INTRODUCTION

The respiratory rate estimation framework in this thesis is much the same as what is introduced in chapter 3. Figure 4.1 gives flowchart of the framework.
In this thesis, the developed framework consists mainly of four parts as follows and each stage has already been labelled below the framework in Figure 4.1.

Step 1: RR estimates from each individual signal, IP and ECG, are optimized to be as accurate as possible based on the idea that the more accurate the individual method is, the better the fusion methods could work.

Step 2: Signal quality indicators(SQI) for each data segments are estimated to tell the data of good quality from the bad ones and also help to smooth the RR estimates since SQI could indicate the reliability of the RR estimates from underlying signals.

Step 3: Investigate the feasibility of attenuating the motion artefact with the available reference signal accelerometer (Acc) recordings.

Step 4: the methods based on information fusion to fuse RR estimates from all the underlying signal are also investigated and they are rather related to the signal quality indicator.

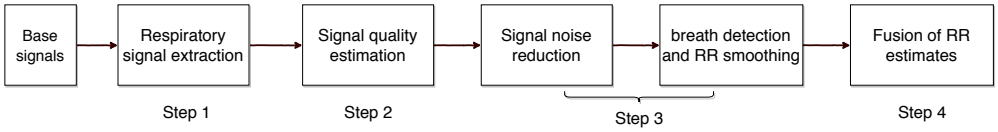


Figure 4.1: The flowchart of the RR estimation development framework.

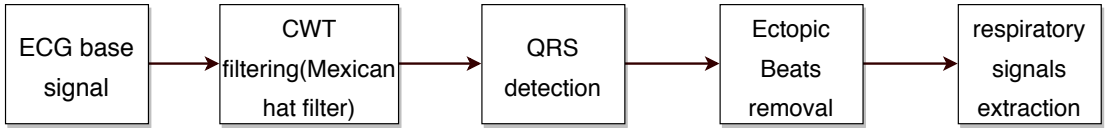


(a) flow chart of ECG preprecessing

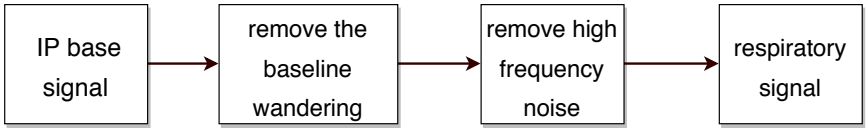


(b) flow chart of IP preprecessing

Figure 4.2: flow chart of base signals proprecessing

A development environment is built in Matlab and this environment uses a parametric approach where the processing methods for RR estimation can be created. Meanwhile, it was also capable to give visualizations of the developed framework, calculate performance evaluation metrics against the reference RR from a gold-standard signal, spirometer recordings.

## 4.2. ALGORITHM DEVELOPMENT

The following subsections give the principles used in the algorithm development under each method. First, we evaluate the RR detection performance of each individual EDR signals from the literature and then only the best performing individual methods were used in the fusion phase. We also introduce the innovations of the developed framework.

### 4.2.1. PRIMARY SIGNALS PREPROCESSING AND RESPIRATORY SIGNAL EXTRACTION

In this section, we introduce the selected methods for extracting the respiratory signals from the ECG and IP signals.

Figure 4.2a shows the flowchart of ECG processing. First, the ECG signals are filtered based on the continuous wavelet filter (CWT) method from imec [59], which helps to filter out the frequency band of no interest and also maximize the R peak in the ECG for a better peak detection. Then a peak detection algorithm is applied to the filtered ECG to detect all the R peaks.

In order to make the ECG processing framework more complete, modifications for detecting the $Q$,$S$ point and also the onset and end of the waveform, according to the study in [60], are done in this thesis due to the request from some techniques for extracting the EDRs, e.g. calculating the amplitude difference between $R$

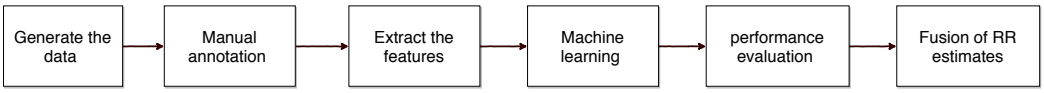


Figure 4.3: The block diagram of SQI evaluation for ECG

and $Q$ peak. Furthermore, after detecting all the $QRS$ waveform, the ectopic beats also needed to be removed as these ectopic beats could have abnormal morphology and R peak interval. Thus, the ectopic beats are removed based on the heartbeat timing signal in [61]. Finally, a set of EDR signals are extracted based on the detected QRS complex waveform.
All the $EDR$ methods used in this thesis are listed in table 3.1 except for the PCA-based method. All the EDR signals of discrete values from the ECG signal were transformed into evenly sampled waveform at a constant frequency of 8 Hz using interpolation based on the cubic spline.
As is shown in the Figure 4.2b, the IP signal is filtered using a 4th order Butterworth band-pass filter with a frequency band of $[0.1-0.8]Hz$ (6 and 48 bpm), which is helpful to remove the baseline wandering, low-frequency noise, and also the cardiogenic oscillations, high-frequency noise.

### 4.2.2. SIGNAL QUALITY AND RESPIRATION QUALITY ESTIMATE

In this section, we introduce the methods for evaluating the signal quality (SQI) for ECG signals from the aspect of mythologies and the respiratory signal quality (RQI) for IP and EDR signals for the aspect of how much respiratory information is present in the signals. Both these two quality indicator will be used for smoothing the RR estimate from underlying signals, as well as for data fusion. For the EDR signal, the overall signal quality (OSQI) is the product of the SQI and RQI. The **idea** is that EDR signal is derived from the ECG and normally it requires an accurate QRS detection and if the raw ECG signal is of low quality (troublesome for QRS waveform detection), the EDR signal should be less reliable even if the RQI is low, thus the corresponding RR estimate is of low trust. On the other hand, if the raw signal is of good quality but the corresponding RQI of EDR is low (the modulation of respiration on the ECG is not distinguishable enough), the RR estimated from the EDR should also be less reliable.

#### SQI FOR ECG SIGNAL

in this section, we introduce the way how we estimate the SQI for ECG signal for the aspect of morphology based on machine learning.
Many studies investigated the way to evaluate the signal quality of ECG signals and in [11], machine-learning based methods are applied in this thesis to classify the ECG of different quality into two categories: "Good" and "Poor" in terms of the reliability for diagnosis purpose. A set of features quantifying energy distribution in the spectrum, higher order moments in the statistical sense and inter-algorithm agreement are calculated and certain classifiers are used to give the final classification based on these features.
With the help of the study [11], a completely automated algorithm to derive the SQI is proposed. The algorithm is based on signal quality metrics which are published previously and some new ones are proposed to estimate the signal quality of ECG for the purpose of providing a better EDR signal. The block diagram for the methods is shown in Figure 4.3.
The **database 3** introduced in Chapter 2 is used for the investigation of SQI for ECG. Totally 10 recordings of clean ECG from 10 subjects together with realistic noise from the same people are utilized to generate the dataset. The realistic noise includes **motion artifact (em)** and **muscle noise (ma)**. It is well-known that in the machine-learning area, the imbalanced classes, which means one class outnumbers all the other classes much, is not good for establishing good classifiers as it causes bias during the design and results in a poor performance with a bad generalization ability [11]. Therefore, to generate a balanced dataset, for the ECG recording of each subject, we add the noise on the top of the clean ECG in an alternating way: for the first 2-min clean ECG segment, a randomly chosen segment with a length of 2 minutes from either em or ma real-

istic noise record was firstly calibrated based on a certain value of signal to noise ratio (SNR) and then added on the top of clean ECG signal with the same length of 2 minutes and then for the next 2min segment in the ECG recording, it keeps clean and no noise is added. The noise was added so that the SNR was equal to a certain value and the data is generated under a range of SNR $[0, 6, 12, -6]dB$, which results in ECG signals distorted by noise of descending intensity.
As for calibrating the noise and ECG signal power based on the SNR, as is suggested in [18], the ability of typical QRS peak detectors to localize the QRS is related to the size of QRS complex. As a consequence, the calculation of the ECG power will be mainly based on the power of QRS complex and the methods for calculating the power of the clean ECG and noises are summarized in Figure 4.3. In order to calculate the power of the QRS complex, firstly all the R peaks are detected and peak-to-peak amplitudes of all the points within the window with a length of 100ms centred at R peak are recorded. Then a trimmed mean of all the amplitudes, after removing a certain amount of the data with relatively low and high values. This mean value is the ECG signal power. As for the calculation of the power of noise $P_v$, it's similar to the calculating of the power of the ECG signal but the root mean squared difference is calculated instead of the peak-to-peak amplitude.
A data example under SNR equal to -6dB is shown in Figure4.5. The $SNR$, $S$, was controlled and the value is

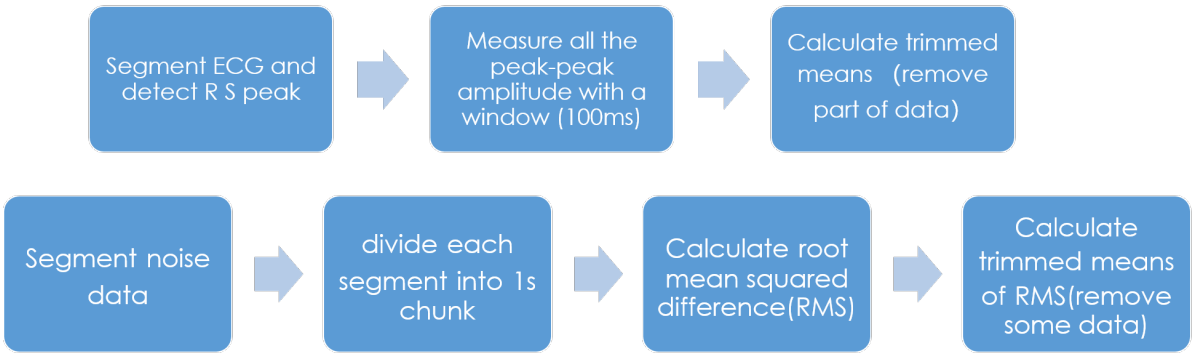


Figure 4.4: The block diagram of calculating the ECG power (upper section) and the noise power (lower section).

calculated as follows:

$$y = x_{cleanECG} + a \cdot noise$$
$$SNR = 10log(P_x/(P_v \cdot a^2))$$
$$a = \sqrt{10^{(\frac{SNR}{10})}\frac{P_x}{P_v}}$$

where $y$ is the is the noisy signal which is generated from the mixtures of realistic noises and the clean ECG data, $x$ is the clean ECG signal, $noise$ is the 2-min segment from the realistic noise recordings. $P_x$ is the power of the clean ECG recordings and $P_v$ is the power of realistic noise recordings.
As for annotation, based on the extended classification scheme described in [11] , it is noted that each class of acceptability was has a certain value between -1 to +1, where -1 means the worst quality while +1 means the best quality, considering the QRS waveform detection accuracy and also the morphology of the signal, we take the class above $C+$ is categorized into "Good", otherwise categorized "Poor". Then together with the EDR signals derived from the ECG, visual inspection is applied to see if the EDR signal is representing a regular respiratory activity. In order to annotate the quality of the ECG signals, a Matlab GUI is developed and the labels can be automatically generated after the annotator select certain buttons. The GUI is shown in Figure 4.6.
As for the Signal quality indices, totally ten features are extracted mainly based on [11] [62] and all the SQI

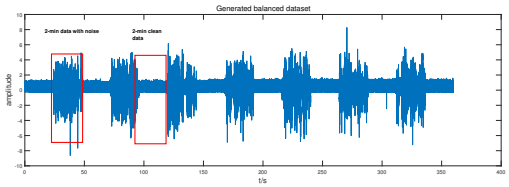


(a) A data example of 6 mins length with clean segment and noisy segment alternating.

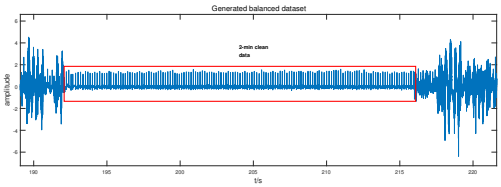


(b) A zoom-in part of the clean segment

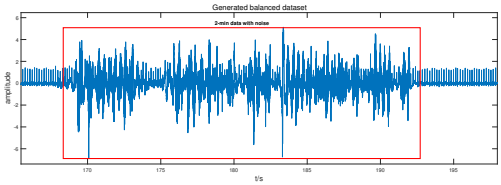


(c) A zoom-in part of the noisy segment

Figure 4.5: An example of the generated balanced dataset

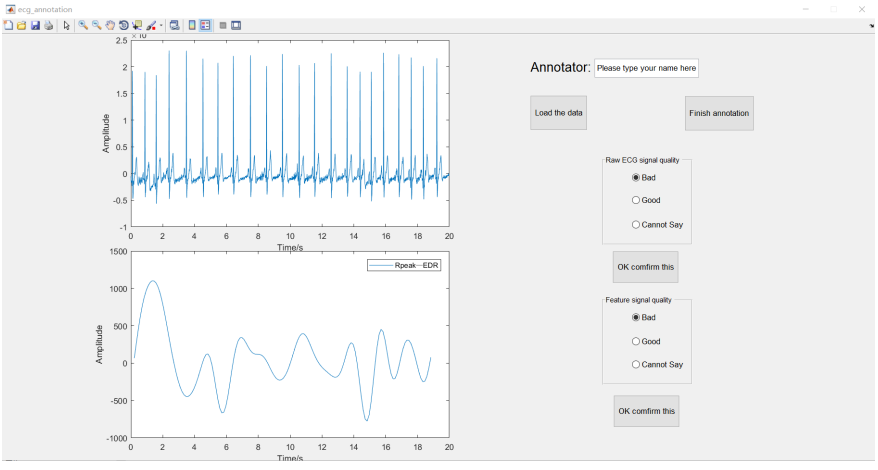


Figure 4.6: The designed Matlab GUI for ECG data annotation

| Quality | Class | Description given to annotators |
|---|---|---|
| 1.00 | A | An outstanding recording with no visible noise or artefact; such an ECG may be difficult to interpret for intrinsic reasons, but not technical ones |
| 0.75 | B+ | A good recording with transient artefact or low-level noise that does not interfere with interpretation |
| 0.5 | B- | A good recording with more transient artefact or low-level noise that does not interfere with interpretation or the QRS detection |
| 0.25 | C+ | An adequate recording that can be interpreted with confidence despite visible and obvious flaws, but no missing signals |
| -0.25 | C- | An adequate recording that can be interpreted with confidence despite visible and obvious flaws with missing data. |
| -0.5 | D+ | a poor recording that may be interpretable with difficulty, or an otherwise good recording with one or more missing signals. |
| -0.75 | D+ | A poor recording that may be interpretable with difficulty. |
| -0.1 | F | an unacceptably poor recording that cannot be interpreted with confidence because of significant technical flaw |

Table 4.1: The criterion for ECG data classification adapted from [11].

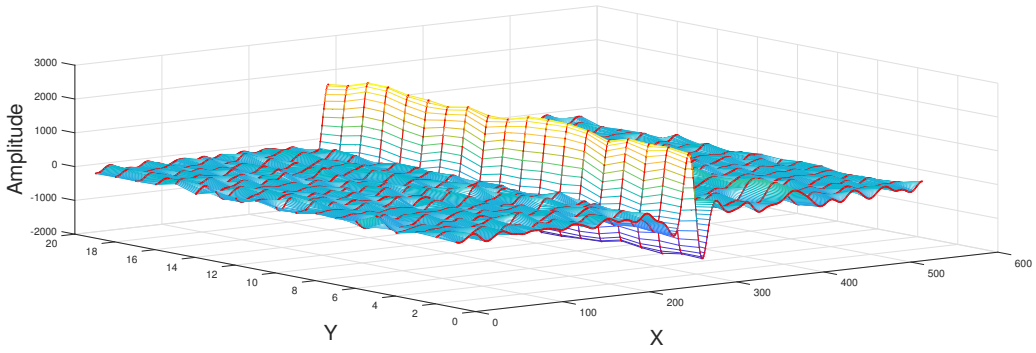


Figure 4.7: Data example of a number of QRS complex in an ECG segment. Along the Y-axis, the time is increasing, corresponding to the occurrence time of each QRS complex. The X-axis indicates the samples of each QRS complex

are summarized in table 4.2 .

**Waveform template matching**
This is a measure of the similarities among all the detected QRS complex of an ECG segment. The principle of the template matching approach, used in [63], is that first all the QRS complex are detected based on certain detection methods and then a template is created by calculating the mean of all the RQS complex. then the Pearson's correlation coefficient is calculated between this template and all the QRS complex and finally, the mean of all the correlation coefficients is calculated taken as the final feature. Pearson's correlation coefficient is a measurement typically used for testing the similarity between two time-series and more details can be found in [64].

**RR energy**
From the observation of the noisy ECG signal, the energy between the R-R intervals can be taken as a feature indicating the signal quality since it is noted that more energy occurred between R peaks during the movement [65]. First, the data is normalized by the maximum. Meanwhile, the RR energy needs to be normalized by the number of points during the RR interval in order to remove the effect of HR variation. Normally, From the data, the normalized RR energy will be larger when the motion artefacts are present, resulting in a large variation of the ECG baseline.

**Relative power in the PCA**
This feature proposed based on the principal component analysis (PCA) which is a typical method for dimension reduction. Based on the idea in [41], the QRS complex, T wave, or P wave in the ECG signals could be characterized by PCA from all the beats within an ECG segment. Thus, the power difference of clean and noisy ECG signals should able to detect by eigenvalues of the covariance matrix of the data matrix of which each column is one aligned QRS complex with the same length. This feature is further taken as the ratio of the sum of all the relatively larger eigenvalues of the first $n$ principal components with over the sum of all eigenvalues extracted based on the principal component analysis (PCA) [66]. In [66], the $n$ is taken as 5 while in this thesis, $n$ is optimized from a range of [1,6]. A data example is shown in Figure 4.7 and this is a 3-D plot of a number of QRS complex in an ECG segment. Along the Y-axis, the time is increasing, corresponding to the occurrence time of each QRS complex. The X-axis indicates the samples of each QRS complex.
All the SQI for the ECG signal are summarized in table 4.2.
In order to find the optimal SQI for indicating the signal quality of ECG, two classifiers are tested to derive the best SQI: **linear discriminant analysis (LDA)**, **quadratic discriminant analysis (QDA)**. The SQI that is able to distinguish data of good quality from bad ones consistently with the highest accuracy based on these two classifiers will be taken as the best SQI.
Due to the limited amount of data in **database 3**, leave-one-subject-out cross-validation method is used to test the performance of each SQI, which means that each time the data from one subject is randomly selected out of all data and the classifiers are trained on the remaining data and the corresponding performance on the selected subject is obtained. Two typical statistical measures for evaluating the performance of these two

classifiers used in [67] are sensitivity ($SE$) and positive predictivity ($PP$). The former is calculated using the formula $TP/(TP+FN)$ while the latter is calculated as follows $TP/(TP+FP)$, where $TP$ is the number of true positives while $FP$ is the number of false negatives and $FN$ is the number of false positives. Furthermore, the F1 score recommended in [67] is also applied to each SQI and it's calculated as follows: $2\cdot(SE\cdot PP)/(SE+PP)$.

| Features | Description |
|---|---|
| | morphology |
| waveform template matching | Measure of the regularity of ECG QRS waveform: similarities in the morphology of the QRS complexes within a segment [62] |
| | Energy distribution |
| average RR energy | A indicator of motion artifact: extra energy occurred between tow consecutive R peaks [65]. |
| relative power of QRS waveform | Spectral distribution ratio between two frequency bands: 5-14Hz band and 5-50Hz band, where the spectrum is calculated by FFT [11]. |
| relative power in the PCA | PCA is applied on the QRS waveform matrix and relative power ration is calculated based on eigenvalues [41]. |
| Wavelet and Shannon entropy | Measure of the distortion of energy distribution of HRV signal: Wavelet transform is used to calculated the power in different frequency bands [62] |
| | Statistical metrics |
| Skewness and kurtosis | Two typical metric used to indicate the presence of outlier in the ECG signal [11]. |
| Matching of two QRS detector | Matching of two existing QRS detection algorithm for the ECG segment [11]. |
| R-R interval variability | Measure of regularity in the R-R time intervals based on the detected R peaks of ECG [62]. |

Table 4.2: SQI candidates for clarifying the signal quality of ECG

### RQI MODEL DEVELOPMENT FOR RESPIRATORY SIGNALS

The respiratory quality indicator is used to indicate whether the respiratory modulation is present in the underlying signal or not and further test how much of respiratory information is actually present. Based on the study[68], several RQIs candidates are introduced in this section and more details are described in appendix A.2. The RQIs proposed in [68] are mainly tested on the respiratory signal derived from ECG and PPG in this thesis all of these RQI together with two novel RQI are tested on the IP signal from the $database1$ introduced

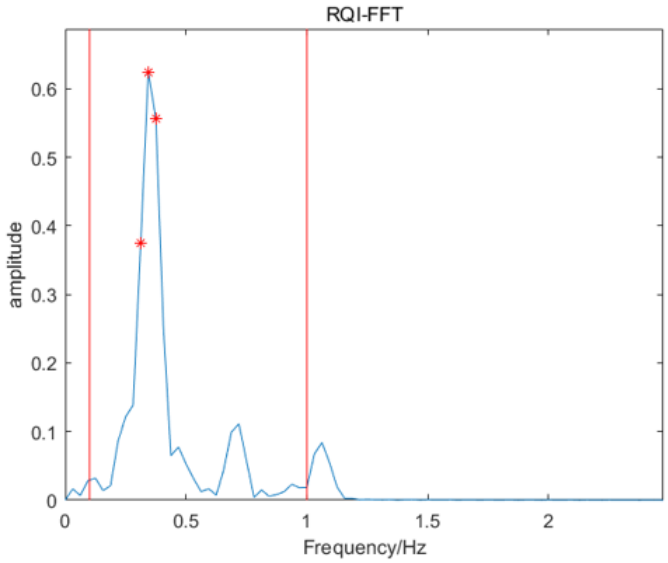


Figure 4.8: An example of the FFT RQI

in Chapter 2. Three key RQIs are introduced as follows.

**Fast-Fourier Transform RQI** The first RQI method is based on the Fast Fourier transform in [68]. The FFT method is applied to estimate the spectrum of the underlying signals and then a value is derived from zero to a unit to presents how much respiratory information is present in the corresponding respiratory waveform. Specifically, The FFT is applied to the data $x(n)$, a data segment of the 20s with a Hamming window to prevent the leakage of the spectrum. The output is the derived spectrum $X(m)$. All the peaks in the $X(m)$ within the predefined respiratory frequency range from 0.1 Hz to 0.8 Hz (6 bpm to 48 bpm) are detected and maximum peak area (MPA) is calculated as the sum of the three largest peaks centralized on the largest value of $X(m)$ while the respiratory area (TRA) is taken as the sum of all the detected peaks. $RQI_{fft}$ is calculated as follows.

$$RQI_{fft} = \frac{\sum_{i=1}^{3} X(m_i)}{\sum_{m=0.1}^{1} X(m)} \tag{4.1}$$

where $sum_{i=1}^{3} X(m_i)$ is the $MPA$ and $\sum_{m=0.1}^{1} X(m)$ is corresponding to $TRA$. The $RQI_{fft}$ is a value in the range from zero to unit and higher values represent a more dominant frequency component in the respiratory range, thus a stronger respiratory modulation for this segment, which means the RR estimate from this segment is more reliable. An example is shown in Figure 4.8.

An relevant RQI can also derived from the frequency sepctrum, denoted as $RQI_{powerration}$. To get a more smoothed spectrum, Welch's power spectral density estimate method is utilized and the ratio between the power of the respiratory frequency range 0.1-0.5 Hz band and the band of 0-1 Hz is calculated as $RQI_{powerration}$.

**Autocorrelation RQI** The autocorrelation is a typical statistical method to find periodical patterns in the signal and normally, the respiratory signals are pseudo-periodic in a short time frame so that an RQI based on autocorrelation is derived and also tested, denoted as $RQI_{auto}$, in [68].

Autocorrelation is a measurement of the correlation of a signal with a delayed copy of itself and the value of correlation is related to the latency. It's also a way to measure the similarity between various data series as a function of the time latency between them. the autocorrelation for lag k is defined as follows [68] :

$$r_k = \frac{1}{\sum_{i=1}^{N}(y_i - \hat{y})^2}) \sum_{t=1}^{N-k} (y_t - \hat{y})(y_{t+k} - \hat{y}) \tag{4.2}$$

The autocorrelation value is in the range of 0-1, where one indicates a perfect alignment while zero means there is no repeating patterns in the underlying signal. The $RQI_{auto}$ is derived based on the autocorrelation of a data segment. Under the assumption that the ideal respiratory signal is expected to be sinusoidal and the better the signal is, the more visible the repeating pattern is shown in the signal, the $RQI_{auto}$ is taken as the maximum autocorrelation within the lag range of k = 102 seconds to k = 819, corresponding to from 6 bpm to

60 bpm. The $RQI_{auto}$ is then assigned to be the maximum correlation value at the specified time lag $k$ within the corresponding respiratory frequency range of and $k$ indicate the time lag where the signal matches to itself most. As a consequence, the larger the correlation value is at a time lag $k$, the more sinusoidal the signal is and the better quality of the underlying respiratory signal.

**Kurtosis and Skewness** These two statistical metrics have been introduced before in subsection of the SQI for ECG signal. Again making the assumption that the ideal respiratory waveform would be a perfect sinusoidal, the corresponding Kurtosis and Skewness for the ideal sinusoidal waveform are 1.5 and 0. Thus a reasonable RQI from the data can be derived based on the deviation from these two standard values:

$$RQI_{kur,k} = \begin{cases} 1 - \frac{|Kur_k - 1.5|}{1.5} & |Kur_k - 1.5| < 1.5 \\ 0 & \text{otherwise} \end{cases} \tag{4.3}$$

$$RQI_{ske,k} = \begin{cases} ske_k & 0 < ske_k < 1 \\ \frac{1}{|Kur_k - 0|} & \text{otherwise} \end{cases} \tag{4.4}$$

**Peak-interval variability** This RQI is based on standard deviation (std) of the time interval between successive peaks in the respiratory signal. For an ideal respiratory signal, this measure will be zero. Thus it is calculated based on the deviation of this std from zero as follows:

$$RQI_{kur,k} = \begin{cases} 1 - \frac{Peakpari^2_{std}}{4^2} & \text{Peakpari}_{std} < 4 \\ 0 & \text{otherwise} \end{cases} \tag{4.5}$$

where the $Peakpari_{std}$ is the standard deviation of the time-interval between successive peaks.
The proposed RQIs is summarized in table 4.3.

**RQIs validation**
Each RQI is scaled in certain methods such that the RQI values are expected to be capable to indicator the actual respiratory information in the underlying signal and the higher the RQI is the better the signal is while lower RQI indicator signal of poor quality.
For comparison, an ideal SQI $iSQI$ is a generated by the product of the error $E$ and the minus one, where $E$ is the error between the RR from the underlying signals and the RR estimate from the gold standard spirometer recordings.
The ability of all the RQI to discriminate data of good quality from the ones with poor quality was assessed using two methods proposed in [68]:

- Error curve plot
- Metric-based methods: by observing the performance difference between each RQI and the idea RQI in terms of error E and the Pearson correlation coefficient.

For the former method, error curve plot, the mean absolute error(MAE) is taken as the mean absolute difference of the estimate (from the existing "$Count - adv$" breath detection in Chapter 3) and reference estimate (from spirometer). Firstly, MAE is calculated for the whole dataset and then the segments with the lowest RQIs are removed and then MAE is recalculated for the remaining segments. This process is repeated by removing increments of 1% of the data, from segments with lower RQI to segments with higher RQI. This process is evaluated independently for each RQI and in principle, the more capable the RQI is to distinguish the segment of good quality from the ones of poor quality, the more likely it is to remove the segments of poor quality and keep the segment of good quality on every increment, thus the MAE will decrease. The MAE is defined:

$$MAE = \frac{1}{N} \sum_{i=1} |(\hat{x}_i - x_i)| \tag{4.6}$$

where N is the amount of samples, and $x_i$is RR estimate from the underlying signals and $\hat{x}_i$ is the RR estimate from the reference spirometer signal.

| RQI | denotation | Description |
|---|---|---|
| | | morphology |
| Autocorrelation | $RQI_{auto}$ | Measure of repeating patterns of the respiratory signals distorted by noise [68]. |
| Skewness and kurtosis | $RQI_{ske}, RQI_{kur}$ | measures of symmetry of distribution and the sharpness of the distribution for the morphology of the signal, respectively. |
| | | Energy distribution |
| FFT RQI | $RQI_{fft}$ | Energy distribution in the respiratory frequency band based on FFT [68]. |
| Welch RQI | $RQI_{powerartion}$ | Energy distribution in the respiratory frequency band based on welch method. |
| Autoregression RQI | $RQI_{ar}$ | Measure of the power of the dominant frequency component in the pre-defined respiratory frequency range as the amplitude of the pole [68]. |
| | | Frequency variation |
| Hjorth parameter RQI | $RQI_{Hjorth}$ | compares the signal's similarity to a pure sine wave based on the calculation of Hjorth parameter which indicating the frequency variation [68]. |
| peak-interval variability | $RQI_{stadparigap}$ | measure of the variability of the peak-interval in the respiratory signal. |

Table 4.3: summary of the proposed RQIs

For the latter evaluation method, we have two metrics:

$$E_{50} = \frac{\sum_N E}{N} - \frac{\sum_m E}{m} \tag{4.7}$$

$$E_{RCM} = MAERQI_{50\%} - MAEidea_{50\%} \tag{4.8}$$

where N is the number of all the data segment and thus $E_{50}$ is presenting the difference between the average error of the whole dataset and the error of segments whose RQI are larger than the RQI median. Thus, this metric $E50$ will take larger values when the RQI is capable to distinguish segments of good quality with a lower error in RR estimate from the segments of poor quality from which an RR estimate with a larger error may be derived. As for the metric $E_{RCM}$, where $MAERQI_{50\%}$ is taken as the mean absolute error of the remaining segments after 50% of the segments has been removed based on the RQI and $MAEIdeal_{50\%}$ is the same mean absolute error after 50% data removed from the same dataset based on $iSQI$. The RCM represents how much better the $iSQI$ performs compared to the RQI after 50% segments are removed and the smaller the $E_{RCM}$ is, the better the RQI is.

### 4.2.3. MOTION ARTIFACT REDUCTION

As is described in Chapter 3, some studies investigated the methods to remove the noise buried in the signal, most of them used the adaptive filtering and the most commonly used reference signal for this filter is accelerometer recording, e.g. in [48], The ACC outputs from three orthogonal directions are used as the input of a bank of gradient adaptive laguerre lattice (GALL) filter to estimate the motion artefact in the ECG. Since reference signal is essential to the performance of adaptive filtering to attenuate the noise and the only possible reference from the $database3$ is the accelerometer recordings, in this subsection, with the help of the method proposed in [69], we use the method of combining constrained independent component (cICA) algorithm in [70] and adaptive filters to first extract the motion artefacts in the noise-contaminated IP signal and then evaluate the correlation between the motion artefact and the accelerometer recordings. By using cICA, the respiratory component of interest could be automatically estimated from the IP and spirometer by the use of cICA. Taking the output from cICA as the input to the adaptive filtering, the true respiratory signals in the IP signal could be extracted with the correct amplitude. Besides, some simpler methods to extract the motion artefact are also used. All the methods are applied to the real data from $database3$.

#### METHODS

ICA is a typical method to extract several independent components (IC) from the observed signals which are mixtures of the ICs [71]. The relationship between the independent components S and the observed mixture signals X is expressed as the equation as follows:

$$X = AS \tag{4.9}$$

where A is the mixing matrix to mix the source signal S. If the A is known, a weight matrix $W$, $W = A^{-1}$, can be used to recover the source $S$ from the observation $X$ as follows:

$$S = WX \tag{4.10}$$

However, in practice, the prior knowledge of the sources S and the matrix A are not always available, the desired signal can not be automatically selected from the output of ICA due to the permutation ambiguity. One algorithm proposed in [72] named constrained ICA (cICA) could effectively extract the desired signal from the mixed observation signal with the help of a reference signal. One study introducing the formulation of the cICA is in [70] and it can be modeled as follows.

$$\begin{aligned} \max_{y} \quad & J(w) \approx \rho[EG(w^T z) - E(G(v))]^2 \\ \text{subject to} \quad & g(w) = \epsilon(y,r) - \xi \leq 0,\ h(w) = E\{y^2\} - 1 = 0 \end{aligned} \tag{4.11}$$

where the object function $J(y)$ is formulated as the negentropy with a positive constant $\rho$ . $G(\cdot)$ is defined as $G(y) = e^{-a_2 y^2/2}/a_2$ as suggested in [70]. Both the object function $J(y)$ and the desired vector $w$ for recovering the true signal from the mixture signal are bounded by the the equality constraint $h(w)$ . $\epsilon(y,r)$ measures the closeness between the extracted signal $y$ from the observation signal and the reference signal $r$. Note that the desired output signal is the independent component in the mixture signal which is closest to the reference signal r.
A solution to solving the cICA problem is proposed in [72] and now summarized in table 3:
After we get the optimal estimate of the true respiratory signals with the help of the cICA method, we still

**Algorithm 3** cICA

1: **procedure** CICA — The procedure of cICA
2: **Initialization** $b$ — Initialize the parameters

$$\mu = 1 \quad \lambda = 1$$
$$\gamma = 1 \quad \eta = 1$$
$$threshold = 0.00001$$

3: **while** $norm(w_k - w_{k-1}) > threshold$ **do** stop the loop when the changed value of weighted vector is less than threshold
4: $\mu_t = max\{0, \mu_{t-1} + \gamma g(w_{t-1})\}$
5: $\lambda_t = \lambda_{t-1} + \gamma h(w_{t-1})$
6: $\Gamma_1 = \overline{\rho} E\{z G'_y(y)\} - \frac{1}{2}\mu E\{z g'_y(y)\} - \lambda E\{zy\}$
7: $\Gamma_2 = \overline{\rho} E\{G"_{y^2}(y)\} - \frac{1}{2}\mu E\{g"_{y^2}(y)\} - \lambda$
8: **end while**
9: **return** $w$ — The optimal weight vector $w$
10: **end procedure**

need to recover the amplitude information based on adaptive filtering. As is described in section 3.2, the principle of Least Mean Square (LMS) adaptive filtering method is as follows:

$$y(n) = w^T(n)u(n)$$
$$e(n) = d(n) - y(n)$$
$$w(n+1) = w(n) + \mu e(n)u(n)$$

where $u(n)$ is the reference signal as the input to the adaptive filter, which could be either related to the MA or the true respiratory signal in the IP signal. $d(n)$ is the desired signal of the adaptive filter and it is the mixture of the true respiratory signal in IP and the motion artefact. $w(n)$ is the weight needed to be applied on the desired signal $d(n)$ for recovering the true respiratory component, $e(n)$ is the corresponding error between the desired signal and the observation $y(n)$ and $\mu$ is the step size.
Similar to the idea in [69], in this application, the noisy IP and spirometer signal($\mathbf{X}$) are mixed in a linear way of MA and respiratory signal sources($\mathbf{S}$). Unlike the typical ICA algorithm, the cICA algorithm doesn't need any prior knowledge about the number of independent sources could be extracted from the underlying signals. The respiratory signal in the noisy IP signal could be recovered based on the cICA algorithm when the reference signal from the smoothed spirometer signal is used. Furthermore, the output from the cICA method is taken as the input of the adaptive filter to recover the amplitude information of the amplitude information. The data used for evaluating this method are from the protocol we designed and mainly from stage $d$ in section 1, where volunteers are required to move randomly on the bed and the MA are most visible because the

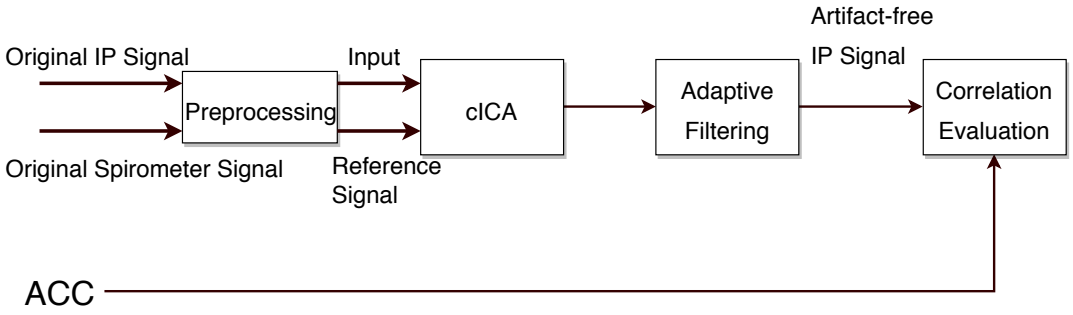


Figure 4.9: The flowchart of the correlation evaluation between motion artefact and Acc recordings

motion artefacts are most visible in this stage. Totally we have 40 segments with a length of 20 s for evaluating this method.

### PREPARATION FOR THE PROPOSED METHOD

Following the preprocessing in [69], figure 4.9 shows a similar primary flowchart includes: preprocessing, cICA implementation and adaptive filtering.
**Band-pass filtering** The signals from spirometer may have non-respiratory component, like high-frequency noises which are the mixture of air leakage and movement. Meanwhile, the IP signal has a cardiac component and is also distorted by quantization noise. A band-pass filtering is enough to remove both high-frequency noises as well as the baseline wandering with low frequency. Due to the fact that the frequency of respiratory component normally lies in the range of 0.1-0.8 Hz, we use a fourth order Butterworth filtering with a band-pass of [0,0.8] Hz to remove the unwanted noise and the baseline wandering.

**The reference signal generation for cICA** The generation of the reference signal can be based on the prior information about the desired signal. Spirometer recordings show a robust pattern of the respiration though sometimes slightly distorted by noise. thus, the reference signal can be generated with the help of the periodic patterns present in the spirometer signal. Firstly the spirometer is pass through a band-pass filtering and then both autocorrelation and peak detection are used obtain the estimate the periodic patterns in the spirometer signal together with the help of manual modification. After we have the respiratory rate from the last step, we use a notch filter to extract a relative clear respiratory signal from the spirometer recordings. After this, we use crosscorrelation to align this respiratory signal with the noisy IP signal since it's required in cICA that the occurrence time of each impulse of the reference signal is needed to be consistent with that of the desired signal [70].

**cICA implementation** After getting the preprocessed spirometer recording, IP signal and the reference signal generated in step 'preprocessing', all of these are then taken as the input of the cICA algorithm. Then the true respiratory-component in IP signal is extracted.

**Adaptive filtering** In this step, we utilize the LMS adaptive filtering to extract the true respiratory signal from the IP signal with the artefact-free respiratory-component in IP signal from step'cICA implementation' as a reference signal. the step size $\mu$ is taken as 0.001 to have a good trade-off between convergence rate and accuracy.

**Other methods for MA estimation**

In order to evaluate the performance of potential ways to extract the motion artefact, three simpler methods are also used as comparisons. They are summarized in the following table 4.4 and the FFT-LMS method is adapted from [69].

**Correlation Evaluation** After we get the MA estimate from the noisy IP signal, we need to evaluate the correlation between the MA and ACC recordings, which is indicating to what extent the ACC can help to remove the noise. The ACC recordings have acceleration data from three orthogonal directions: x,y and z and the correlations between each of them and the MA are evaluated.
We have two metrics for this: linear correlation (Pearson correlation)[64] and coherence[73].

- **Linear correlation** Pearson correlation coefficient is used to indicate the correlation between tow data series X and Y. It has a value in the range of [+1, 1] and the value of 1 represents a total positive linear correlation while -1 means a total negative linear correlation. It's defined as following [64]:

$$r = \frac{\sum_{n=1}^{N}(x_i - \hat{x})(y_i - \hat{y})}{\sqrt{\sum_{i=1}^{N}(x_i - \hat{x})^2}\sqrt{\sum_{i=1}^{N}(y_i - \hat{y})^2}} \tag{4.12}$$

  Because pearson correlation coefficient is affected by phase difference, we need to align the MA estimate with the ACC recordings by crosscorrelation and then calculate the pearson correlation between the aligned signals then.

- **Coherence** The linear correlation between two signals x and y in frequency domain is measured as a function of frequency by the magnitude squared coherence function defined as [74]:

$$|\gamma_{xy}(f)|^2 = \frac{|P_{xy}(f)|^2}{P_{xx}(f)P_{yy}(f)} \tag{4.13}$$

  In 4.13, $Pxy(f)$ is the complex cross-power spectral density and of x and y signals while $P_{xx}(f)$and $P_{yy}(f)$ are the corresponding power spectral densities of the individual x and y signals respectively. The value of coherence is in the range of [0,1] and a value of zero means no correlation is found between these two signals while a value of one indicate the best linear correlation at the corresponding frequency.
  The maximum possible attenuation of the noise which can achieved by the adaptive filtering is a function of frequency given in [74]:

$$attenuation(f) = -10log_{10}(1 - |\gamma_{xy}(f)|^2)[dB] \tag{4.14}$$

  based on this equation, the attenuation of the noise at certain frequency is determined by the value of the coherence. Since the length of the data segment used in this method is 20s with data points of 20480 at sampling rate of 1024Hz, the spectra were calculated using Welch's method based on the Fast Fourier transform (FFT) with $2^{15}$ point together with the hamming window. We evaluate the coherence in two ways: i) maximum coherence that occurred at the respiratory frequency ii) the mean coherence of the peaks in respiration range. An example is shown in Figure 4.10.

### 4.2.4. BREATH DETECTION

The algorithm used for the breath detection is the modification of "$Count - adc$" method introduced in [8] and the details has already been described in chapter 2. The threshold of this detection method is taken related to the value of third quartile $\hat{Q_3}$ and the factor $k$ multiplied to $Q_3$ is optimized in a part of the data resulting in $threshold = k * Q_3$. Breath-detection threshold multipliers $k$ for the respiratory signals of IP $EDR_{RSA}$ is set to 0.3 while for the $EDR_{QRSslope}$, $EDR_{RSamp}$, $EDR_{QRSarea}$ and $EDR_{Ramp}$ is set to 0.6.
This method returns instantaneous RR estimates for the segment based on the peaks detection and the algorithm is summarized in the table:

| Algorithm name | core method |
|---|---|
| FFT-LMS [69] | a) Estimate the respiration rate from the spirometer recording with manual correction and the spectrum of the MA contaminated IP signal.<br>(b) The spectrum of MA is generated by setting the coefficients of the frequency corresponding to the true respiratory component in FFT to zero.<br>(c) The MA estimate in the time domain is generated by the inverse FFT transform on the MAE spectrum from step b).<br>(d) The MA estimate is then taken as the input of the LMS adaptive filter while the corresponding desired signal is the noisy IP signal. The output will be the estimate of the respiratory signal and then subtracted from the noisy IP to generate the final estimate of MA. |
| Notch filter-LMS | a) Estimate the respiration rate(RR) from the spirometer recording with manual correction.<br>(b) Use a notch filter with the stop band centred at the frequency of RR with a bandwidth of 0.2Hz. The output is a synthetic MA reference signal in time-domain. |
| ICA-LMS | a) apply typical ICA to the MA contaminated IP signal and extract the first three independent component.<br>(b) align the three independent components with the preprocessed spirometer by cross-correlation. Then take the one which has the highest correlation with the preprocessed spirometer as the estimate of the clean IP signal. The MA estimate is obtained by subtracting the clean IP from the noisy IP signal.<br>(c) The MA estimate is then taken as the input of the LMS adaptive filter while the corresponding desired signal is the noisy IP signal. The output will be the estimate of the respiratory signal and then subtracted from the noisy IP to generate the final estimate of MA. |
| cICA-LMS | already described above. |

Table 4.4: Summary of the methods utilized for estimating the true respiratory signals from the MA contaminated IP signal

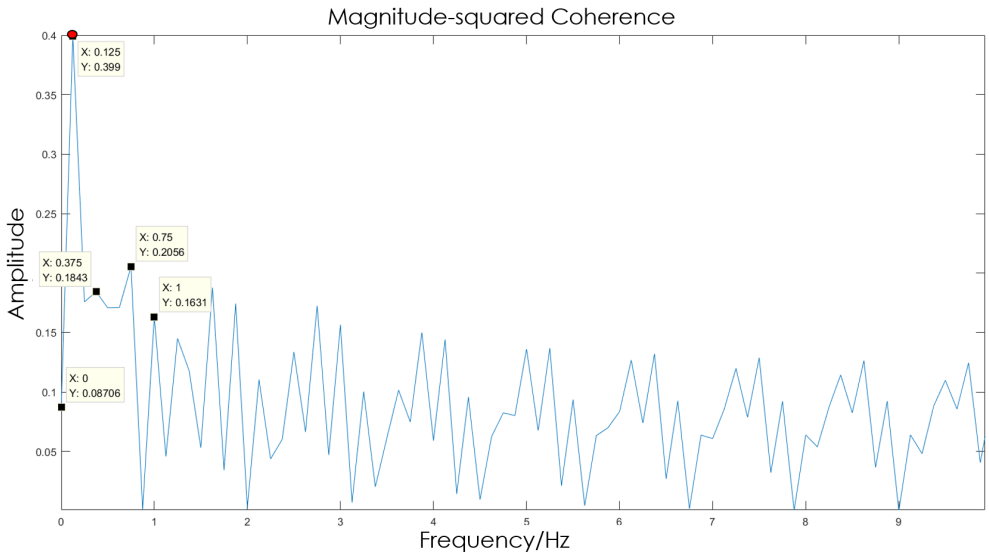


Figure 4.10: All the peaks of coherence that occurred at the respiratory frequency band. The red dot indicates the largest peak and the black solid squares denote the other peaks in this band

**Algorithm 4** Advanced Counting Method (Count-adv)

**Initialization** All the local pairs of extrema are found in the band-pass filtered curve. The absolute values of the amplitude difference of the subsequent pairs of extrema are calculated for further determining the threshold. The threshold is taken as the third quartile $\hat{Q}_3$ multiplied by a factor of k. Set $flag$ to 1.

**while do** $flag = 1$

The pair of subsequent extreme separated by the minimum difference $Amp$ is selected.

**if** $Amp < threshold$ **then**

the pair is considered to be a random fluctuation which is not representing the respiratory activity and hence further removed and set $flag$ to 1.

**else**

Set $flag$ to 0.

**end if**

**end while**

The remaining detected pairs of extremes are considered to be representing the true respiratory activity.

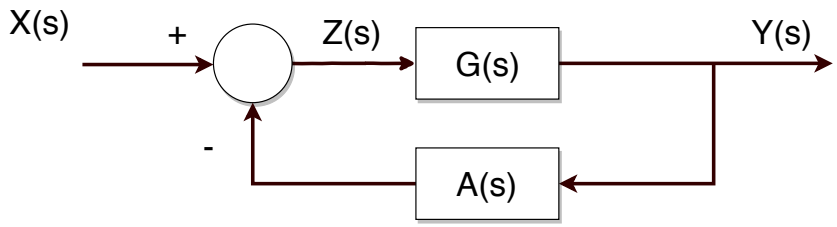


Figure 4.11: Block diagram of the IIR filter

### 4.2.5. RR SMOOTHING

Based on the help of the SQI derived before and the ideas in [23], a filtering method for correcting the RR estimate is introduced.
The infinite impulse filter (IIR) is firstly modified with the help of SQI and RQI introduced in the previous chapters and then the RR estimate series from the underlying respiratory signal are further smoothed with this modified IIR filter. The block diagram is shown in Figure4.11. The related functions of the IIR filter can be derived as follows:

$$\begin{cases} Y(s) = Z(s)G(s) \\ Z(s) = X(s) - Z(s)G(s)A(s) \end{cases} \tag{4.15}$$

Furthermore, the transfer function is as follows:

$$H(s) = \frac{Y(s)}{X(s)} = \frac{G(s)}{1 + G(s)A(s)} \tag{4.16}$$

In this application, the gain $G(s)$ is equal to one. converting these function into time domain, the output of the filter is:

$$RR_k = RR_{k-1} + \alpha(RR_k^{inst} - RR_{k-1}) \tag{4.17}$$

This equation means that the current RR estimate should be a weighted sum of the current instantaneous RR estimate as well as the RR estimate in previous one.
Furthermore, the derived SQI between 0-1 are used to scale the forget factor to limit RR variation as follows:

$$\alpha_k = \alpha \cdot SQI_k \tag{4.18}$$

The final RR estimate from the current data segment will be determined by the SQI estimate and this filter can handle the situations when the SQI is low thus resulting in a poor $RR_{inst}$ by relying more on the previous estimate instead of the current one to generate the final estimate.

### 4.2.6. INFORMATION FUSION FOR RESPIRATORY RATE ESTIMATE

We have introduced a set of fusion methods to fusion the RR estimate from the IP and EDR signals.
The first two methods are the mean and median of all the RR estimate from all the underlying respiratory signals. Mean is the simplest way for information fusion. The median method could work well when part of the RR estimates are overestimated against the true RR while the others are underestimates of the true RR.
More complicated methods are introduced as follows.

**Weighted RR with SQI and RQI**

Since we have derived the SQI and RQI for both respiratory signals derived from IP and ECG signals previously in section 4.2.2, another reasonable way is to calculate the weighted mean of the RR estimate from all the methods, which is following a similar idea in [69]. The equation for weighted RR is as follows:

$$RR = \frac{\sum_{i=1}^{N} RR_i \cdot SQI_i}{\sum_{i=1}^{N} SQI_i} \tag{4.19}$$

**Kalman filter**

We summarize the Kalman dynamical system model again in following equations:

$$x_K = A_k x_{k-1} + B_k u_k + w_k$$
$$z_k = H_k x_k + v_k$$

In this study, there is no control vector $u_k$ so that the control-input model $B_k$ is set to zero. In order to determine the remaining parameters, we did some statistical analysis on the **dataset 3** and more details of this can be found in Appendix A.3.

$A_k$ In [12], the RR of a healthy people cannot have great changes during a relatively long time frame [12]. In order to determine the dynamic model parameter $A_k$, The difference in RR between two adjacent segments of 20 s is analyzed including over 1021 segments. The histogram and bivariate Gaussian distribution fitting are analyzed for specific motion type and overall dataset. More details can be found in Appendix A.3. Since from the results most of the pairs of two consecutive segments have almost same RR value (This can be seen in the middle heat map in FigureA.1a, most of the points are on the diagonal) This $A_k$ is set to one and the Kalman dynamic model is simplified to a scalar equation.

$w_k$ and $v_k$ are process noise and observation noise under the assumption that they are zero-mean Gaussian white noise with covariance $Q_0$: $w_k \sim N(0, Q_0)$and variance $R_0$: $v_k \sim N(0, R_k)$. To estimate this two covariance, since we can get the true continuous RR series from the spirometer recordings, the $Q_0$ can be directly estimated by calculating the variance of the RR series. Furthermore, the errors of the RR estimate from the measured IP and ECG signal can be calculated with the help of true RR from spirometer, then the observation noise covariance can also be simply estimated by taking the variance of the errors. As a consequence, evaluated from the overall dataset, the $Q_0$ is set to 4 for EDR while for IP is 2.

As for the initialization, the initial values $x_0$ and $P_0$ were set to the SQI-weighted sum of the RR from respiratory signals of which the SQI is above 0.5, which could make sure that the initial value $x_0$ is very close to the true state.

In one study [75], the measurement noise covariance $R_K$ is modified to be various based on the signal quality and the relationship was modified from:

$$R_k = R_0 * e^{SQI^{-2}-1}$$

The idea of the modification is that when the signal is of low quality, a low value of SQI, the measurement noise should be forced to be large since the corresponding RR estimate is less reliable. This will force the Kalman filter to focus more on the prior state transition model instead of the measurement. On the other hand, for the signal of good quality, a high value of SQI will force the measurement noise to be small, resulting in the KF trust more on the trust more the current RR estimate. In this way, the measurement noise of the KF could be determined in an adaptive way by the corresponding SQI and then track the true state better.

After the KF smoothing applied to the RR estimates from each individual respiratory signal, they are still needed to be fused in order to give the final RR estimate based on the corresponding confidence indicated by the SQI and RQI. Based on the study [12], all the independent Kalman filtered estimates from individual signals could be combined based on equation 4.20 in and for simplicity, two RR from two respiratory signals are fused in the way by equation 4.21:

$$X_k = \sum_{s=1}^{S} \left( \frac{\prod_{i=1, i\neq k}^{S} \sigma_{k,i}^2}{\sum_{s=1}^{S} (\prod_{j=1, j\neq i}^{S} \sigma_{k,j}^2} \cdot x_{k,s} \right) \tag{4.20}$$

$$RR_k = \frac{\sigma_{k,2}^2}{\sigma_{k,2}^2 + \sigma_{k,1}^2} x_{k,1} + \frac{\sigma_{k,1}^2}{\sigma_{k,2}^2 + \sigma_{k,1}^2} x_{k,2} \tag{4.21}$$

where $x_k$ and $\sigma_{k,s}$ are the RR estimate from individual respiratory signals and the confidence of this estimate for the $s-th$ respiratory signal at the $k-th$ time-step, respectively. Based on one study [75], the confidence $\sigma_{k,s}$ is determined with the help of Kalman residual values as well as SQIs in the following equation 4.22.

$$\sigma_{k,s}^2 = \frac{r_{k,s}^2}{SQI_{k,s}^2 \lambda_s^2} \tag{4.22}$$

Where the $\lambda_s^2$ is the corresponding factor of trustfulness between different signals since different respiratory signals have different ability to provide a correct RR estimate and in this thesis for the EDR signals, $\lambda_s^2$ is in the range of [0,0.4] while for the IP signal, $\lambda_s^2$ is one. The fusion methods in equation 4.21 can handle the situations when motion artefacts are presents in certain respiratory signals. For example, if the motion artefact is present in one respiratory signal $s$, while all the others signals are of good quality. This will result in a larger residual and low value of SQI in signal $s$, thus a low weight will be assigned to the RR estimate from this signal and the final RR estimate will be more determined by the RR estimates from the other respiratory signals.
The processing block diagram is shown in the following Figure 4.12.

**Viterbi algorithm**


Figure 4.12: Block diagram of the KF fusion method

Viterbi algorithm is a commonly used method for tracking the change of the true states by searching for the most possible sequence of the observations which are closest to the true state. More details of the Viterbi algorithm can be found in[76]. In this RR monitoring application, after the RR estimates from all underlying respiratory signals are obtained, the Viterbi algorithm can be applied on them to search for the most possible RR estimate per time frame closest to the true RRs.
In this application, the state space is composed of the true RR, denoted as $RR_{true}$, from each segment and the observation space are the estimated RR, denoted as $RR_{inst}$, from individual respiratory signals. The joint distribution of $RR_{true}$ of two successive segments for different motion types are introduced in Appendix A.1.1 and the transition probability from one to other states is actually the conditional probability of this joint distribution. The emission probability, the probability of an observation from the state, is taken as the RQI introduced above. The Viterbi algorithm then can be used to decide the final transmit probability of $RR_{inst}$ between every two frames and eventually, the most likely sequence of state can be generated. The following table summarized the setting of the Viterbi algorithm.

| Vertibi parameters | denotation | descripition |
|---|---|---|
| Time frame | $S$ | Time frames (20s) of the respiratory signals |
| RR estimate | $RR_{inst}$ | RR estimate from individual respirotary signal |
| true RR | $RR_{true}$ | True RR for each time frame |
| State space | $s = \{RR_{true,1}, RR_{true,2}...RR_{true,N}\}$ | The true RR |
| Observation space | $o = \{RR_{inst,1}, RR_{inst,2}...RR_{inst,N}\}$ | $RR_{inst}$, instantaneous RR estimate from all channels |
| Transition probability | $T_{s_i,s_j}$ | transition probability from $s_i$ to state $j$ and this is calculated as the conditional probability of the joint distribution : $s_j \| s_i = s_i \sim N(\mu_1 + \frac{\sigma_{12}}{\sigma_{22}}(s_j - \mu_2), \sigma_{11} - \frac{\sigma_{12}^2}{\sigma_{22}})$, where $N$ means a normal distribution and the $\sigma$ and $\mu$ are the parameters of the joint distribution. |
| Emission probability | $E_{o_j,s_i}$ | the probability of observing $o_j$ from state $s_i$ and it is taken as the RQI of each data frame. |

## 4.3. FRAMEWORK EVALUATION

All the different algorithms were evaluated against the reference respiratory rate derived from the spirometer recordings. In this section, we have introduced a set of statistical metrics in [23] for evaluating the framework for RR monitoring and compared them with each other. The details of the metrics are introduced in the following subsections.

### 4.3.1. EVALUATION COEFFICIENT

In this section, we give an introduction to the statistical metrics used for evaluating the performance of the raised framework suggested in [23].

#### MEAN ABSOLUTE ERROR

For all $N$ measurements, the mean absolute error can be derived as follows

$$MAPE = \frac{1}{N}\sum_{n=1}^{N}\left|RR_n - RR_{ref,n}\right| \tag{4.23}$$

where the $RR_n$ and $RR_{ref}$ are the RR estimate from framework and the true RR estimate from spirometer reference signal.

#### MEAN ABSOLUTE PERCENTAGE ERROR

As is suggested in [23], in RR monitoring, the error of the RR estimate against the reference in terms of percentage is commonly since a small error in RR estimate may also result in clinical consequences if the true RR is already small. For example, an error of 3bpm against the true RR of 4 bpm is considered to be severe in a clinical sense. The absolute value percentage error and the mean absolute percentage error are give as:

$$MAE = \frac{1}{N}\sum_{n=1}^{N}\left|\frac{RR_n - RR_{ref,k}}{RR_{ref,k}}\right|100\% \tag{4.24}$$

### RELIABILITY ON PERCENTAGE ERROR

In this thesis, absolute percentage error is used to derive a metric namely reliability. If the RR estimate is within ±20% of the true RR, this estimate can be taken as reliable one. This metric is given as:

$$reliability_n = \begin{cases} 1 & \left|\frac{RR_k - RR_{ref,n}}{RR_{ref,n}}\right| < 0.2 \\ 0 & \text{otherwise} \end{cases} \tag{4.25}$$

calculating the total proportion, we get:

$$reliability = \frac{sum_{n=1}^{N} reliability_n}{K} \tag{4.26}$$

### LINEAR CORRELATION BETWEEN REFERENCE AND ESTIMATE

As is introduced in previous chapter 3, the Pearson correlation is a measurement indicating the linear correlation between the RR estimate and true RR.

### BLAND–ALTMAN PLOT

The Bland–Altman is a graphical visualization method to compare two measurements in terms of agreement [77]. The agreement is typically visualized by 95% limits of agreement which is calculated by the mean difference plus and minus 1.96 standard deviations of the difference and a smaller range of this limits indicates a better agreement between the two tested measurements. In a word, Bland–Altman is a good way to test of if the proposed framework can work interchangeably with reference spirometer to derive correct and robust RR estimates.

# 5

# EVALUATION AND RESULT

This chapter presents the evaluation results of the developed framework and can be divided mainly into two sections. In the first sections, following the block diagram of the complete framework introduced in Chapter, the performance of every sub-block is shown and discussed in more details. As for the second section, the evaluation result of the whole complete framework presented at a higher level.

## 5.1. PERFORMANCE EVALUATION OF THE KEY SUB-BLOCK IN THE FRAMEWORK

In this section, following the block diagram of the complete framework introduced in Chapter 4 shown in Figure 4.1, the performance of the key sub-block is shown and discussed in more details.

### 5.1.1. SIGNAL QUALITY INDICATOR AND RESPIRATION QUALITY INDICATOR

This sub-section presents the result of SQI and RQI investigation on ECG and both IP and EDR respiratory signals, respectively.

#### SQI FOR ECG SIGNAL

Totally 9 SQI candidates for ECG signal are tested by two classifiers, LDA and QDA, the optimal SQI will be taken as the one which is capable to distinguish the data of good quality from those ones of bad quality with the best performance. Due to the limited number of samples used in this application, leave-one-out cross-validation is used. Three statistical metrics which have already been introduced in section 4.2.2 are used to evaluate the performance of the classifiers based on each SQI: sensitivity, predictivity (PP) and $F_1$ score.
For a clear visualization of the performance of each SQI, the statistical metrics of each SQI are shown in Figure 5.1 and the values of the measures are shown in Table 5.1. In Figure 5.1, the SQIs are listed on the histogram with their predictivity, sensitivity and overall $F_1$ score. The left part is the output from the LDA classifier and the right part is from the QDA classifier. In Table 5.1, all the SQIs are ranked based on the average of $F_1$ from two classifiers in an ascending order. Clearly, from both the figure and table, for both classifiers, it can be seen that the template matching SQI is the optimal one since it has the best performance in distinguishing data of

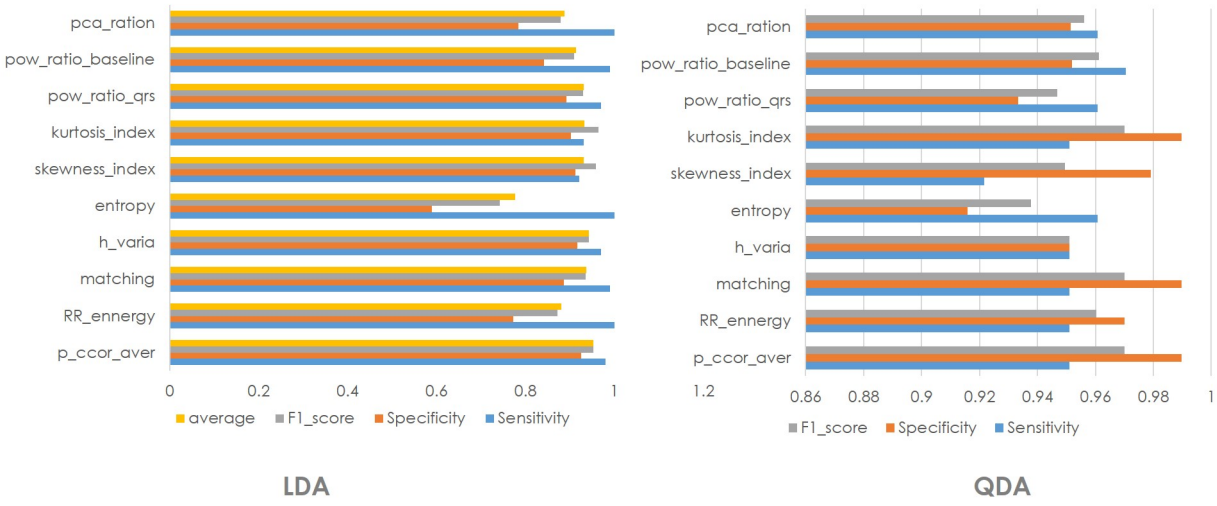


Figure 5.1: Performance evaluation of the SQIs

| | LDA | | | QDA | | | Overall |
|---|---|---|---|---|---|---|---|
| Indicator | sensitivity | predictivity | $F_1$ | sensitivity | predictivity | $F_1$ | Average of $F_1$ |
| $powerratioqrs$ | 0.78 | 0.70 | 0.74 | 0.74 | 0.69 | 0.71 | 0.72 |
| $waveletentropy$ | 0.99 | 0.56 | 0.72 | 0.98 | 0.64 | 0.77 | 0.74 |
| $kurtosis$ | 0.64 | 0.95 | 0.76 | 0.72 | 0.93 | 0.81 | 0.79 |
| $hrvaria$ | 0.85 | 0.82 | 0.84 | 0.85 | 0.82 | 0.83 | 0.83 |
| $pcaration$ | 0.99 | 0.71 | 0.83 | 0.95 | 0.79 | 0.86 | 0.84 |
| $RRennergy$ | 1.00 | 0.71 | 0.83 | 0.96 | 0.83 | 0.89 | 0.86 |
| $skewness$ | 0.81 | 0.93 | 0.87 | 0.82 | 0.92 | 0.87 | 0.87 |
| $ratiobaseline$ | 0.97 | 0.79 | 0.87 | 0.94 | 0.84 | 0.89 | 0.88 |
| $ratiomatch$ | 0.92 | 0.87 | 0.90 | 0.92 | 0.89 | 0.90 | 0.90 |
| $F_1matching$ | 0.97 | 0.82 | 0.89 | 0.96 | 0.87 | 0.917 | 0.90 |
| $qrscorraver$ | 0.97 | 0.89 | 0.93 | 0.93 | 0.94 | 0.94 | 0.93 |

Table 5.1: Classification rate of the SQIs which are ranked by the average of $F_1$ score from two classifiers in ascending order.

good quality from the bad ones among all SQIs for the whole dataset, with the highest $F_1$ score, thus we take the template matching-based SQI as the optimal SQI for ECG quality.

#### INDIVIDUAL RQI FOR RESPIRATORY SIGNALS

The evaluation methods of the RQIs are already introduced in section 4.2.2, including the error curve plot and three more statistical measures.
For a clear understanding, RQI comparison metrics introduced in section 4.2.2, $E_{50}$, $E_{RCM}$ and $correlation$ are shown in the Figure 5.2 and this bar plot summarizes the performance of all the derived RQIs. The largest $E_{50}$ is seen when using $RQI_{FFT}$ (5.51 bpm) and the smallest $E_{RCM}$ is seen when using $RQI_{powerration}$. The values of all the RQIs are summarized in Table 5.2 and ranked in an ascending order based on the value of $E_{50} - E_{RCM}$ and the larger this value is, the better the corresponding RQI will be.
The error curve is shown in Figure 5.3. As for the idea RQI, the lowest one in this figure, it is capable to distinguish the data of good quality from the bad ones since because of the decrease on MAE when more data with the lowest idea RQI removed from the whole dataset. It's clear that the three closest curves to the idea RQI one are: $RQI_{fft}$, $RQI_{powerratio}$ and $RQI_{auto}$.
Interestingly, the average performance across all of the data analyses for the $RQI_{FFT}$, $RQI_{powerration}$, and $RQI_{auto}$ was almost the same. Finally, we can draw a conclusion that $RQI_{fft}$, $RQI_{powerratio}$ and $RQI_{auto}$ can tell signals of good quality from the bad ones.

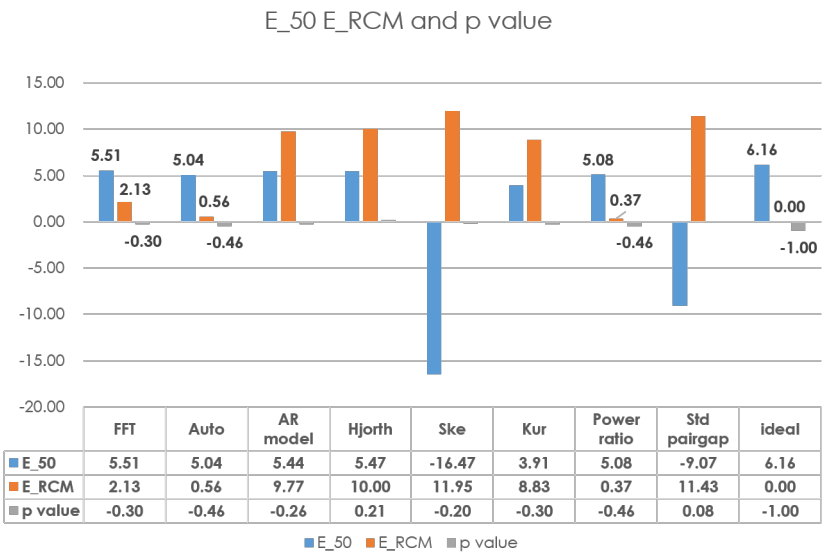


| | FFT | Auto | AR model | Hjorth | Ske | Kur | Power ratio | Std pairgap | ideal |
|---|---|---|---|---|---|---|---|---|---|
| E_50 | 5.51 | 5.04 | 5.44 | 5.47 | -16.47 | 3.91 | 5.08 | -9.07 | 6.16 |
| E_RCM | 2.13 | 0.56 | 9.77 | 10.00 | 11.95 | 8.83 | 0.37 | 11.43 | 0.00 |
| p value | -0.30 | -0.46 | -0.26 | 0.21 | -0.20 | -0.30 | -0.46 | 0.08 | -1.00 |

Figure 5.2: The summary of the performence of all the derived RQI

### 5.1.2. MOTION ARTIFACT REDUCTION

In this subsection, the results of the methods proposed in section 4.2.3 are presented and can be mainly divided into two parts. Four methods for extracting the true respiratory signals from the artefact-distorted IP signals are summarized in Table 4.4 and in the first part, the results of these methods are presented. As introduced in 4.4, after extracting the MA using the best method, constrained ICA, the coherence and Pearson correlation are used to evaluate the correlation between the Acc recordings and the MA. and the results are present in the second part.

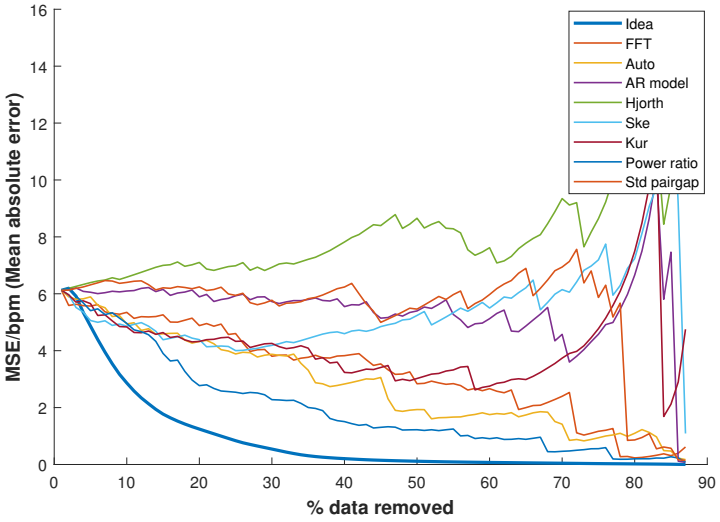


Figure 5.3: The error curve of all the derived RQI

| RQI indicator | $E_{50}$ | $E_{RCM}$ | p value | $E_50$ - $E_{RCM}$ |
|---|---|---|---|---|
| Ske | -16.47 | 11.95 | -0.20 | -28.41 |
| Std pairgap | -9.07 | 11.43 | 0.08 | -20.50 |
| Kur | 3.91 | 8.83 | -0.30 | -4.92 |
| Hjorth | 5.47 | 10.00 | 0.21 | -4.53 |
| AR model | 5.44 | 9.77 | -0.26 | -4.34 |
| FFT | 5.51 | 2.13 | -0.30 | 3.38 |
| Auto | 5.04 | 0.56 | -0.467 | 4.48 |
| Power ratio | 5.08 | 0.37 | -0.46 | 4.71 |
| Ideal | 6.16 | 0.00 | -1.00 | 6.16 |

Table 5.2: The summary of the performence of all the derived RQIs

| Correlation between the true bioz estimate and the smoothed spirometer recordings | | | | | |
|---|---|---|---|---|---|
| segment | Raw bioz | Notch filter | FFT | cICA+LMS | ICA+lms |
| 1 | 0.168 | 0.085 | 0.07 | 0.94 | 0.992 |
| 2 | 0.151 | 0.453 | 0.654 | 0.81 | 0.846 |
| 3 | 0.537 | 0.602 | 0.618 | 0.987 | 0.640 |
| 4 | 0.5 | 0.678 | 0.558 | 0.87 | 0.518 |
| mean | 0.339 | 0.4545 | 0.475 | 0.90175 | 0.742 |

Figure 5.4: Correlation between the estimated respiratory signal in IP signal with the smoothed spirometer recordings.

### INDIVIDUAL METHODS EVALUATION

In this section, the performance of the four methods is shown, which are used to estimate the true respiratory signal from the noisy IP signal. The data used for this evaluation are from stage d section 1 of the **database 3** introduced in section 2.5, totally 10 volunteers involved. In stage d section 1, the volunteers are required to move randomly while lying on the bed, where the motion artefacts are most visible in the IP signal, making it the most representative one of the artefacts-distorted data sample.
The data of stage 4 are chopped into 4 segments with a length of the 20s with a overlapping of 5s.
As is shown in Figure 5.4, the estimate of the true respiratory signal based on the $cICA-LMS$ methods has the highest correlation, 0.90, with the smoothed spirometer recordings, followed by the estimate from the method of typical $ICA-LMS$ with an average correlation of 0.74. It is clear that the rest two methods based on FFT, notch filter don't work well and can't provide a promising estimate of the true respiratory signal from the noisy IP signal since the estimate from these two methods only have a correlation of 0.46 and 0.47, respectively. Thus, in the further investigations, only these two ICA-based on methods are utilized to evaluate the correlation between Acc and motion artefacts.

### CORRELATION BETWEEN ACC AND MOTION ARTIFACTS

In this section, the results of correlation between Acc recordings and motion artefacts are presented. This correlation is evaluated based on two metrics $Pearson correlation$ and $spectrum coherence$ and the results are shown in the following Figure 5.5. In Figure 5.5a, we can see that the mean correlation in the time domain of Pearson correlation between the estimated motion artefact and the ACC recording, all channels of 3 axis, is really low and the maximum is 0.31, not high enough to attenuate the motion artefacts effectively.
As for the spectrum coherence, we use the best tow methods $cICA-LMS$ and $ICA-LMS$ to estimate the true respiratory IP signal from the noisy ones and then subtract this from the noisy IP signal to get the estimate of the motion artefacts. Finally, the coherence between Acc and motion artefacts is calculated and the results are shown in Figure 5.5b and 5.5c. In the former sub-figure, the coherence values of the largest peak in the respiratory frequency range based on two methods motioned above, shown in two columns for each Acc channel, are really low and the maximum one is only 0.37, which can only achieve an attenuation of only 0.57dB on the corresponding frequency component.
In the latter sub-figure, the average coherence values of all the peaks in the respiratory ranges are not large either and the maximum is 0.5, which can only achieve an attenuation of 1.24dB in an average meaning. From the analysis above, we can conclude that the ACC recordings are not correlated with the motion artefacts well tush it's not a good reference signal for noise removal of IP signals for this particular movement where most

representative motion artefacts are present.
It is noted that during the data collection in **database 3**, the accelerometer is attached on the same position of human body shown in Figure 2.7, in the middle chest due to the limitation of the wire length. Strictly speaking, the effect of the different positions should also be explored in the future work.

#### RR SMOOTHING FILTER WITH SQI AND RQI ASSISTED

In section 4.2.5, the SQI-assisted RR smoothing methods are introduced. An example of IP signal in the following Figure 5.6 shows how this RR smoothing filtering helps follow true RR when the signal quality is not good for a certain part of the data. The IP data example is part of section $freebreath$ of the protocol introduced in the section 2.5, where the volunteers are required to sit still for a while and then move randomly to generate motion artefacts, which could result in some overestimated RR due to the bad signal quality.
In Figure 5.6a, for the first part of the data, the volunteers are asked to breathe freely without any movement and the data is of great quality. In the middle part, the volunteer is required to move randomly to generate motion artefacts on the top of the clean IP data, which results in a data of very poor quality. The following part is that the volunteer is asked to breathe freely again though there is a baseline drift in the data.
In Figure 5.6b, the RR smoothing filter with varying $\alpha$, from 0 to 1 with a step size of 0.1, is applied to the data in 5.6a and the corresponding Mean absolute errors(MSE) between the RR estimate from this filter and RR from the reference data are shown in the lower section. For a clear comparison, the unfiltered RR from IP, the RR filtered by moving average and the RR filtered by this smoothing filter are also present in the upper sub-figure, which are the green solid square, black solid square and the dark red curve. From the lower part, it's obvious that smoothing filter when $\alpha = 0.2$ has the best performance with an MSE of 0.64, which means the weighed assigned to the current estimate RR is only 0.2. Thus, when giving an estimate of the current $RR_k$ in equation 4.17, the A-IIR with fixed $\alpha$ work best in a way that weights much more on the previous $RR_{k-1}$ instead of the current instantaneous estimate, denoted as $RR_k^{inst}$. The MSE of moving average filter is approximately 2 bpm, which is equal to A-IIR filter with $\alpha = 0.7$.
In order to have a clear understanding of the RR smoothing method, $\alpha$ modified by SQI in equation 4.18, denoted as $A-IIR_{\alpha-SQI}$, In Figure 5.6c, we make a comparison between the RR smoothing filter with the best $\alpha = 0.2$ , denoted as $A-IIR_{\alpha=0.2}$ and $A-IIR_{\alpha-SQI}$. In the upper sub-figure, The blue band gives the ±20% range of the spirometer RR values. The reference value of the dark blue curve is in the middle of this band. Meanwhile, the RR values of $A-IIR_{\alpha=0.2}$, $A-IIR_{\alpha-SQI}$ and moving average are in purple, red and yellow curves, respectively.
From the lower sub-figure, the RQI is high for segments from 1 to 7 and suddenly drop to very close to 0 for segment 8,9, while both RR curve of $A-IIR_{\alpha=0.2}$ and $A-IIR_{\alpha-SQI}$ lie in the blue band all the time in the upper sub-figure, as it resists any changes in RR as long as the signal quality is estimated to be poor. However, RR curve of moving average is outside where the RQI is poor, which means it cannot handle segment of poor quality.
It is noted that the MSE of $A-IIR_{\alpha=0.2}$ and $A-IIR_{\alpha-SQI}$ are very close, 0.64 and 0.65, which means they have almost the same performance for this data example. However, in practice, the best $\alpha$ is hard to obtain since it requires the knowledge of the true RR while the SQI of data can be estimated based on the methods proposed in section 4.2.2 and the method of $A-IIR_{\alpha-SQI}$ can still work to track the true RR estimate from the underlying signals especially when data segment of low quality are present.

### 5.1.3. INFORMATION FUSION FOR RESPIRATORY RATE ESTIMATE

In section 4.2.6, five fusion methods are introduced and in this subsection, two examples of the most novel methods, Kalman filtering and Viterbi algorithm, present in the following figures shows how these two methods work for a more detailed interpretation.

#### KALMAN FILTERING FUSION

An example of the Kalman filter fusion is shown in Figure 5.7. In this example, RR estimates from four respiratory signals are utilized to create a fusion estimate of RR. This data example is also part of the database 3

**Linear Correlation between the motion artifact and ACC**

| segment | notch | | | fft | | | cica_lms | | | lca_lms | | |
|---|---|---|---|---|---|---|---|---|---|---|---|---|
| | x | y | z | x | y | z | x | y | z | x | y | z |
| 1 | 0.231 | -0.154 | -0.220 | 0.159 | -0.157 | -0.270 | 0.140 | 0.022 | -0.417 | 0.149 | 0.117 | -0.051 |
| 2 | 0.146 | -0.214 | -0.298 | 0.198 | -0.228 | -0.323 | 0.095 | -0.165 | -0.429 | 0.089 | -0.142 | -0.473 |
| 3 | 0.111 | 0.044 | 0.032 | 0.048 | 0.207 | -0.099 | 0.285 | -0.022 | 0.159 | 0.516 | -0.023 | 0.072 |
| 4 | -0.232 | 0.110 | 0.263 | -0.238 | 0.093 | 0.266 | -0.223 | 0.176 | 0.235 | -0.075 | 0.051 | 0.093 |
| Absolute mean | 0.31 | 0.13 | 0.20 | 0.16 | 0.17 | 0.24 | 0.19 | 0.10 | 0.31 | 0.21 | 0.08 | 0.17 |

(a) Pearson correlation between the ACC and the motion artefact

**Coherence of ACC with largest peak**

| Segment/acc | X | | Y | | Z | |
|---|---|---|---|---|---|---|
| 1 | 0.30 | 0.15 | 0.24 | 0.13 | 0.44 | 0.24 |
| 2 | 0.30 | 0.13 | 0.23 | 0.11 | 0.37 | 0.22 |
| 3 | 0.39 | 0.26 | 0.48 | 0.24 | 0.31 | 0.17 |
| 4 | 0.42 | 0.27 | 0.33 | 0.24 | 0.37 | 0.25 |
| Absolute mean | 0.35 | 0.20 | 0.32 | 0.18 | 0.37 | 0.22 |
| *attenuation*(dB) | 0.57 | 0.18 | 0.47 | 0.14 | 0.64 | 0.22 |

(b) The coherence of the largest peak in the respiratory frequency range. The two columns are corresponding to ICA-LMS and cICA-LMS methods

**Coherence of ACC with all the peaks**

| Segment/acc | X | | Y | | Z | |
|---|---|---|---|---|---|---|
| 1 | 0.55 | 0.33 | 0.41 | 0.25 | 0.63 | 0.44 |
| 2 | 0.49 | 0.21 | 0.42 | 0.18 | 0.39 | 0.19 |
| 3 | 0.53 | 0.34 | 0.15 | 0.06 | 0.19 | 0.10 |
| 4 | 0.42 | 0.27 | 0.47 | 0.34 | 0.32 | 0.15 |
| Absolute mean | 0.50 | 0.29 | 0.36 | 0.21 | 0.38 | 0.22 |
| *attenuation*(dB) | 1.24 | 0.38 | 0.60 | 0.20 | 0.68 | 0.22 |

(c) The coherence of the average of all the peak in the respiratory frequency range

Figure 5.5: Correlation evaluation of the ACC recordings with the motion artefact

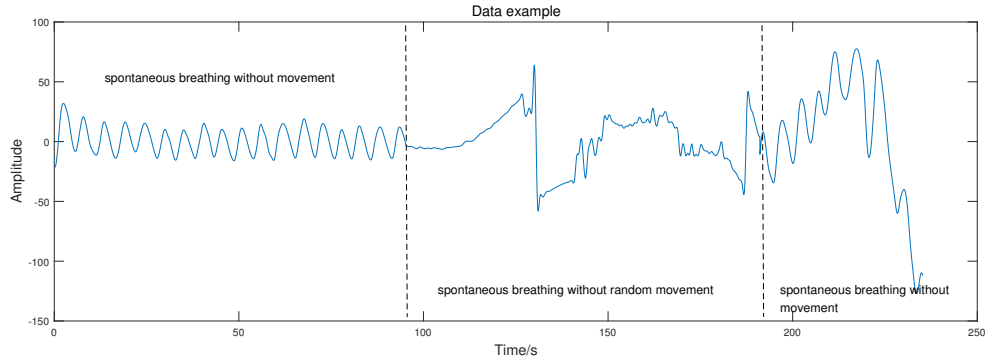


(a) Data example including three part:spontaneous breathing without movement, randomly moving, back to spontaneous breathing

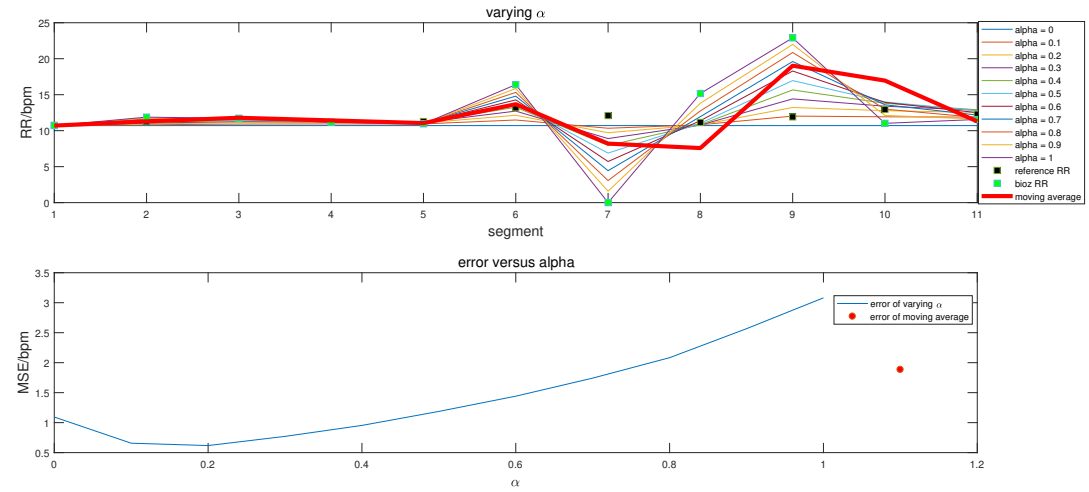


(b) filtering with varying $\alpha$ and the corresponding errors. Moving average is also present as a comparision.

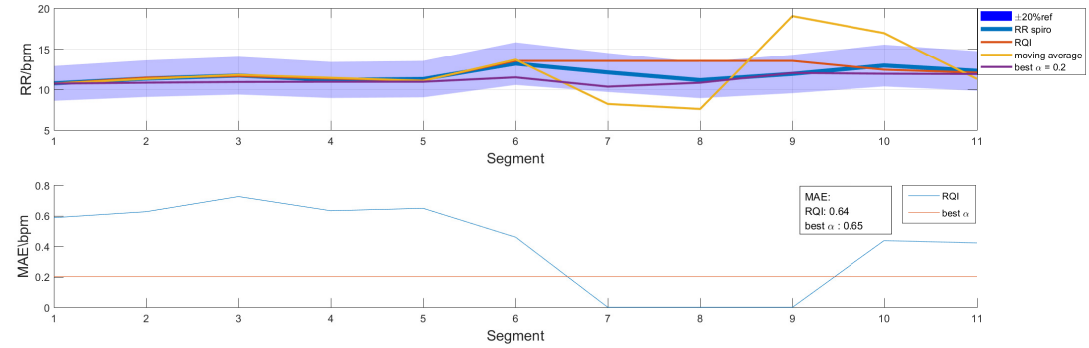


(c) Comparison between the filter with the best fixed $\alpha$ and with the $\alpha$ modified by the SQI

Figure 5.6: A segment of data where quality-assisted IIR filter is performed

introduced in section 2.5.1. In the upper left subfigure, the blue shade is the area of ±20% , similar to the metric 'reliability' introduced in chapter 4, against the reference RR. The dotted lines are the raw RR estimated from the four source signals and the solid lines with the same colours are the corresponding RR after Kalman filtering. The initialization of the state RR is set as the quality-weighted RR estimate from the subset of four signals, of which the SQI is above 0.5. It's clear that after KF filtering all individual RRs are staying with the ±20% area against the reference RR. In the upper right figure, the solid black squares are the fused RR estimate and all of them stay within the ±20% area against the reference RR. Thus, the Kalman filtering fusion method works well on tracking the true RR for this data example.
The lower two subfigures present the corresponding weight and RQIs for each individual RR. Not surprisingly, in most cases the source signals which have the best signal quality, the corresponding weight is also the largest one. Thus, the Kalman filter fusion method works in a way of giving a proper weight to each source signal with the help of the corresponding RQI to provide a good track of the true RR.

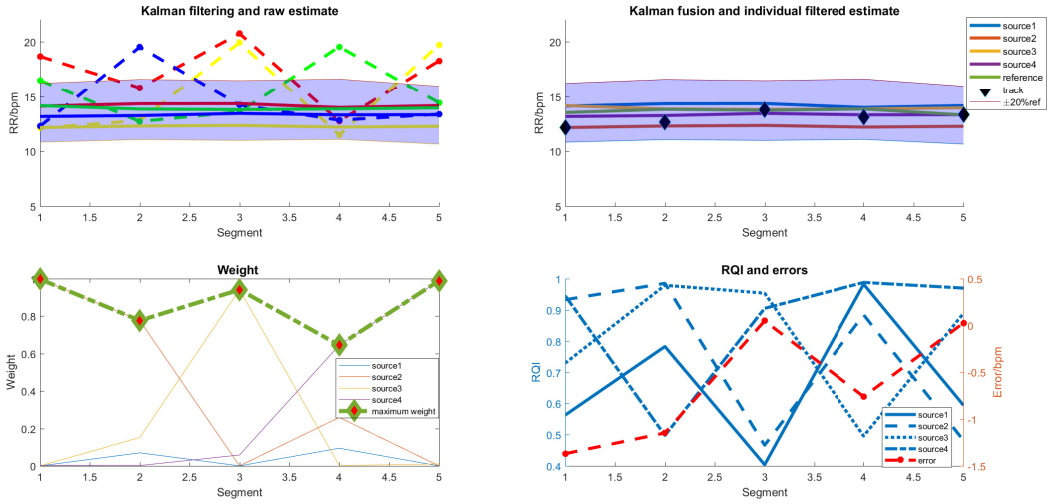


Figure 5.7: a) the raw RR estimates and the RR estimates after Kalman filtering of four individual methods; b) The RR estimates after Kalman fusion against the individual RR after Kalman filtering; c) The corresponding signal quality of the individual methods; d) The weight assigned to each individual method in Kalman fusion.

### VITERBI ALGORITHM

As is introduced in section 4.2.6, the Virerbi algorithm is used to track the changes of the true RR from all the RR estimates from all the respiratory signals.
A data example of explaining how Viterbi works is shown in the following Figure 5.8. Figure 5.8a shows the $RR_{isnt}$ in 5 time segments from four individual respiratory signals. Each blue arrow means the calculated transmit probability between two corresponding states. The back-forward track of red arrows means that once reaching the last segment, a back-forward search will start from the state with the largest probability at the last segment and the Viterbi path can be retrieved by saving back state in last segment which has the largest transmit probability with the current one. For example, the transmit probability ,from state 1 in time segment 1 to state 1 in time segment 2, is calculated by the equation below, where the $P(R_{2,1}|R_{1,1})$ is the transition probability, $V_{RR_{1,1}}$ is the initialized probability of state 1 in time segment 1 by the corresponding RQI and SQI. Finally, $P(R_{2,1,observation}|R_{2,1,true})$ is the emission probability.
Figure 5.8b shows the tracking performance of Viterbi algorithm. The blue shade indicators the area of errors of ±20%$against the reference RR and the \mathrm{RR}_{inst}$ curve from four individual respirotary signals are also present. Clearly, the Viterbi path has found the certain individual $RR_{inst}$ closest to the true RR for each segment, resulting in a minimum error among the errors between the true RR and each $RR_{inst}$.
It is noted that, in this data example, there is always one certain RR estimate close to the true RR and the

Viterbi algorithm can pick it as the final RR estimate for the corresponding time segment.

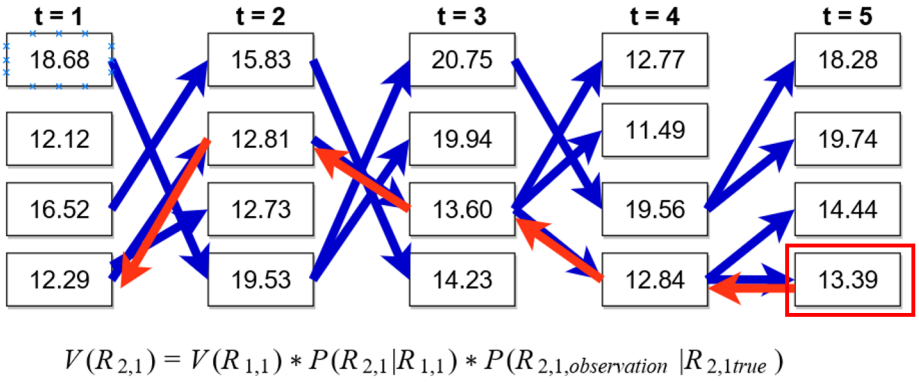


(a) Schematic diagram of Viterbi algorithm

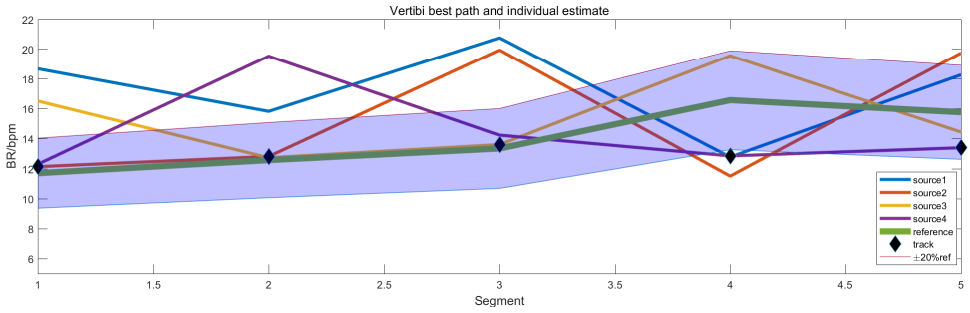


(b) The tracking performence of Viterbi algorithm

Figure 5.8: An example of Viterbi algorithm

## 5.2. PERFORMANCE EVALUATION OF THE COMPLETE FRAMEWORK

This section gives the evaluation result of the complete framework shown in Figure 4.1 and can be mainly divided into two sub-sections. The first sub-section presents the results from the whole $dataset3$ introduced in section 2.5.1. This means that the evaluation carried out on all the recordings without considering the activity difference of the five sections in database 3. The latter subsection analyses the results from different activity classes.

### 5.2.1. OVERALL MEASUREMENT EVALUATION

This section presents the overall results of the dataset we have.

#### INDIVIDUAL ALGORITHM

In Table 5.3, we summarize all the individual methods which are combinations of the base signal, breath detection method and filtering method, evaluated against the reference spirometer recordings. Different evaluation metrics, reliability, MAE and MAPE, are further divided into subsections as follows.

| Algorithm name | base signals | Breath detection | filtering |
|---|---|---|---|
| 1 adc QRSslope | QRSslope | Count-adv | No |
| 2 adc RSamp | QRS-RSamp | – | – |
| 3 adc QRSarea | QRS-area | – | – |
| 4 adc RRinterval | RRinterval | – | – |
| 5 adc Ramp | Ramp | – | – |
| 6 adc bioz | bioz | – | – |
| 7 adc IIR QRSslope | QRS-slope | Count-adv | SQI-IIR |
| 8 adc IIR RSamp | QRS-RSamp | – | – |
| 9 adc IIR QRSarea | QRS-area | – | – |
| 10 adc IIR RRinterval | RRinterval | – | – |
| 11 adc IIR Ramp | Ramp | – | – |
| 12 adc IIR bioz | bioz | – | – |
| 13 adc mov RSslope | QRS-slope | Count-adv | Kalman filter |
| 14 adc mov RSamp | QRS-RSamp | – | – |
| 15 adc mov QRSarea | QRS-area | – | – |
| 16 adc mov RRinterval | RRinterval | – | – |
| 17 adc mov Ramp | Ramp | – | – |
| 18 adc mov bioz | bioz | – | – |
| 19 bioz comp | bioz | original | No |

Table 5.3: Respiratory rate estimation algorithms from individual respiratory signal

**Reliability**

In this evaluation, the reliability defined in the previous chapter is used as one essential indicator of the performance of different methods throughout the evaluation section. It indicates the percentage of time the measured RR has a maximum of 20% error of the true RR value obtained from the reference spirometer recordings. In the following figure 5.9, the overall results are shown as a bar chart in a descending order by the reliability.

The first impression from Figure5.9 is that the IP-based methods could provide a more accurate RR estimate compared with the EDR-based methods in a general sense. The reliability of the IP-based methods is in the range of 73%~82%, while the range of EDR-based methods is 38%~67%, where large variations are present among the EDR methods. One possible reason is that the respiration modulation on the ECG signals are not visible for most times even on the clean-ECG data segment and both from the literature [12] and the data, the respiratory modulations can be invisible if the breathing rate is too low or too high.

It is also noted that in this Figure 5.9, the SQI-based IIR filtering, denoted as $SQI-IIR$, can improve the general reliability. This means that the SQI-based IIR filtering method could help to correct the poor RR estimate due to random fluctuations in the corresponding signals which are resulted from motion artefacts. Figure 5.9 also shows what value every step of the framework in Figure 4.1 adds. The reliability of the method from imec, $biozcomp$ has a general reliability of 73.8%, while for the modified method $adciirbioz$, where the RR estimates of $adcbioz$ going through the SQI-assisted filtering, it can achieve a higher reliability of 82.27%, which means that the proposed individual method $adciirbioz$ could provide a more reliable RR estimate. However, $adcbioz$ has almost the same general reliability as $adciirbioz$ but a larger MAP and MAPE (shown in the next subsection). This means the SQI-assisted filtering gain little on the general reliability for IP signals. But for the EDR signals, the SQI-assisted filtering could help gain more in terms of the reliability, e.g. $adciirQRSslope$ can achieve 56% while $adcQRSslope$ can only provide 50% reliability, which means the SQI-assisted filtering could gain an improvement of 6% on $EDR_{QRSslope}$ respiratory signal. The gain from the information fusion will be discussed later.

The methods that were filtered using Moving average filter are denoted with *mov* in their names. From Figure 5.9, the *mov* filter have a lower general reliability compared with $SQI_{IIR}$ for both IP and EDR signals. Due to the principle of moving average filter, equal weights are assigned the current RR estimate and the previous one and then the average of these two is taken as the final RR estimate, which isn't taking the signal quality into consideration. Hence, it can not reduce the estimation errors when both of the current and previous RR estimates deviate from the true RR too much.

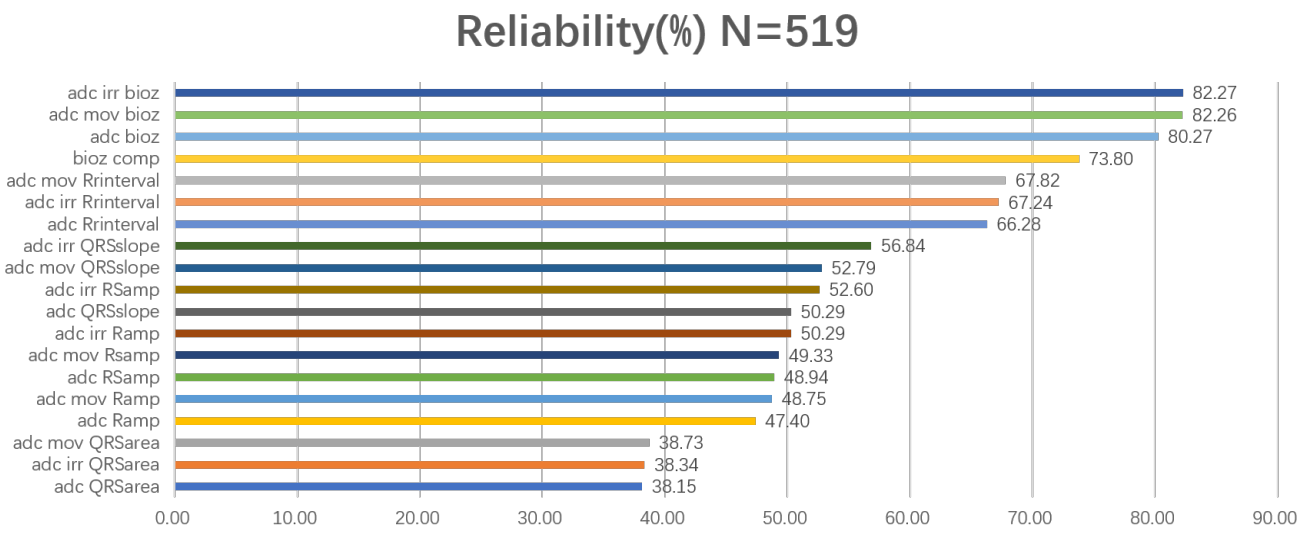


Figure 5.9: Reliability of the individual methods in table 5.3

**Mean absolute error and Mean absolute percentage error**

In the following Figure 5.10, the Mean absolute error(MAE) and mean absolute percentage error(MAPE) are shown to indicate the performance of all the individual methods. In this figure, we rank all the individual methods by MAE in a descending order. As expected, both MAE and MAPE metrics give the same rank order. The most impressive finding is that IP methods could give a more accurate RR estimate compared with ECG signals, which have a much lower MAE and MAEP. It can be also seen that the $SQI_{IIR}$ smoothing method could help to obtain more accurate RR estimate especially for EDR signals since almost all the EDRs could provide less MAE and MAPE after $SQI_{IIR}$ filtering, e.g. $adciir\,QRSslope$ outperforms $adcQRSslope$. However, there is no big difference in the MAE and MAPE between $adciir\,bioz$ and $adcbioz$, since these values are already low enough with MAE:1.63bpm and 1.73bpm and MAPE 11.11% and 11.64%, respectively.

**Bland-Altman plot**

In this subsection, the Bland-Altman plot in percentage error and correlation plot of $adciir\,bioz$ are shown in Figure 5.11. From the left sub-figure, the RR estimate and RR reference show a good correlation of 0.87 and most of the pairs are lying on the line of $y = x$, although there is a slight bias of 0.28. For a more intuitive understanding how the derived RQI works, we divided the points into three subgroups: good quality of $RQI > 0.6$, red solid square, moderate quality of $> 0.6 RQI > 0.3$ and low quality of $RQI < 0.3$. An intuitive impression from this figure is that almost all the points of good quality with $RQI > 0.6$ are lying on the line of $y = x$, which means they are very close to the true RR. As for the points of moderate and low quality, they are more spread on both sides of $y = x$, which means not all of them are modified to get closer to the true RR after the filtering methods.

The Bland-Altman plot based on the percentage error for RR measurement is shown in the right sub-figure. The mean difference is 1% and the limit of agreement is between -16% and 14%. Similar to the correlation plot, almost all the points of good quality with $RQI > 0.6$ are within the limit of agreement although there are few outliers outside this range, which means that the RQI could tell the data of good quality from others in a general sense. As for the points of moderate and low quality, they are more spread and it's noted that for the data of bad quality with $RQI < 0.3$, more points (51%) are within the limit of agreement while fewer outliers are outside(40%), which means that the $adciir$ methods could provide promising help to modify the RR from

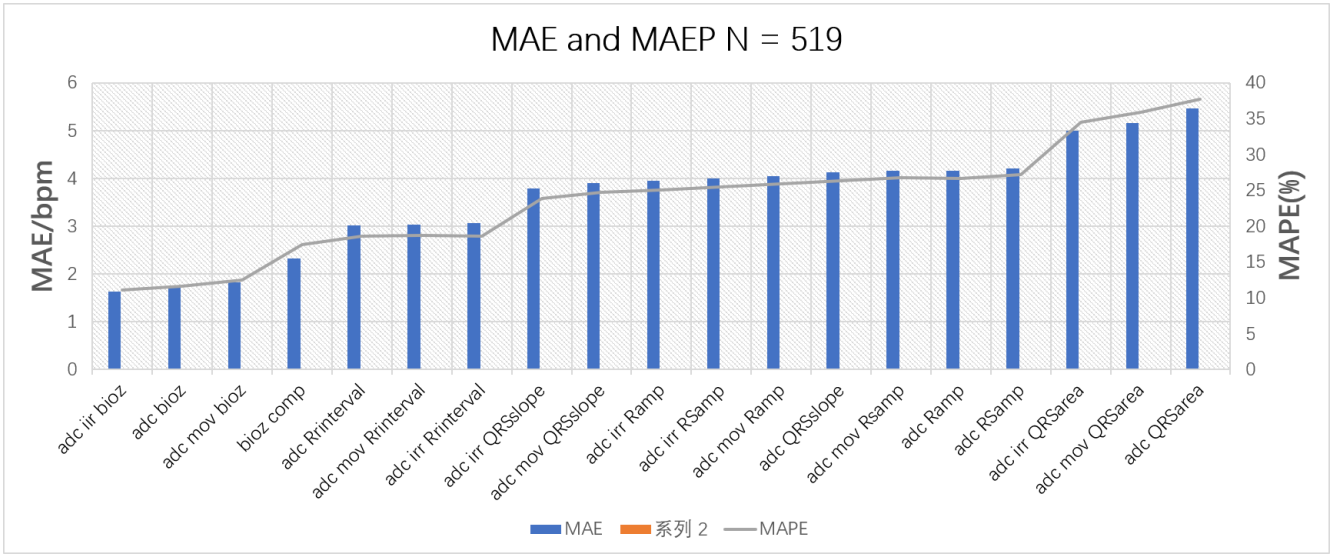


Figure 5.10: MAE and MAEP for the individual methods in table 5.3

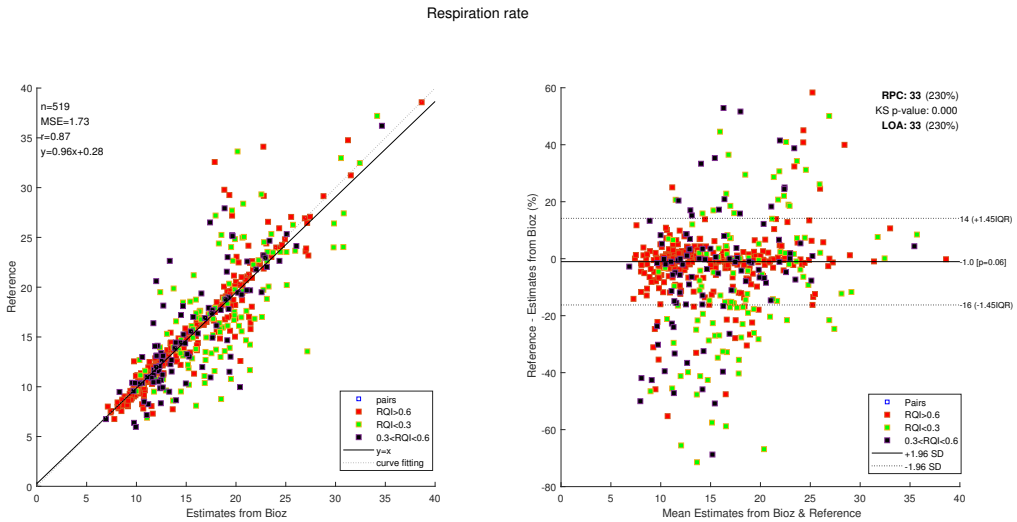


Figure 5.11: Bland-Altman plot and the correlation between RR estimate from reference and from *adc iir bioz*

| Algorithm name | base methods | Breath detection | filtering |
|---|---|---|---|
| 1 RR Kalman | 7,8,12 | adc | SQI-IIR kalman filtering |
| 2 Weighted RR | – | – | SQI-IIR |
| 3 RR average | – | – | – |
| 4 RR median | – | – | – |
| | KF smoothing in a fusion way | | |
| 5 adc iir KF QRSslope | QRSslope | Count-adv | SQI-IIR & Kalman filter |
| 6 adc iir KF RSamp | QRS-RSamp | – | – |
| 7 adc iir KF QRSarea | QRS-area | – | – |
| 8 adc iir KF RRinterval | RRinterval | – | – |
| 9 adc iir KF Ramp | Ramp | – | – |
| 10 adc iir KF bioz | bioz | – | – |

Table 5.4: Summary of fusion algorithms for respiratory rate estimation. The column "Base methods" refer to the individual methods in Table 5.3 which are fused together in each fusion method.

data of bad quality to be closer to the true RR.

### INFORMATION FUSION ALGORITHM

This section presents the result of Information fusion algorithm. The following table 5.4 summarize all the fusion methods which are a combination of the individual methods in 5.3. Mainly the filtered RR methods by SQI-assisted filtering, which are methods 7,8,12 in Table 5.3. The main target is to see if the fusion methods could provide better performance on RR monitoring in terms of evaluation metrics. It is noted that the $adciirKF$ fusion methods in table 5.4 work in way of "information fusion" for initialization, which means the initialization of $x_0$ is taken as the weighted average of the RR from respiratory signals of which the SQI is larger than 0.5. There is no further fusion step for the RR after Kalman filtering.

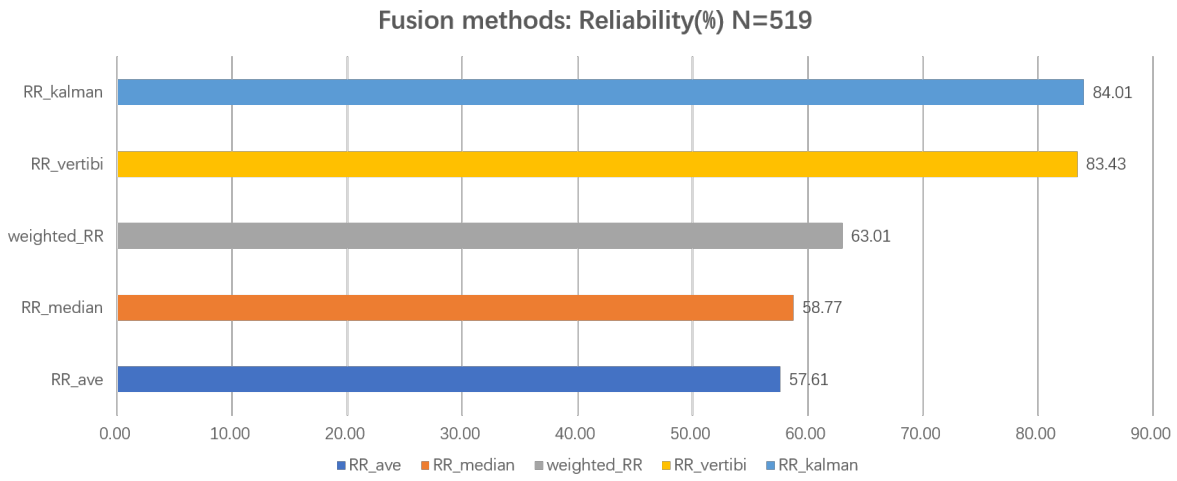


Figure 5.12: Reliability of the first four fusion methods in table 5.4

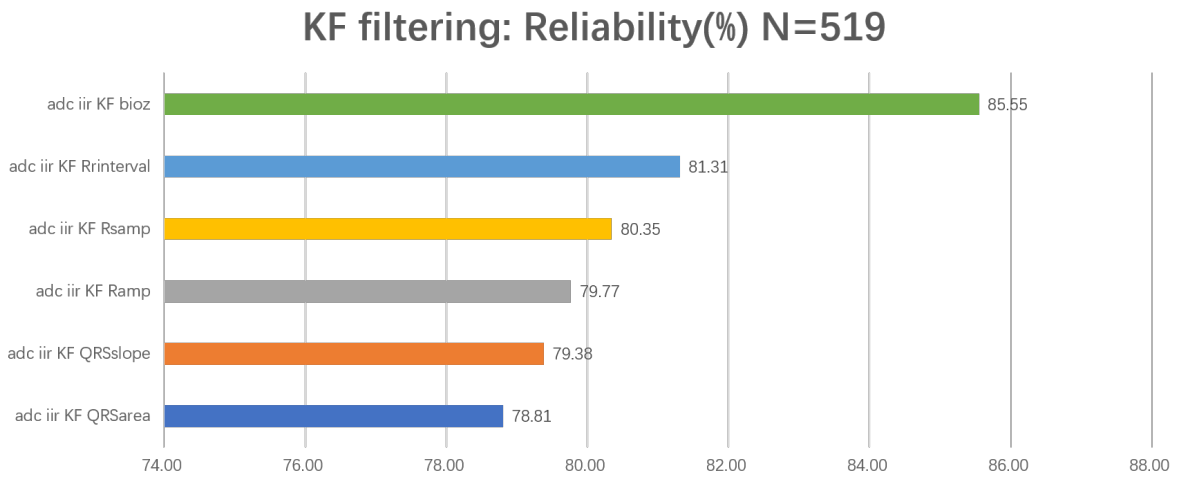


Figure 5.13: Reliability of the last five fusion methods in table 5.4

**Reliability**

The reliability of the fusion methods from 1 - 4 are shown in Figure5.12. It can already be stated that neither $RRaverage$, $RRmedian$ nor $weightedRR$ methods could not provide a high reliability on RR monitoring thus more attention will be given the other two fusion method, $RRkalman$ and $RRviterbi$ in the following. The two best fusion methods are $RRkalman$ and $RRviterbi$, with the reliability of 84.01% and 83.43%, respectively.

As for the methods from 5-10, we only initialize the Kalman filter setting for each individual base signal in a fusion way, e.g the initial state values $x_0$ is set to the SQI-weighted sum of the RR from all respiratory signals of which the SQI is above 0.5. There is no further fusion step for the RR after Kalman filtering. The reliability of these five methods is shown in the following Figure 5.13. Surprisingly, the best method in these five is the $adciirKFbioz$ with a reliability of 85.5%, a slightly larger than that of the best fusion method $RRkalman$ by 1.5%, which means the fusion doesn't gain improvement on reliability compared with only KF filtering the RR. One possible reason for this could be that the RR estimate from the EDRs signals is too noisy compared with that from the IP signal, with the reliability of 82% and less than 50% respectively. Thus the fusion method could not gain improvement if the quality of the individual RR estimate is too spread.

**Mean absolute error and Mean absolute percentage error**

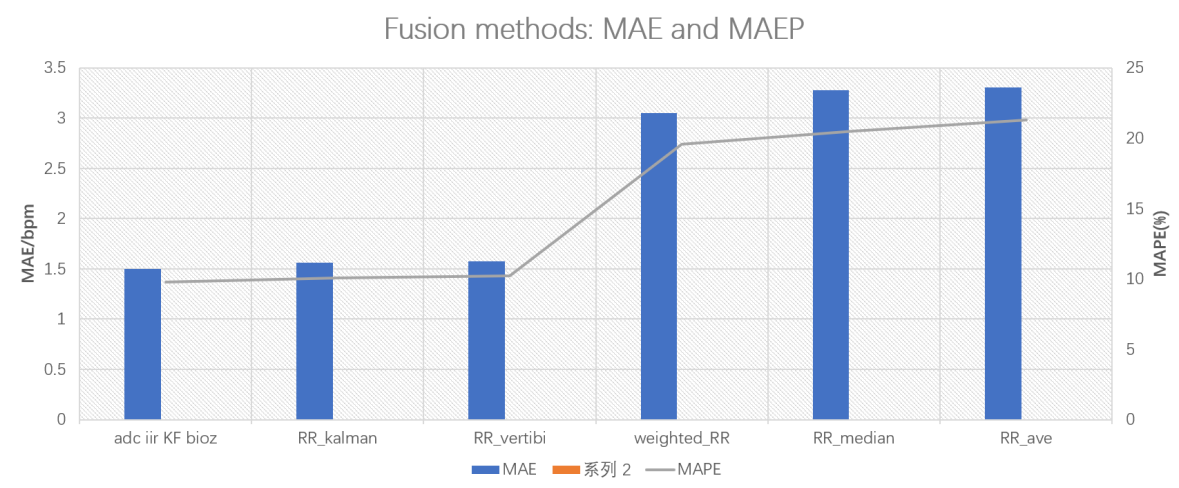


Figure 5.14: MAE and MAEP for the first four fusion methods in table 5.4

Figure 5.14 shows the MAE and MAPE of the fusion methods. Majority of the values of MAE are in 1.5-3.5 bpm while for MAPE are in 10% - 20%. $adciirKFbioz$ method has the minimum MAE of 1.50 bpm followde by $RRKalman$, which has a slightly larger value 1.56 bpm. As for the MAPE, the values of $adciirKFbioz$ and $RRKalman$ are 9.78% and 10.05%, respectively.

**Bland-Altman plot**

Figure 5.15 shows the Bland-Altman plot and correlation plot of the $RRkalman$ method. Compared with

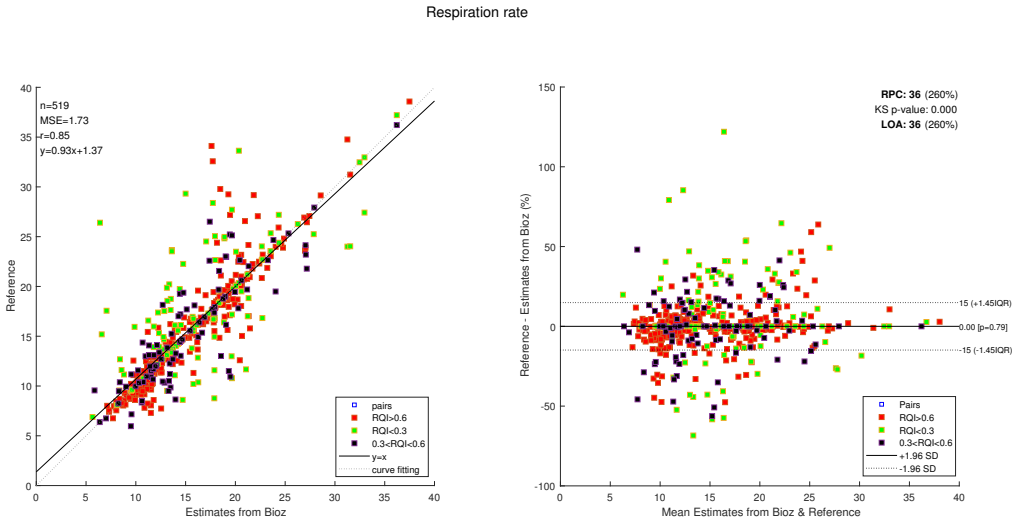


Figure 5.15: Bland-Altman plot and correlation between RR estimate from reference and from $RRKalman$

Figure5.11 of $adciirmethod$, the correlation value is decreased from 0.87 to 0.85 by 0.02 and the limit of agreement stays the same at 30%. It is noted that 60% of the data of bad quality, solid square, stay in the limit agreement compared with that of the method $adciirbioz$ which is 50%. This means the $RRkalman$ method works better than $adciirbioz$ on correcting the RR estimate from data of bad quality.

### OVERALL ALGORITHMS EVALUATION

In this section, we evaluated all the proposed methods of both individual methods and fusion methods by ranking them with multiple factors. Table 5.16 gives clinical reliability(%), mean absolute error(bpm), mean absolute percentage error (%) and Pearson correlation value (unitless). Base on the idea from [23], the sum of the rank values for each method is presented. Sum of the ranks could make more senses to make a more generalized evaluation if a method performs really well on some metrics but poor on the others.
Overall, $adcirrKFbioz$ has the minimum rank sums of 4 which is much less than that of the other methods. When comparing the individual methods with the fusion ones, only two fusion methods, $RRKalman$ and $RRViterbi$ perform similarly to the best individual method. Looking at the individual ranks, $adciicbioz$ has the most uniform performance.

## 5.2.2. ACTIVITY TYPE EVALUATION

In this section, we evaluate the performance of the developed framework of five different activities in total introduced in the appendix A.1( including lying, sitting, standing, walking and running and free breathing with random motion). This section can be divided into three parts. In the first part, the overall evaluation results on all the motions of the five categories are given. In the last two parts, more details of the evaluation results of the motions are present, including data collected when volunteers are lying still against data from activities as well data from periodic activities and non-periodic activities.

| Methods | Reliability | MAE | MAPE | Pearson correlation | rank sum |
|---|---|---|---|---|---|
| adc iir KF bioz | 85.55 | 1.50 | 9.78 | 0.89 | 4 |
| RR kalman | 84.01 | 1.56 | 10.05 | 0.88 | 9 |
| RR vertibi | 83.43 | 1.57 | 10.19 | 0.88 | 11 |
| adc iir bioz | 82.27 | 1.64 | 11.11 | 0.87 | 17 |
| adc bioz | 82.26 | 1.73 | 11.65 | 0.87 | 19 |
| adc iir KF Rrinterval | 81.31 | 1.81 | 11.17 | 0.85 | 24 |
| adc irr QRSslope | 56.84 | 3.80 | 23.87 | 0.43 | 76 |
| adc mov QRSslope | 52.79 | 3.91 | 24.78 | 0.40 | 81 |
| adc irr Ramp | 50.29 | 3.94 | 25.01 | 0.42 | 84 |
| adc irr RSamp | 52.60 | 4.00 | 25.53 | 0.40 | 87 |
| adc QRSslope | 50.29 | 4.13 | 26.29 | 0.37 | 95 |
| adc mov Ramp | 48.75 | 4.05 | 25.95 | 0.39 | 95 |
| adc mov Rsamp | 49.33 | 4.15 | 26.77 | 0.34 | 101 |
| adc Ramp | 47.40 | 4.17 | 26.67 | 0.36 | 103 |
| adc RSamp | 48.94 | 4.21 | 27.25 | 0.31 | 106 |
| adc irr QRSarea | 38.34 | 4.99 | 34.49 | 0.16 | 113 |
| adc mov QRSarea | 38.73 | 5.16 | 35.88 | 0.12 | 115 |
| adc QRSarea | 38.15 | 5.46 | 37.68 | 0.12 | 120 |

Figure 5.16: Ranks of all the individuals methods and fusion methods

### OVERALL RESULTS

Figure 5.17 shows how well individual a set of individual methods together with fusion methods perform in terms of reliability for tasks classified into lying (number of measurement points for each method is 81), sitting (75), standing (38), walking and running (110) and free breathing with noise (215) activity stages and the results are in each sub figure. Reliability is selected as it probably conveys most information from short data segments. In each subfigure, Each bar represents the reliability of one selected method for one activity class. As to be guessed, the errors of RR estimate should have a trend of increasing when the activity is becoming more intensive, making the RR estimate worst in the walking section. However, surprisingly, walking stages are best caught with individual IP methods and even better with the fusion method, $adciirKFbioz$. But the ECG doesn't perform well. For the latter one, this could be explainable: more active classes could result in a motion-distorted ECG from which less reliable EDR could be derived. For the former one, a deeper investigation would be needed, as it is an intuitive taught the proposed methods should provide more accurate RR estimates for the activity of less intensity than that with higher intensity.
For the first three activity classes, lying, sitting and standing, the best results are from the methods $RRViterbi$ and $RRKalman$, with the highest reliability of 93%, 89% and 89%, respectively, which means this fusion method did help to provide a better RR estimate. It's also noted that the reliability of the lying section is the largest, indicating that $RRKalman$ would be optimal choices over fusion methods, considering all the uncertainties fusing multiple signals has-if the data is measured mainly from the patients in bed or on the chair.
For the last two activity classes, walking and running and free breathing with random movement, the best results are from the fusion method of $adciirKFbioz$, which means for these two activities, the RR estimate from method $adciirbioz$ further filtered by Kalman filter could provide a good performance. Meanwhile, the fusion method, $RRKalman$ could also provide comparative results since the differences between it and $adciirKFbioz$ are small, 1.5% and 1.8%.
The Figure 5.18 shows the MAE and MAPE for each activity class and the best method is also labelled on the top of each bar. The MAE range for all the activity classes is [1,1.8] bpm and the MAPE is [7,12]% and this indicates that the proposed methods have a generally good performance in different activity classes. it is obvious that the worst result is from the free-breathing section. This could be explainable: breathing section has the longest data length and almost half of the data are generated under random movement ( the volunteers are asked to move randomly in the second 4 min in free-breathing section, which has a total length of 8min.), which could make it more difficult to obtain an accurate RR estimate from the underlying signals.

### RESULTS OF STILL AGAINST ACTIVITY

In this section, the evaluation results of data collected when volunteers are lying still, stage b in section 1, against data from activities from other sections in **database 3**.
Figure 5.17 shows how well a set of individual methods together with selected fusion methods perform in terms of reliability, MAE and MAPE for RR estimate from still data and activity data the results are in each sub figure. In the upper two subfigure, each bar represents the reliability of one selected method and in the lower two subfigures, the MAE and MAPE of each selected method are present. All the selected methods are methods 7, 10, 12, 19 in table 5.3 and methods 1, 4, 5, 8 10 in table 5.4 since they are the most representative individual methods and fusion methods in term of reliability.
In Figure 5.19a and Figure 5.19c, the reliability, MAE and MAPE of each method of the still data are present. The first impression from Figure 5.19a is that the best results for still data are from five methods with reliability of 100%, which means the RR estimates are all reliably based on these methods, $adciirbioz$, $adciirKFRrinterval$, $adciirKFbioz$ and two fusion methods $RRKalman$ and $RRViterbi$. This indicates that the proposed framework can achieve 100% reliably for RR estimate from still data. The corresponding MAE and MAPE of these five methods are present in Figure 5.19c. The MAE and MAPE of these five methods are in the range of [0.5,0.7]bpm, [5,10]%, which means and this indicates that the proposed methods have a Good performance on still data.
In Figure 5.19b and Figure 5.19d, the reliability, MAE and MAPE of each method of the still data are present. The first impression from Figure 5.19a is that the best result for activity data is from method $adciirKFbioz$ with reliability of 84%. The corresponding MAE and MAPE of the best method are present in Figure 5.19c. The MAE and MAPE of $adciirKFbio$ are 1.54 bpm and 10%, which means and this indicates that the proposed methods have a Good performance on still data.
In a conclusion, the best methods for both still data and activity data can achieve a good performance of RR

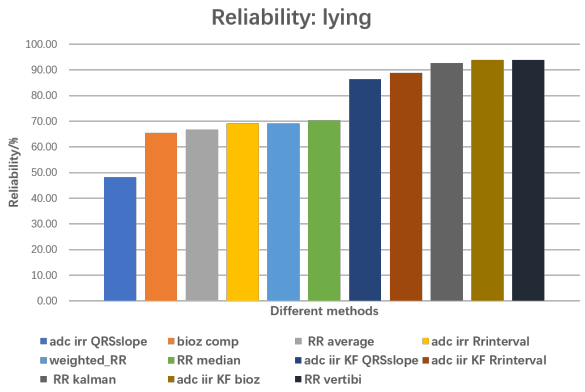


(a) Reliability for lying section

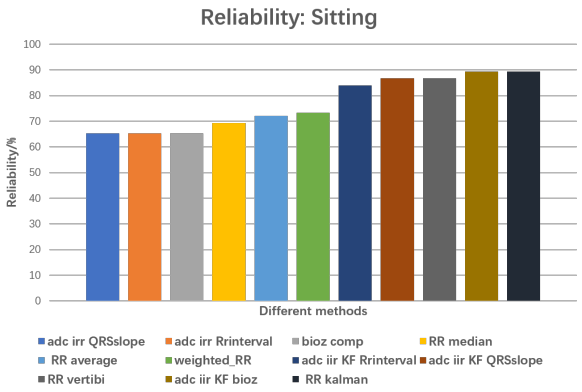


(b) Reliability for sitting section

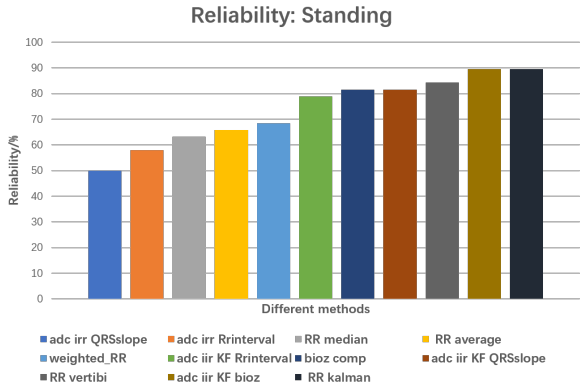


(c) Reliability for standing section

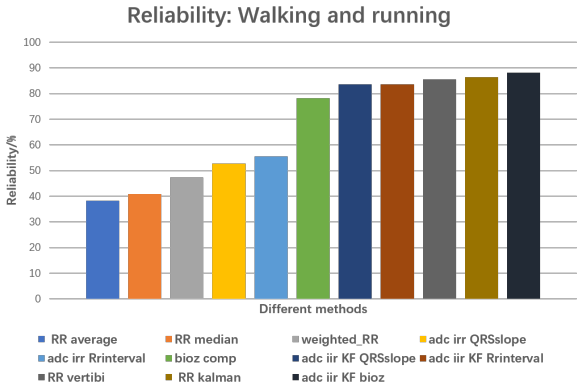


(d) Reliability for walking and running section

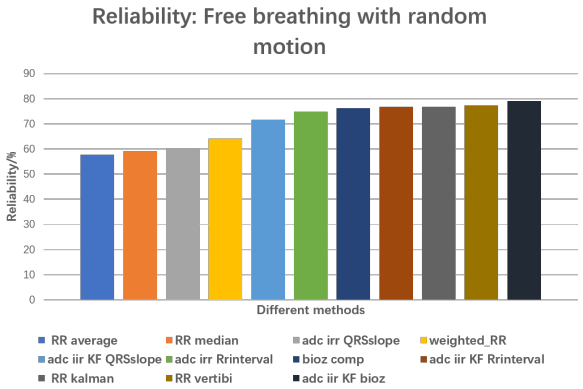


(e) Reliability for free breathing section

Figure 5.17: Reliability evaluation for all the motion types

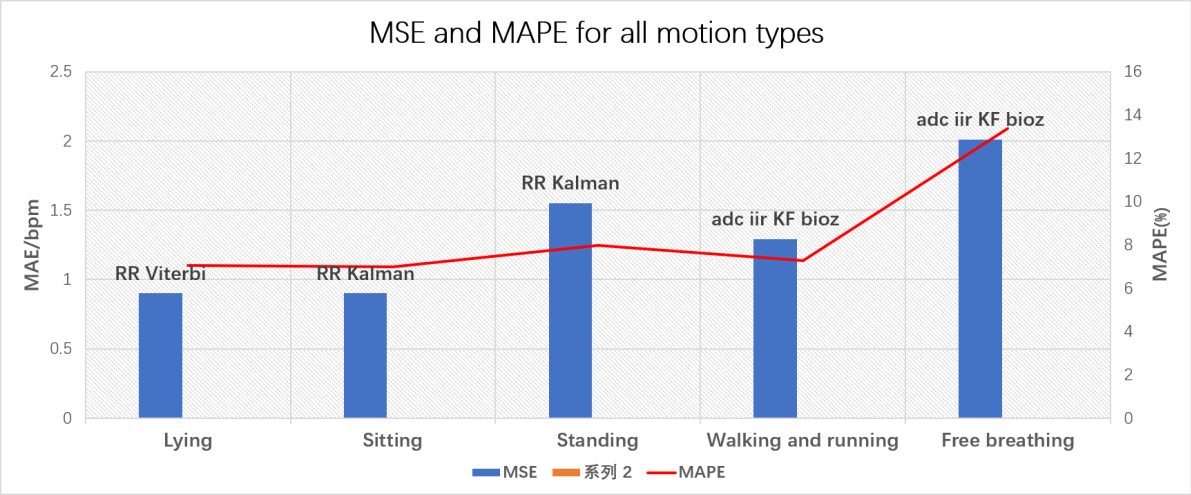


Figure 5.18: MAE and MAPE of all the motion types with the corresponding best method

estimate in terms of reliability, MAE and MAPE. However, it's also found that the amplitude-based EDR methods, $EDR_{QRSslope}$ have a moderate performance for both datasets while the frequency-based EDR method $EDR_{Rrinterval}$ have much better performance. One possible reason is that $EDR_{QRSslope}$ required a more clean ECG signal with a good shape while the $EDR_{Rrinterval}$ only required accurate detections of QRS waveform, which is relatively easier.

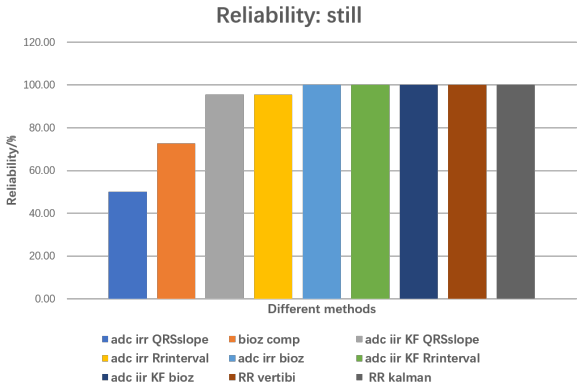


(a) Reliability of still section

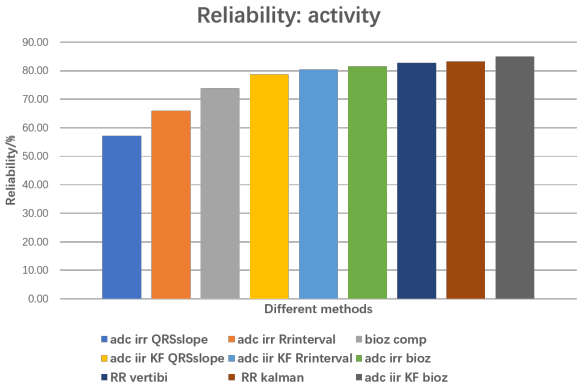


(b) Reliability of activity section

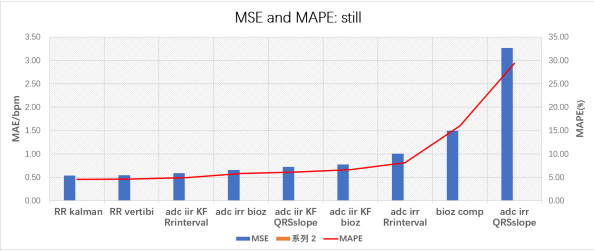


(c) MAE and MAPE of still section

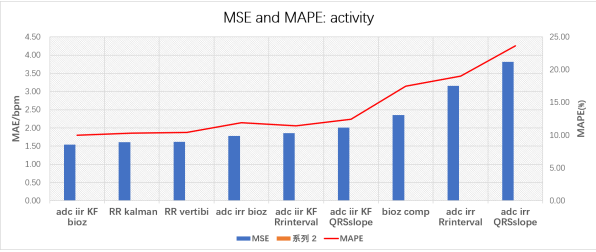


(d) MAE and MAPE of activity section

Figure 5.19: Evaluation for still and activity

#### RESULTS OF PERIODIC ACTIVITY AGAINST NON-PERIODIC ACTIVITY

In this section, the evaluation results of data collected during periodic movement, including stage b in section 1, against data collected from non-periodic movement of **database 3** introduced in section 2.5.1. The data is summarized in the following table 5.5
Figure 5.20 shows how well a set of individual methods together with selected fusion methods perform in

| Data categories | source |
|---|---|
| periodic movement | s1c, s1e, s2f, s4a, s4b, s4c, s4d, s4e |
| non-periodic movement | s1d, s2d, s2e, s3a,s3b |
| Description | All the data are from $dataset3$ introduced in 2.5.1. The source indicates which stage and section the data is from, e.g. $s1c$ means stage c in section 1, lying section. |

Table 5.5: Data of periodic and non-periodic activity

terms of reliability, MAE and MAPE for RR estimate of periodic activity and non-periodic activity the results are in each sub figure. In upper two subfigure, each bar represents the reliability of one selected method and in the lower two subfigures, the MAE and MAPE of each selected method is present. All the selected methods are methods 7, 10, 12, 19 in table 5.3 and methods 1, 4, 5, 8 10 in table 5.4 since they are the most representative individual methods and fusion methods in term of reliability.
In Figure 5.20a and Figure 5.20c, the reliability, MAE and MAPE of each method of the periodic are present. The first impression from Figure 5.20a is that the best result for still data is from method,$adciirKFbioz$ with reliability of 89% and the corresponding MAE and MAPE are present in Figure 5.20c, 1.1bpm and 7%, respectively, which means and this indicates that best method,$adciirKFbioz$, have a Good performance on periodic activity. It is also noted all the selected methods achieve reliability above 50%, however, the EDR-based methods don't have comparative relusts with IP-based methods.
In Figure 5.20b and Figure 5.19d, the reliability, MAE and MAPE of each method of the non-periodic data are present. The first impression from Figure 5.19b is that the best result for non-periodic activity is from method $adciirKFbioz$ with reliability of 86%. The corresponding MAE and MAPE of the best method are present in Figure 5.19d. The MAE and MAPE of $adciirKFbioz$ are 1.4 bpm and 8%, which means and this indicates that the proposed methods have a Good performance on still data.
In a conclusion, the best methods for both periodic activity and non-periodic activity can achieve a good performance of RR estimate in terms of reliability, MAE and MAPE. However, it's also found that the EDR-based methods, either $EDR_{Rrinterval}$ or $EDR_{QRSslope}$ don't have comparative results with IP-based methods during movement.

## 5.3. DISCUSSION

### 5.3.1. INDIVIDUAL RR ESTIMATE METHODS

As for the individual methods, in this thesis, the basic RR estimation method is the "$count-adc$" method and then a number of filtering methods are proposed to smooth the RR estimate from the individual respiratory signal. From the result shown in section 5.2, for both IP and EDR respiratory signals, the simple moving average filtering doesn't really help gain a lot on tracking the true RR while the SQI-assisted filtering method could make the RR estimate more robust against the motion artefacts.
When comparing the IP and EDR signals, IP signal could provide a more robust and accurate RR estimate with the help of the proposed filtering methods, achieving the highest of the reliability of 83% while the EDR signals are less reliable, with the highest reliability of 67% for $EDR_{Rrinterval}$ from the overall performance. This is as expected since, from the literature, many studies have already introduced the limitations of RR es-

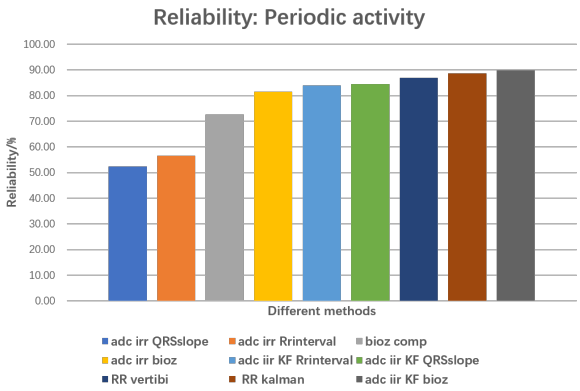


(a) Reliability of periodic activity

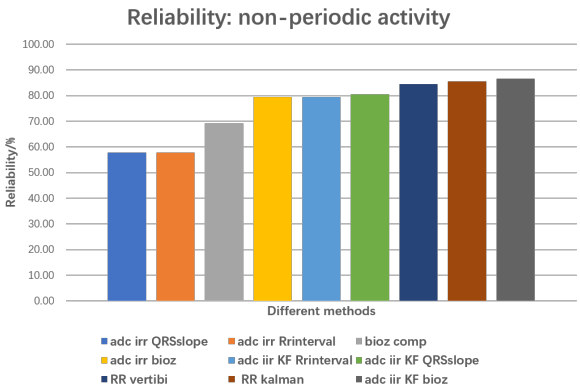


(b) Reliability of non-periodic activity

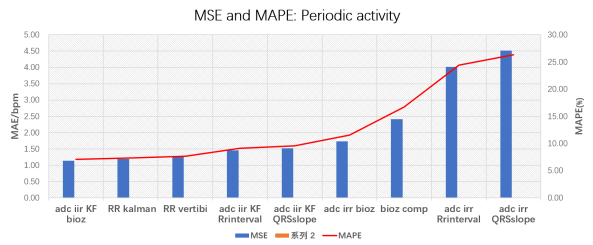


(c) MAE and MAPE of periodic activity

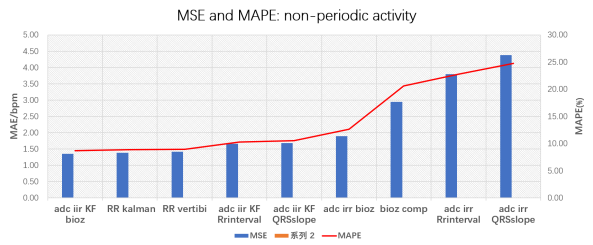


(d) MAE and MAPE of non-periodic activity

Figure 5.20: Evaluation for periodic activity and non-periodic activity

timate from EDR signals, e.g the limitations of RSA introduced in section 2.3.1. As for the amplitude-based EDR signals, it requires an accurate shape of the ECG signal to extract a good EDR signal, however, the morphology of the ECG signal can deteriorate much easier when there are motion artefacts, resulting in a poor EDR signal with no respiration information.

The basic breath detection was mainly done using a slightly modified algorithm in [8]. To optimize the parameters of this methods, the factor multiplied to the third quartile, the data from the section free breath of the database 3 introduced in Chapter 2 are used, where volunteers are asked to breathe freely with random movement. Since the threshold parameter is optimized at certain activities, where people are moving randomly, it may really have problems handling other situations where people are breathing during other activities which make the current threshold work poorly on RR estimation. Thus, a better way to determine the threshold should be further investigated.

Study in [52] used Fast Fourier Transform to estimate the RR from $EDR_{RAmp}$ and $EDR_{RSA}$ and it's reported that these two respiratory signals could provide similar performance. The study collected data from 24 subjects and all of them were under the full standard sleep test. The Correlation coefficients between these two methods and the true RR from the reference signal are approximately 0.70. The best individual methods proposed in this thesis of $EDR_{RAmp}$, and $EDR_{RSA}$ have lower value correlation coefficients, 0.67,0.42, compared with that in [52]. The reason for this is that, in this thesis, the ECG signal is much more easily distorted by motion artefacts since there is a lot of movement during the data collection compared with that in [52], resulting in a poor EDR signal especially for the amplitude-based method, $EDR_{RAmp}$. Thus the RR estimate will be less accurate.

Compared with ECG, there are much fewer studies on RR estimation based on the IP signal. In one study in [27], the respiratory rate is extracted using the Short-Time Fourier Transform (STFT) from both IP and reference respiratory signal. A sliding window of size 15 seconds which moves 5 seconds each time is used for this purpose. The dominant frequency in each window is chosen to be the respiratory rate in that window. It's found that an accuracy of 65.66% can be achieved by this method, where the accuracy means the percentage of the times when the respiratory rate extracted from the impedance signal and the reference signal are equal. In this thesis, the best individual method for IP signal can achieve a reliability of 82.28%. It's noted that no comparison can be made between the performance between these methods since the reliability and accuracy

for evaluating these two methods have different statistical meaning.

### 5.3.2. SIGNAL QUALITY: SQI AND RQI

In Chapter 4, we introduced a set of SQI and RQI together to tell the data of good quality from the bad ones. These two quality indicators are further used in the RR smoothing filter and also the two fusion methods, Kalman filter and the Viterbi algorithm. Thus, an accurate SQI and RQI are very essential to each block of the signal processing chain in this thesis. Take the SQI-assisted RR smoothing method, for example, if the data of good quality is estimated to be of low quality, the RR estimate will be closer to the previous one RR, resulting in giving incorrect data in the further fusion phase. From the result in Chapter 5, all the proposed SQI and RQI are not perfect and probably cannot always distinguish the data of good quality from the bad ones. More investigation should also put on the RQI and SQI and A human-annotated signal quality indicators could make an interesting study and comparison between this and the RQI and SQI proposed in this thesis should also be interesting.

### 5.3.3. INFORMATION FUSION METHODS

The results show that certain signal fusion can provide more accurate and robust RR estimate for different types of data in terms of activities, however, the differences between the fusion methods and the best individual methods are small.
Five fusion methods, $RRKalman$, $WeightedRR$, $RRaverage$ $RRmedian$ and $RRViterbi$, are proposed and the best two are $RRKalman$ and $RRViterbi$. The first one is a modification to a published algorithm in [75] and the latter one is a novel application of the Viterbi Algorithm on the bio-medical study. Both of them use the proposed SQI and RQI.
Median and weighted average don't perform well on the RR estimate due to their simple principle. Since SQI and RQI are the most sensitive part of the signal processing chain and the accuracy of these two can determine the performance of all the methods with signal quality indicator assisted. The weighted mean approach most probably suffers from the signal quality indices not being directly comparable with each other during different activities. Investigation on which respiratory signals could provide underestimated RR and which can provide overestimated RR could be an interesting study and better signal quality indicator should also be explored.
The two best fusion method, $RRViterbi$ and $RRKalman$, behaved almost similarly and both of them performed well in the aspect of reliability with values above 80%. Overall performance for $RRKalman$ was found to be a zero-sum approach to the best IP methods, while the $RRViterbi$ decreases the reliability by 2% compared with the best IP method. As for the $RRKalman$ with no improvement to the best individual method, one possible reason is that it only to filter individual RR estimates and the KF residuals are later used to weight final RR value. The shortcomings for this the residual could also be small for even if when the RR estimate has a large error against the true RR. This can happen when there is a big variation between the two true RR from the two successive data segments while some RR estimates didn't react to this change and are still close to the RR estimate from the first segment, from the Kalman model in this thesis, the residual will be small and during the fusion step, these RR estimates would also be assigned a larger weight, resulting in a poor RR estimate. This is proved by the comparing between the RR estimate filtered by Kalman filtering before and after the fusion step. The former one achieved a 2% improvement in reliability compared with the best IP method while the latter one achieved no improvement. On possible study could also be on the Kalman filter and a proper setting should be explored.
As for the $RRViterbi$ algorithm, it's used to track the true RR by picking on RR estimate per segment from the RR estimate series after Kalman filtering of all the respiratory signals. It achieves a good performance reliability of 80% but a decreased reliability compared with the best IP signal. This show, even after the Kalman filter, the picked RR, most possible state, could not always be close to the true RR. Thus, better fusion methods should also be explored in future studies.
In order to reduce the RR estimate errors as much as possible, some suggestions could also be taken into consideration. The first one it that some data of bad quality could be excluded simply based on the corresponding signal quality. The benefit of this is that the effect of the RR estimate from data of bad quality could be totally

ignored and this could help a lot when a set of consecutive poor RR estimate from a long-term data of bad quality. The second suggestion is that more motion artefacts attenuation methods should also be explored. It's really hard to derive an accurate RR estimate from a heavily artefact-distorted respiratory signal since the respiratory information could be totally buried under the noise. If the signal quality could be improved much with the help of certain motion attenuation methods, the RR estimate will be more accurate.

# 6

# CONCLUSIONS AND FUTURE WORK

This chapter makes conclusions of the results shown in the previous Chapter 5 in section 6.1 and since there are still space of improvement for the current framework, some suggestions regarding how the algorithms could be improved in the future are also present in section6.2

## 6.1. CONCLUSIONS

The main result of this thesis was the proposed framework could generally provide a reliable and robust RR monitoring under different motions. For more details, two signal quality metrics are proposed and it was found that was that RR estimates from both single IP and ECG signals improved with RQI and SQI assisted based on some smoothing and tracking techniques. These signal quality indicators work well on distinguishing data of good quality from the bad ones, however, it can not always achieve this in any situation. Thus, some further studies could be carried on SQIs and try to make both of them more accurate and individualized for different people.
IP methods could provide a more robust RR estimate than EDR methods, which is not a surprise. The best individual EDR signal is $EDR_{Rrinterval}$ with the highest reliability of 67% while the worst one is $EDR_{QRSarea}$. The reason for the poor performance of the EDR signals is that compared with the IP signal, the EDRs requires a more accurate peak detection and also a more correct shape of the ECG signal. However, motion artefacts could distort the shape of the ECG and make the EDR signal less reliable even with no respiratory information. Meanwhile, normally the modulations on the ECG signal are much weaker compared with IP which means it may not always present in the ECG, e.g. $EDR_{RSA}$ may not present under many situations introduced in section 2.3.1. Thus, further investigation could be on better methods to extract the EDRs. Regarding $EDR_{RSA}$, certain classification methods could be explored to distinguish data where RSA is present from that where RSA is not present. This would make the fusion step easier.
A set of fusion methods are also applied on the RR estimates from each individual methods and it is found that none of these fusion methods can achieve improvements on all the evaluation metrics and normally if one is improved, some other one could be worse, e.g. when $RRKalman$ is used, the Mean absolute errors decreases but the general reliability increases compared with the best IP methods. However, the best two fusion methods, $RRKalman$ and $RRViterbi$ can still achieve a high performance on RR monitoring for a certain type of activity, e.g. $RRViterbi$ has the best performance for data from the lying section while $RRKalman$ works best in sitting section and standing section in $database3$. The other fusion methods, $RRaverage$,$RRmedian$, due to its simplicity and more strict requirements for a good performance, they

don't work well on RR monitoring. Further investigation could also be on exploring better fusion methods. Activity class evaluation showed that free breath with random movement is difficult for all methods. Random movement, as well as non-periodic movement, are found to be troublesome. IP was found to be particularly sensitive to movements while it is also superior to the EDR methods. In general, each activity classes can be effectively handled using certain individual methods or fusion methods.

## 6.2. FUTURE WORK

In this section, we summarize the potential future work which could add improvement to the current framework in this thesis.
Since the threshold parameter in the basic breath detection method, "adc count", are ultimately pre-define and the generalized parameter could not work well on certain situations even it has been optimized by using a learning period from the signal itself. For example, the IP data from different activities have different amplitudes and even variant among the volunteers. More investigations could be put on how to determine the parameter in an adaptive way and individualized. It may also gain an improvement on the performance of peak detection if the time information is taken into consideration.
Some possible future work could also be improving the signal quality indices performance on distinguishing the data of good quality from the bad ones. From the result we have so far, the proposed SQI and RQI could not work perfectly and if better signal quality indices could be explored, all the current methods with the SQI and RQI assisted would benefit a lot and the RR estimate of the current framework could also be more robust and accurate.
More investigation could also be put on exploring more respiratory information from the underlying biomedical signals. In this thesis, only the respiratory rate is of interest and the current framework only output the RR estimate with no respiratory information. There are more respiratory information like tidal volume, flow rate and possible future work could be an assessment of the suitability of IP signal for measuring the volume of the airs inhaled and exhaled during the breath cycles.
In this thesis, we tested the feasibility of accelerometer(Acc) recordings as a reference signal for motion artefacts attenuation and from the result, the correlation between the motion artefacts and Acc recordings is not high enough for the adaptive filtering methods to attenuate the motion artefacts. Thus Acc is a proper signal and better reference signal should be explored. Based on the fact that the motion artefacts are mainly from relative sliding between the electrodes and the skin during movement, a better reference signal could measure this relative movement. One possible way is to embed the relevant sensors to measure the stretching strength at the joint point of the electrodes and the wires.

# A

# APPENDIX

## A.1. MEASUREMENT PROTOCOL

This section gives the details of the protocol that was used for respiration information estimate study conducted at holst center imec, the Netherlands. The five sections have the associative movement categories and enough time length for each stage.
Note: Since wearing the nose clip for a long time may cause discomfort to the volunteers, during each section of the protocol, a flexible break period for the subject to relax can be set during two activities if needed (e.g. set a break between stage b and c in section A). The breath-hold part at the beginning of each section is used for synchronization.

### A.1.1. MOTION ACTIVITIES

The details of the activities in five sections are introduced in this subsection.

#### LYING ON THE BED

a) Breathe in deeply and then hold the breath of 7s

b) Sit on the chair with a normal breathing [2 min]

c) Raise the arm and then drop it every 4 seconds [40 s]

d) Move lightly in the bed (imagine that you cannot get sleep or have pain) [40 s]

e) Lie in the bed on the back, bend and straighten legs repetitively [30 s]

#### SITTING AT THE CHAIR

a) Sit down and breathe without spirometer [30 s]

b) Sit down and hold the spirometer but breathe not through the spirometer [30 s]

c) Sit down and hold the spirometer and breathe through the spirometer [30 s]

d) Surf the Internet on smartphone [30 s]

e) Clean the designated area of a table [30 s]

f) Stand up and sit down continuously every 4 seconds [6cycles]

#### STANDING

a) Move body randomly and lightly without hand waving [30 s]

b) Move body and wave hands randomly and lightly [30 s]

#### WALKING AND RUNNING

a) Walk on the treadmill at a speed of 3.0 km/h [40 s]

b) Walk on the treadmill at a speed of 4.0 km/h [40 s]

c) Walk on the treadmill at a speed of 5.0 km/h [30 s]

d) Jog on the treadmill at a speed of 6.0 km/h [30 s]

e) Running on the treadmill at a speed of 7.0 km/h [30 s]

#### FREE BREATH AND MOVEMENT

a) Free breathing with 2min no-movement period alternating with 2 min of motion [4 min]

b) Free breathing with 2min no-movement period alternating with 2 min of motion [4 min]

#### SYNCHRONIZATION

The following mechanisms will provide easy synchronization between Robin and Biopac spirometer recordings:
To distinguish the five sections of motion:

1. Making time markers on the spirometer data
2. Deep breathing as a mark of starting time for each phase.
3. Writing down the time (laptop clock) for each phase.
4. Tapping Robin at the right beginning and end of each phase.

To distinguish each stage (e.g a,b) in a section:

1. Making time markers on the spirometer data.
2. Writing down the time (laptop clock) for each step.
3. Tapping Robin at the right beginning and end of each stage.

## A.2. SQI AND RQI

In this section, the details of the proposed SQI and RQI candidates are introduced.

### A.2.1. SQI FOR ECG SIGNAL

The proposed SQIs are as follows.

**Wavelet and Shannon entropy** One SQI for ECG signal is from [62] and the idea is that the ECG data of good quality can be distinguished from those of bad quality based on the features in the frequency domain. The heart rate variability(HRV) is used to derive the frequency features as the ECG data of bad quality has the potential problems of resulting in a distorted HRV signal which may not have normal distribution of the power in the different frequency band. Thus, the wavelet entropy is used to measure the distortion in the frequency domain which can be calculated based on discrete wavelet transform (DWT) and more details can be found in [78]. By using DWT, the signals can be decomposed into different frequency band and two output, *approximation wavelet coefficients* and *detail wavelet coefficients* are representing the temporal features in the corresponding frequency. Finally, we can derive the features based on approximation wavelet coefficients and detail wavelet coefficients in the corresponding frequency band.
For the HRV signal, the distorted signal can have rather high-frequency noises in the frequency band of 1-2 Hz which is not present in the clean signal and based on this, the Shannon entropy [79] of this frequency band is then calculated to indicate the level of disorder to indicate the signal quality.

**Skewness and kurtosis** Skewness and Kurtosis are two typical statistical metrics to characterize the distributions of the signal and skewness measures the symmetry of the distribution while Kurtosis is measuring the sharpness of the distribution and more details can be found in [80]. For ECG signals, if the quality is low which means there are noises present, the Skewness will be of a larger value while the Kurtosis will become smaller since the noise can result in the asymmetry in the distribution of ECG and a much flatter distribution in terms of sharpness. As a consequence, these two statistical metrics, Skewness and Kurtosis can be used to indicate the quality of the ECG signal.

**Matching of two QRS detector** One SQI for ECG based on the matching of peak detectors of QRS complex is proposed in [66] and the idea is different types of noise could have a different impact on the accuracy of QRS detection [81], the noise level of the ECG data can be indicated by the performance of different QRS detectors. In this study, two peak detectors are used. One is based on digital filtering (DF) and integration [82] and one is a detection algorithm from imec. The SQI is defined to be the ratio of beats detected by both algorithms to all the detected beats (by either algorithm).

**R-R interval variability** The R-R interval is the time interval between two subsequent R peaks in the ECG signal. The variations of the R-R intervals is thus can be a signal quality indicator for ECG signal proposed in [62]. This regularity is affected by the performance of QRS detectors under the noise as the QRS could miss some peaks or wrongly detect the noise as true peaks. Thus, the standard deviation of R-R intervals could be large when the ECG is of distorted by noise. Thus, the SQI can be taken as variability in the R-R intervals and this can be calculated as follows:

$$C_v = \frac{\widehat{\sigma_{RR}}}{\widehat{\mu_{RR}}} \tag{A.1}$$

where $\hat{\sigma_{RR}}$ and $\hat{\mu_{RR}}$ are the standard deviation and mean of the data series of the R-R intervals.

### A.2.2. RQI FOR THE RESPIRATORY SIGNALS

**Autoregression RQI**
Another RQI based on Autoregression model (AR) is proposed in [68]. AR model is used to estimate the spectrum of the signal since it can achieve a high resolution for the spectrum. The selection of the best order for the AR model is based on the Akaike's Information Criterion (AIC) and about the AIC more details can be found in [83]. The AR model is trained on the order from 1 to 30 and the best order is taken as the one which can produce the minimum AIC.
After calculating the AR model on the data. the $RQI_{AR}$ is further taken as the pole of the model which has the largest amplitude among all the poles within the predefined respiratory range. If all the poles are out of

the respiratory range, the $RQI_{AR}$ is set to zero. Actually, the $RQI_{AR}$ is indicating the power of the domain frequency in the predefined respiratory frequency range the signal from which the most possible RR can be derived.

**Hjorth Parameter RQI** Three Hjorth parameters have been defined: activity, mobility, and complexity [84]. Activity is a measure of the squared standard deviation of a signal's amplitude which indicates the mean power of the signal. The standard deviation of the slope against the activity is taken as the mobility. Finally, complexity is a measure of the frequency uniqueness of a data series and when the signal has only one frequency component, which is actually a sinusoid wave, the corresponding complexity will be one. The calculations of these three Hjorth parameters can be found in [84]. Based on the idea in [68], one assumption can be made that the respiratory waveform of best quality would be a perfect sinusoid wave, thus the Hjorth parameter of interest for the $RQI_{Hjorth}$ is complexity as it represents the most sinusoidal signal when its value is equal to one. Thus the calculated Hjorth complexity can indicate the quality of the underlying respiratory signal by measuring how close it is to a sinusoidal signal thus indicate the reliability of the RR estimate from this underlying signal.

## A.3. STATISTICAL ANALYSIS ON THE RR OF CONSECUTIVE TWO SEGMENTS

This statistical analysis is based on spirometer recordings of 10 subjects from the protocol introduced in Chapter **??** and the joint distribution of the RR of two successive segments (20 s) are investigated on four categories of motion, including lying, sitting, standing and walking and running. Totally a number of more than 800 segments from the protocol are utilized.
The following Figure A.1 shown the histogram together with the bivariate distribution fitting plot. The purpose of this analysis is to help decide the dynamic model of the Kalman filter and also the relevant bivariate distribution parameters for the Vertibi algorithm introduced in introduced in section 4.2.6.
The corresponding bivariate distribution parameters are summarized in the following table A.1.

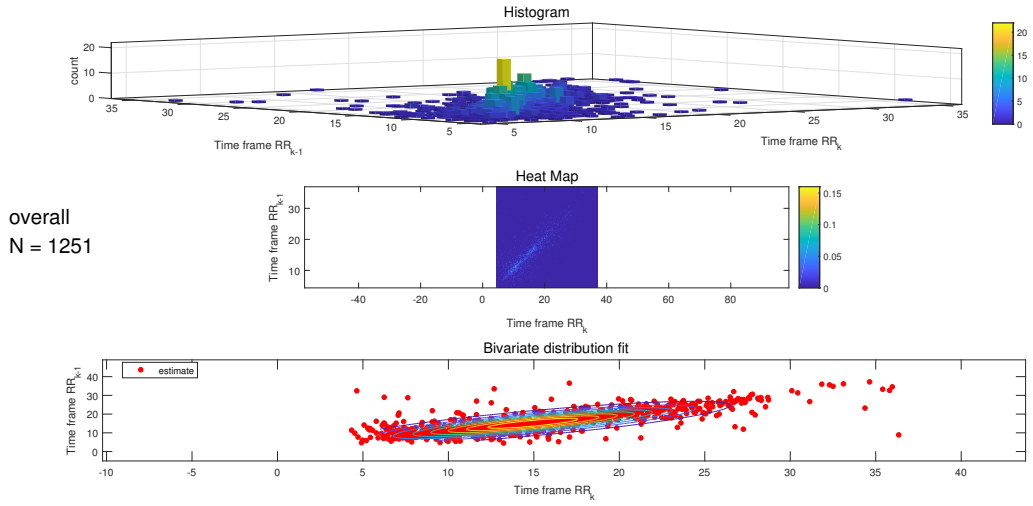


(a) statistical analysis on overall dataset

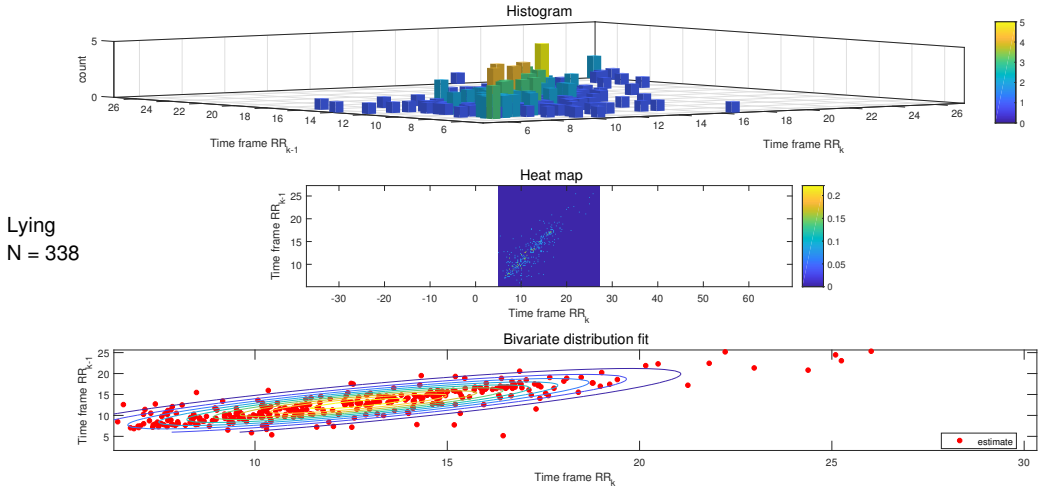


(b) statistical analysis on dataset of specific motion: lying

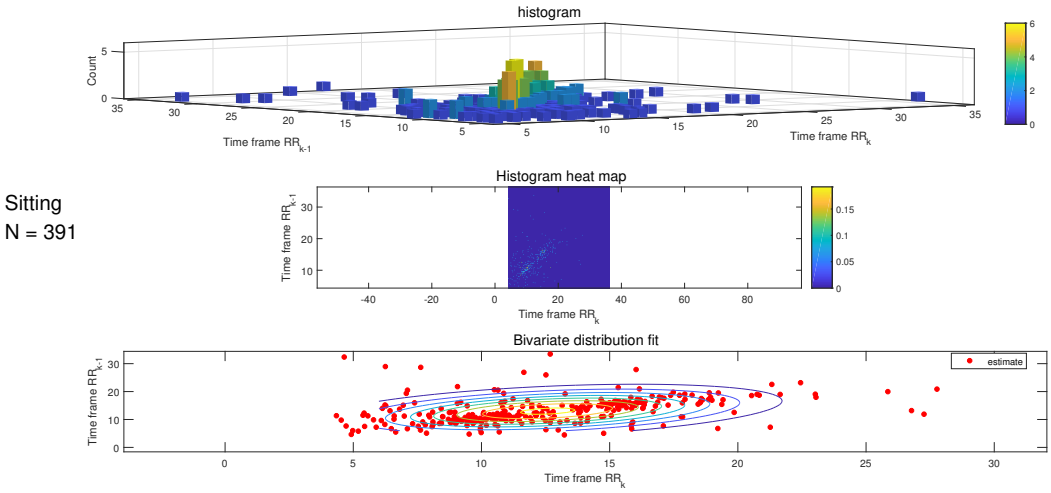


(c) statistical analysis on dataset of specific motion: sitting

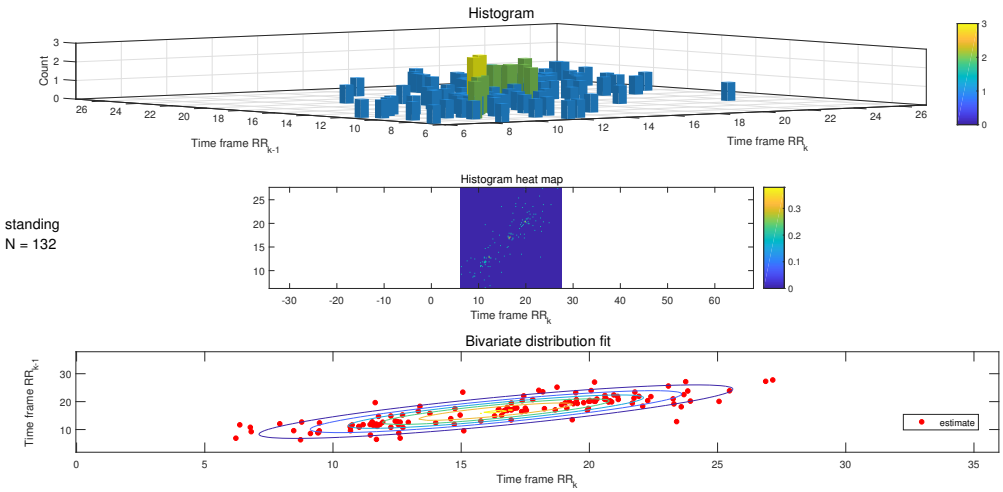


(d) statistical analysis on dataset of specific motion: standing

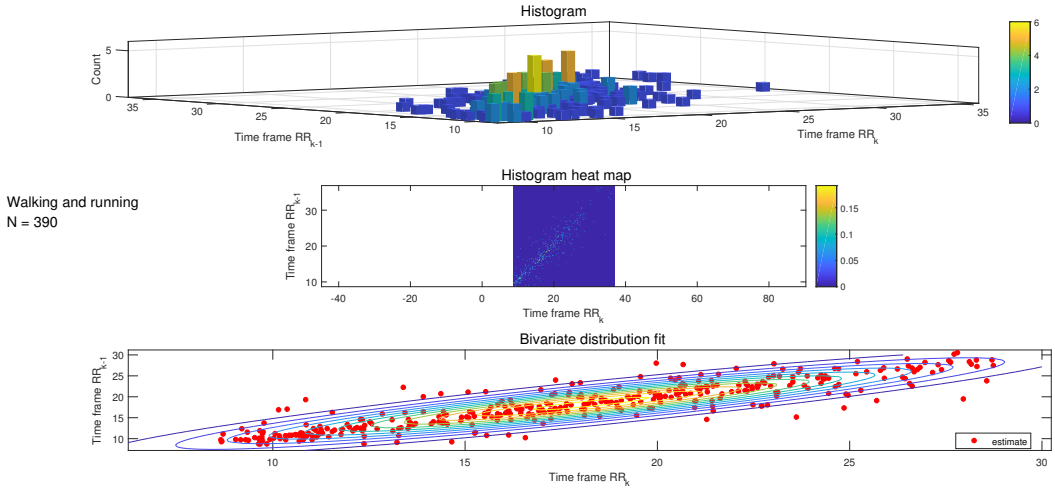


(e) statistical analysis on dataset of specific motion: walking

Figure A.1: Statistical analysis on the RR of consecutive two segments for overall dataset and specific motion dataset

| Motion categories | Mean:$\mu$ | convariance matrix: $\sum$ |
|---|---|---|
| Lying | $\begin{bmatrix} 12.68 \\ 12.79 \end{bmatrix}$ | $\begin{bmatrix} 15.63 & 13.26 \\ 13.26 & 15.73 \end{bmatrix}$ |
| Sitting | $\begin{bmatrix} 12.57 \\ 12.98 \end{bmatrix}$ | $\begin{bmatrix} 19.79 & 7.97 \\ 7.97 & 22.04 \end{bmatrix}$ |
| Standing | $\begin{bmatrix} 16.35 \\ 16.41 \end{bmatrix}$ | $\begin{bmatrix} 23.73 & 20.80 \\ 20.80 & 25.51 \end{bmatrix}$ |
| Walking & running | $\begin{bmatrix} 18.25 \\ 18.37 \end{bmatrix}$ | $\begin{bmatrix} 33.4 & 30.89 \\ 30.89 & 34.39 \end{bmatrix}$ |
| free breath | $\begin{bmatrix} 14.47 \\ 14.48 \end{bmatrix}$ | $\begin{bmatrix} 26.91 & 24.43 \\ 24.43 & 27.08 \end{bmatrix}$ |

Table A.1: Bivariate distribution parameters for five types of motion

# BIBLIOGRAPHY


[1] Electrocardiography. https://en.wikipedia.org/wiki/Electrocardiography. Accessed: 2018-06-18.

[2] 12-lead ecg placement guide with illustrations. https://www.cablesandsensors.com/pages/12-lead-ecg-placement-guide-with-illustrations. Accessed: 2018-06-18.

[3] Peter H Charlton, Timothy Bonnici, Lionel Tarassenko, Jordi Alastruey, David A Clifton, Richard Beale, and Peter J Watkinson. Extraction of respiratory signals from the electrocardiogram and photoplethysmogram: technical and physiological determinants. *Physiological measurement*, 38(5):669, 2017.

[4] Amit K Gupta. Respiration rate measurement based on impedance pneumography. *Texas Instruments application report SBAA181*, 2011.

[5] Orjan G Martinsen and Sverre Grimnes. *Bioimpedance and bioelectricity basics*. Academic press, 2011.

[6] Jesús Lázaro, Alejandro Alcaine, Daniel Romero, Eduardo Gil, Pablo Laguna, Esther Pueyo, and Raquel Bailón. Electrocardiogram derived respiratory rate from qrs slopes and r-wave angle. *Annals of biomedical engineering*, 42(10):2072–2083, 2014.

[7] VP Seppä, J Hyttinen, and J Viik. A method for suppressing cardiogenic oscillations in impedance pneumography. *Physiological measurement*, 32(3):337, 2011.

[8] Axel Schäfer and Karl W Kratky. Estimation of breathing rate from respiratory sinus arrhythmia: comparison of various methods. *Annals of Biomedical Engineering*, 36(3):476, 2008.

[9] Ainara Sobron, Inaki Romero, and Txema Lopetegi. Evaluation of methods for estimation of respiratory frequency from the ecg. In *Computing in Cardiology, 2010*, pages 513–516. IEEE, 2010.

[10] Peter H Charlton, Timothy Bonnici, Lionel Tarassenko, David A Clifton, Richard Beale, and Peter J Watkinson. An assessment of algorithms to estimate respiratory rate from the electrocardiogram and photoplethysmogram. *Physiological measurement*, 37(4):610, 2016.

[11] GD Clifford, J Behar, Q Li, and Iead Rezek. Signal quality indices and data fusion for determining clinical acceptability of electrocardiograms. *Physiological measurement*, 33(9):1419, 2012.

[12] Mason Laura. *Signal processing methods for non-invasive respiration monitoring*. PhD thesis, University of Oxford, 2002.

[13] George B Moody, Roger G Mark, Andrea Zoccola, and Sara Mantero. Derivation of respiratory signals from multi-lead ecgs. *Computers in cardiology*, 12(1985):113–116, 1985.

[14] Stefano Nava, Nicolino Ambrosino, Enrico Clini, Maurizio Prato, Giacomo Orlando, Michele Vitacca, Paolo Brigada, Claudio Fracchia, and Fiorenzo Rubini. Noninvasive mechanical ventilation in the weaning of patients with respiratory failure due to chronic obstructive pulmonary disease: a randomized, controlled trial. *Annals of internal medicine*, 128(9):721–728, 1998.

[15] Sardar Ansari, Kevin R Ward, and Kayvan Najarian. Motion artifact suppression in impedance pneumography signal for portable monitoring of respiration: an adaptive approach. *IEEE journal of biomedical and health informatics*, 21(2):387–398, 2017.

[16] Helmut Hutten. Impedance plethysmography. *Encyclopedia of Medical Devices and Instrumentation*, 2006.

[17] Marcel Młyńczak and Gerard Cybulski. Motion artifact detection in respiratory signals based on teager energy operator and accelerometer signals. In *EMBEC & NBC 2017*, pages 45–48. Springer, 2017.

[18] A. L. Goldberger, L. A. N. Amaral, L. Glass, J. M. Hausdorff, P. Ch. Ivanov, R. G. Mark, J. E. Mietus, G. B. Moody, C.-K. Peng, and H. E. Stanley. PhysioBank, PhysioToolkit, and PhysioNet: Components of a new research resource for complex physiologic signals. *Circulation*, 101(23):e215–e220, 2000 (June 13). Circulation Electronic Pages: http://circ.ahajournals.org/content/101/23/e215.full PMID:1085218; doi: 10.1161/01.CIR.101.23.e215.

[19] VC Moore. Spirometry: step by step. *Breathe*, 8(3):232–240, 2012.

[20] Gandis G Mazeika and Rick Swanson. Respiratory inductance plethysmography an introduction. *Pro-Tech Services Inc., available online at www. protech. com*, 2007.

[21] Gari D Clifford, Francisco Azuaje, Patrick McSharry, et al. *Advanced methods and tools for ECG data analysis*. Artech house Norwood, MA, 2006.

[22] ECG Normal. Electrophysiology of the heart. 1960.

[23] Mika Mäntykangas et al. Improving respiratory rate estimation by combining information from impedance pneumography and electrocardiography. 2016.

[24] Frank N Wilson, Franklin D Johnston, and Charles E Kossmann. The substitution of a tetrahedron for the einthoven triangle. *American heart journal*, 33(5):594–603, 1947.

[25] ENRICO GIANLUCA Caiani, A Porta, M Terrani, S Guzzetti, A Malliani, and Sergio Cerutti. Minimal adaptive notch filter for respiratory frequency tracking. In *Computers in Cardiology, 1999*, pages 511–514. IEEE, 1999.

[26] Christopher M Masi, Louise C Hawkley, Edith M Rickett, and John T Cacioppo. Respiratory sinus arrhythmia and diseases of aging: Obesity, diabetes mellitus, and hypertension. *Biological psychology*, 74 (2):212–223, 2007.

[27] Sardar Ansari, Ashwin Belle, Kayvan Najarian, and Kevin Ward. Impedance plethysmography on the arms: Respiration monitoring. In *Bioinformatics and Biomedicine Workshops (BIBMW), 2010 IEEE International Conference on*, pages 471–472. IEEE, 2010.

[28] Marcel Młyńczak and Gerard Cybulski. Impedance pneumography: Is it possible? In *Photonics Applications in Astronomy, Communications, Industry, and High-Energy Physics Experiments 2012*, volume 8454, page 84541T. International Society for Optics and Photonics, 2012.

[29] Dean Hess. *Respiratory care: principles and practice*. Jones & Bartlett Learning, 2011.

[30] John J Bray. *Lecture notes on human physiology*. Blackwell Publishing, 1999.

[31] Hong-bin Wang, Chen-wen Yen, Jing-tao Liang, Qian Wang, Guan-zheng Liu, and Rong Song. A robust electrode configuration for bioimpedance measurement of respiration. *Journal of healthcare engineering*, 5(3):313–328, 2014.

[32] Ville-Pekka Seppa, Jari Viik, and Jari Hyttinen. Assessment of pulmonary flow using impedance pneumography. *IEEE Transactions on Biomedical Engineering*, 57(9):2277–2285, 2010.

[33] VP Seppä, J Viik, A Naveed, J Väisänen, and J Hyttinen. Signal waveform agreement between spirometer and impedance pneumography of six chest band electrode configurations. In *World Congress on Medical Physics and Biomedical Engineering, September 7-12, 2009, Munich, Germany*, pages 689–692. Springer, 2009.

[34] Douglas A Hettrick and Todd M Zielinski. Bioimpedance in cardiovascular medicine. *Encyclopedia of Medical Devices and Instrumentation*, 2006.

[35] L-G Lindberg, H Ugnell, and PÅ Öberg. Monitoring of respiratory and heart rates using a fibre-optic sensor. *Medical and Biological Engineering and Computing*, 30(5):533–537, 1992.

[36] Walter Karlen, Srinivas Raman, J Mark Ansermino, and Guy A Dumont. Multiparameter respiratory rate estimation from the photoplethysmogram. *IEEE Transactions on Biomedical Engineering*, 60(7):1946–1953, 2013.

[37] Rangsal Ruangsuwana, Gordana Velikic, and Mark Bocko. Methods to extract respiration information from ecg signals. In *Acoustics Speech and Signal Processing (ICASSP), 2010 IEEE International Conference on*, pages 570–573. IEEE, 2010.

[38] Eco J.C. de Geus, Gonneke H.M. Willemsen, Coert H.A.M. Klaver, and Lorenz J.P. van Doornen. Ambulatory measurement of respiratory sinus arrhythmia and respiration rate. *Biological Psychology*, 41(3):205 – 227, 1995. ISSN 0301-0511. doi: https://doi.org/10.1016/0301-0511(95)05137-6. URL http://www.sciencedirect.com/science/article/pii/0301051195051376.

[39] Devy Widjaja, Joachim Taelman, Steven Vandeput, Marijke AKA Braeken, Renée A Otte, Bea RH Van den Bergh, and Sabine Van Huffel. Ecg-derived respiration: Comparison and new measures for respiratory variability. In *Computing in Cardiology, 2010*, pages 149–152. IEEE, 2010.

[40] Christina Orphanidou, Susannah Fleming, Syed Ahmar Shah, and Lionel Tarassenko. Data fusion for estimating respiratory rate from a single-lead ecg. *Biomedical Signal Processing and Control*, 8(1):98–105, 2013.

[41] Philip Langley, Emma J Bowers, and Alan Murray. Principal component analysis as a tool for analyzing beat-to-beat changes in ecg features: application to ecg-derived respiration. *IEEE transactions on biomedical engineering*, 57(4):821–829, 2010.

[42] Eckhard Alt, Michael Heinz, Christoph Hirgstetter, Hans-Peter Emslander, Severin Daum, and Hans Blömer. Control of pacemaker rate by impedancebased respiratory minute ventilation. *Chest*, 92(2): 247–252, 1987.

[43] Shen Luo, Valtino X Afonso, John G Webster, and Willis J Tompkins. The electrode system in impedance-based ventilation measurement. *IEEE transactions on biomedical engineering*, 39(11):1130–1141, 1992.

[44] Olaf Such. Motion tolerance in wearable sensors-the challenge of motion artifact. In *Engineering in Medicine and Biology Society, 2007. EMBS 2007. 29th Annual International Conference of the IEEE*, pages 1542–1545. IEEE, 2007.

[45] Monson H Hayes. *Statistical digital signal processing and modeling*. John Wiley & Sons, 2009.

[46] Dimitris G Manolakis, Vinay K Ingle, and Stephen M Kogon. *Statistical and adaptive signal processing: spectral estimation, signal modeling, adaptive filtering, and array processing*. McGraw-Hill Boston, 2000.

[47] A Bhavani Sankar, D Kumar, and K Seethalakshmi. Performance study of various adaptive filter algorithms for noise cancellation in respiratory signals. *Signal processing: An international journal (SPIJ)*, 4 (5):267, 2010.

[48] Zhengbo Zhang, Ikaro Silva, Dalei Wu, Jiewen Zheng, Hao Wu, and Weidong Wang. Adaptive motion artefact reduction in respiration and ecg signals for wearable healthcare monitoring systems. *Medical & biological engineering & computing*, 52(12):1019–1030, 2014.

[49] Alexander M Chan, Nima Ferdosi, and Ravi Narasimhan. Ambulatory respiratory rate detection using ecg and a triaxial accelerometer. In *Engineering in Medicine and Biology Society (EMBC), 2013 35th Annual International Conference of the IEEE*, pages 4058–4061. IEEE, 2013.

[50] Drew A Birrenkott, Marco AF Pimentel, Peter J Watkinson, and David A Clifton. Robust estimation of respiratory rate via ecg-and ppg-derived respiratory quality indices. In *Engineering in Medicine and Biology Society (EMBC), 2016 IEEE 38th Annual International Conference of the*, pages 676–679. IEEE, 2016.

[51] H Bettermann, P Engelke, P Van Leeuwen, and C Heckmann. Die bestimmung der atemfrequenz aus der respiratorischen sinusarrhythmie (rsa). determination of respiratory rate on the basis of respiratory sinus arrhythmia. *Biomedizinische Technik/Biomedical Engineering*, 41(11):319–323, 1996.

[52] G Dorfman Furman, Z Shinar, A Baharav, and S Akselrod. Electrocardiogram derived respiration during sleep. In *Computers in Cardiology, 2005*, pages 351–354. IEEE, 2005.

[53] Syed Ahmar Shah, Susannah Fleming, Matthew Thompson, and Lionel Tarassenko. Respiratory rate estimation during triage of children in hospitals. *Journal of medical engineering & technology*, 39(8): 514–524, 2015.

[54] Syed Ahmar Shah. *Vital sign monitoring and data fusion for paediatric triage*. PhD thesis, University of Oxford, 2012.

[55] Lionel Tarassenko. *Measurement and fusion of non-invasive vital signs for routine triage of acute paediatric illness*. PhD thesis, Oxford University, UK, 2010.

[56] Susannah Fleming, Lionel Tarassenko, Matthew Thompson, and David Mant. Non-invasive measurement of respiratory rate in children using the photoplethysmogram. In *Engineering in Medicine and Biology Society, 2008. EMBS 2008. 30th Annual International Conference of the IEEE*, pages 1886–1889. IEEE, 2008.

[57] Jesús Lázaro, Eduardo Gil, Raquel Bailón, Ana Mincholé, and Pablo Laguna. Deriving respiration from photoplethysmographic pulse width. *Medical & biological engineering & computing*, 51(1-2):233–242, 2013.

[58] Rudolph Emil Kalman. A new approach to linear filtering and prediction problems. *Journal of basic Engineering*, 82(1):35–45, 1960.

[59] Inaki Romero, Bernard Grundlehner, and Julien Penders. Robust beat detector for ambulatory cardiac monitoring. In *Engineering in Medicine and Biology Society, 2009. EMBC 2009. Annual International Conference of the IEEE*, pages 950–953. IEEE, 2009.

[60] Xiao Hu, JQ Wang, and Ni Zhang. Detecting onset and offset of qrs complex based on measurement of a triangle. *J Appl Sci*, 29(3):289–293, 2011.

[61] Javier Mateo and Pablo Laguna. Analysis of heart rate variability in the presence of ectopic beats using the heart timing signal. *IEEE Transactions on Biomedical Engineering*, 50(3):334–343, 2003.

[62] Christina Orphanidou. *Signal Quality Assessment in Physiological Monitoring: State of the Art and Practical Considerations*. Springer, 2017.

[63] Christina Orphanidou, Timothy Bonnici, Peter Charlton, David Clifton, David Vallance, and Lionel Tarassenko. Signal-quality indices for the electrocardiogram and photoplethysmogram: Derivation and applications to wireless monitoring. *IEEE journal of biomedical and health informatics*, 19(3):832–838, 2015.

[64] Jacob Benesty, Jingdong Chen, Yiteng Huang, and Israel Cohen. Pearson correlation coefficient. In *Noise reduction in speech processing*, pages 1–4. Springer, 2009.

[65] Tianyang Li. Ecg parameter extraction and motion artifact detection. 2016.

[66] J Behar, J Oster, Q Li, and GD Clifford. A single channel ecg quality metric. In *Computing in Cardiology (CinC), 2012*, pages 381–384. IEEE, 2012.

[67] Mohamed Elgendi. Optimal signal quality index for photoplethysmogram signals. *Bioengineering*, 3(4): 21, 2016.

[68] Drew Birrenkott. Respiratory quality index design and validation for ecg and ppg derived respiratory data. *Report for transfer of status, University of Oxford*, 2015.

[69] Fulai Peng, Zhengbo Zhang, Xiaoming Gou, Hongyun Liu, and Weidong Wang. Motion artifact removal from photoplethysmographic signals by combining temporally constrained independent component analysis and adaptive filter. *Biomedical engineering online*, 13(1):50, 2014.

[70] Zhi-Lin Zhang. Morphologically constrained ica for extracting weak temporally correlated signals. *Neurocomputing*, 71(7-9):1669–1679, 2008.

[71] Te-Won Lee. Independent component analysis. In *Independent component analysis*, pages 27–66. Springer, 1998.

[72] Wei Lu and Jagath C Rajapakse. Approach and applications of constrained ica. *IEEE transactions on neural networks*, 16(1):203–212, 2005.

[73] S Lawrence Marple and Claudio Marino. Coherence in signal processing: a fundamental redefinition. In *Signals, Systems and Computers, 2004. Conference Record of the Thirty-Eighth Asilomar Conference on*, volume 1, pages 1035–1038. IEEE, 2004.

[74] Sen M Kuo and Dennis Morgan. *Active noise control systems: algorithms and DSP implementations*. John Wiley & Sons, Inc., 1995.

[75] Shamim Nemati, Atul Malhotra, and Gari D Clifford. Data fusion for improved respiration rate estimation. *EURASIP journal on advances in signal processing*, 2010:10, 2010.

[76] Andrew Viterbi. Error bounds for convolutional codes and an asymptotically optimum decoding algorithm. *IEEE transactions on Information Theory*, 13(2):260–269, 1967.

[77] Davide Giavarina. Understanding bland altman analysis. *Biochemia medica: Biochemia medica*, 25(2): 141–151, 2015.

[78] Mark J Shensa. The discrete wavelet transform: wedding the a trous and mallat algorithms. *IEEE Transactions on signal processing*, 40(10):2464–2482, 1992.

[79] Claude E Shannon, Warren Weaver, and Arthur W Burks. The mathematical theory of communication. 1951.

[80] James Dean Brown. Skewness and kurtosis. *Manoa: JALT Testing & Evaluation SIG Newsletter*, 1997.

[81] Gary M Friesen, Thomas C Jannett, Manal Afify Jadallah, Stanford L Yates, Stephen R Quint, and H Troy Nagle. A comparison of the noise sensitivity of nine qrs detection algorithms. *IEEE Transactions on biomedical engineering*, 37(1):85–98, 1990.

[82] Patrick S Hamilton and Willis J Tompkins. Quantitative investigation of qrs detection rules using the mit/bih arrhythmia database. *IEEE transactions on biomedical engineering*, (12):1157–1165, 1986.

[83] Hirotugu Akaike. Akaike's information criterion. In *International encyclopedia of statistical science*, pages 25–25. Springer, 2011.

[84] Bo Hjorth. Eeg analysis based on time domain properties. *Electroencephalography and clinical neurophysiology*, 29(3):306–310, 1970.